International Pacific Research Center

April 2009–March 2010
Report

School of Ocean and
Earth Science and Technology
University of Hawai‘i at Mānoa

CONTENTS

Editor: Gisela E. Speidel, PhD
Japanese Translator: Keiko Tokinaga
Cover Photo: Gisela E. Speidel, PhD
Design: Susan Yamamoto

THE INTERNATIONAL PACIFIC RESEARCH CENTER

Conceived under the "US–Japan Common Agenda for Cooperation in Global Perspective," the International Pacific Research Center (IPRC) was established in 1997 within the School of Ocean and Earth Science and Technology at the University of Hawai'i at Mānoa. The IPRC mission is "To provide an international research environment dedicated to improving mankind's understanding of the nature and predictability of climate variations and change in the Asia-Pacific region, and to developing innovative ways to utilize knowledge gained for the benefit of society." The core support for the IPRC comes from the State of Hawai'i through the University and from the principal supporting agencies: the Japan Agency for Marine-Earth Science and Technology (JAMSTEC), NASA and NOAA. Financial support for our research is also provided by other government agencies in the US and abroad. The IPRC now has an annual budget of roughly 7 million dollars.

Asia and the Pacific region are home to over half the world's people, all of whom are affected by variations in the climate system. IPRC researchers conduct modeling and diagnostic studies to document these variations and understand their causes, whether such causes are purely natural or have a human component. Through advances in basic research, the IPRC contributes to improving environmental forecasting for the Asia-Pacific region. One focus of IPRC investigations is the understanding of key phenomena rooted in the tropics, such as the El Niño-Southern Oscillation of the ocean-atmosphere system, monsoon circulations, interannual variability in the Indian Ocean, intraseasonal oscillations of the tropical atmosphere, and tropical cyclones. Other examples of important issues for IPRC study include the nature of decadal variability in the extratropical North Pacific Ocean, the dynamics of the very strong Kuroshio and Oyashio ocean currents in the western North Pacific and the role of marginal seas in the climate system. Concerns about climate change are addressed through modeling studies of past climate and through assessment of model predictions for future trends in climate.

国際太平洋研究センター

国際太平洋研究センター（IPRC）は、「地球的展望に立った協力のための日米共通課題」のもと、1997年にハワイ大学マノア校の海洋地球科学技術学部内に設立されました。その使命は、「国際色豊かな研究環境を創り、アジア・太平洋地域の気候変動及び変化について、その性質と予測可能性に対する人類の理解を向上させ、そして得られた知見を社会に役立てるために活用する革新的な手段を生み出すこと」です。IPRCの研究費は主に、ハワイ大学を通してハワイ州から、また主要支援機関である海洋研究開発機構、NASA、NOAAから支援されています。内外のその他の政府機関からも支援を受けており、現在およそ七百万ドルの年間予算により運営しています。

アジア・太平洋地域は世界人口の半分以上が居住する地域で、気候系の変動はこれらの人々すべてに影響を及ぼします。そのような気候変動には純粋な自然現象であるものも人類活動が関係したものもありますが、IPRCでは、それらを記述し原因を探るため、モデルによる研究や診断的研究を実施しています。このような基礎研究を進展させることでアジア・太平洋地域の環境予測の改善に大きく貢献しています。現在IPRCでは、エルニーニョ・南方振動、モンスーン循環、インド洋の経年変動、熱帯大気の季節内振動、そして熱帯低気圧といった、熱帯起源の現象に注目して研究を行っています。その他の重要な課題として、北太平洋亜熱帯域における十年規模変動の性質、西部北太平洋の強い海流である黒潮・親潮の力学、気候系での縁辺海の役割に関する研究を行っています。さらに、過去の気候のモデル研究やモデルによる将来予測の評価により、気候変化に関する様々な課題に取り組んでいます。

FOREWORD

This report summarizes the activities of the International Pacific Research Center (IPRC) for the period April 1, 2009–March 31, 2010. The mission of the IPRC is to conduct research in order to enhance understanding of the nature and mechanisms of climate variability and change, and to improve the tools for modeling and forecasting the climate system. The focus of work is on the Asia-Pacific region.

The IPRC has a scientific staff of over 50, consisting of faculty, researchers, postdoctoral fellows, and extended-term scientific visitors. IPRC faculty also supervise several graduate students in the Meteorology and Oceanography departments of the University of Hawai‘i. The Asia-Pacific Data-Research Center (APDRC) at the IPRC operates a web-based server system that makes data resources readily accessible to IPRC researchers, the international science community and the wider public.

IPRC activities continue to grow in concert with an increasing public interest in understanding the climate system and its impacts on society. This growth is seen in the total funding awarded to IPRC scientists in support of their research and in the growing number of IPRC scientific staff, postdoctoral fellows and visitors. The increase in staff over the past decade has been accommodated by reorganization of existing office space, but this last year the center expanded to occupy the entire School of Ocean and Earth Science and Technology fourth floor space in the Pacific Ocean Science and Technology building.

Another noteworthy milestone this year was the installation of a new 488-core computing cluster at IPRC. This new cluster, named *Kuroshio*, has upgraded IPRC's computing capability by nearly an order of magnitude.

Our staff at the IPRC are grateful to our principal supporting agencies, the Japan Agency for Marine-Earth Science and Technology (JAMSTEC), NASA and NOAA, and to the State of Hawai'i for its sponsorship of IPRC through the University of Hawai‘i. We look forward to many more years of fruitful international collaboration as we address critically important challenges in climate science.

Kevin P. Hamilton
Director

はじめに

本冊子では、国際太平洋研究センター（IPRC）における2009年4月1日から2010年3月31日までの活動概要を報告します。IPRCは、気候変動の性質とそのメカニズムに対する理解を深め、気候系のモデル化と予測に必要な道具を改良するための研究を行っています。対象は、主にアジア・太平洋地域です。

現在、総勢50名を超える、教授陣、研究員、博士研究員、長期訪問研究員を擁し、さらに教授陣は、ハワイ大学気象学科や海洋学科の大学院生を指導しています。また、IPRCのアジア太平洋データ研究センター（APDRC）では、ウェブ上にデータサーバを運用しており、IPRC内だけではなく世界中の気候研究者に向けて、さらには広く一般の方が容易に使える形で、データを提供しています。

IPRCの活動は、気候系そのものや気候が社会に及ぼす影響に一般の方々の関心が高まるのに応じて、日々発展し続けており、研究助成金の総額、そして研究員、博士研究員及び訪問者の数も増加しています。過去10年間は、既存の居室スペースを再配分することにより人員増加に対応してきましたが、昨年遂に拡張を行い、海洋地球科学技術学部（SOEST）がPOSTビル4階に保有するスペースを全てIPRCが使用することになりました。

その他の目立った出来事として、488コアの計算機クラスターを設置しました。「黒潮」と名付けられたこの新しい計算機の導入により、IPRCの計算能力は飛躍的に向上しました。

IPRCの主要支援機関である海洋研究開発機構（JAMSTEC）、NASA、NOAAに対して、またハワイ大学を通し資金を提供してくださるハワイ州に対して、IPRC一同、深く感謝いたします。気候科学における非常に重要な課題に取り組むことにより、今後も末永く実り多き国際的な研究協力が続くことを期待しています。

所長　ケビン P. ハミルトン

Chapter 1: LARGE-SCALE INDO-PACIFIC CLIMATE

Geographical patterns of forced climate change

A major new initiative was begun in the study of regional patterns of climate change, including modes of variability, in response to global warming. Spatial variations in sea surface temperature (SST) and rainfall changes over the tropics were studied in ensemble simulations of the first half of the 21st century under the A1B greenhouse gas (GHG) emission scenario using the coupled ocean–atmosphere general circulation models of the Geophysical Fluid Dynamics Laboratory (GFDL) and the National Center for Atmospheric Research (NCAR). Although the radiative forcing from long-lived GHG emission is nearly uniform in space, pronounced patterns emerge in both SST and precipitation (Figure 1.1). Regional differences in SST warming can be as large as the tropical-mean warming. The tropical Pacific warms, with a temperature maximum along the equator and a minimum in the southeast subtropics. Warming in the northern subtropics tends to be larger than in the southern subtropics. Over the equatorial Indian Ocean, surface wind anomalies are easterly, the thermocline shoals, and warming is less prominent in the east, indicative of Bjerknes feedback. In the midlatitudes, ocean circulation changes generate narrow banded structures in SST warming. The warming is negatively correlated with wind speed change over the tropics and positively correlated with ocean heat transport change in the northern extratropics.

Tropical precipitation changes are positively correlated with geographical deviations in SST warming from the tropical mean. In particular, the equatorial maximum in SST warming over the Pacific anchors a band of pronounced rainfall increase. A comparison of these patterns with the simulated atmospheric response to spatially uniform SST increase shows the impact of the SST warming patterns on rainfall change, an effect overlooked in current discussions of the precipitation response to global warming. Implications for the global and regional responses of tropical cyclones are discussed. [S.-P. Xie (IPRC), C. Deser (NCAR), G.A. Vecchi (GFDL), J. Ma (IPRC), H. Teng

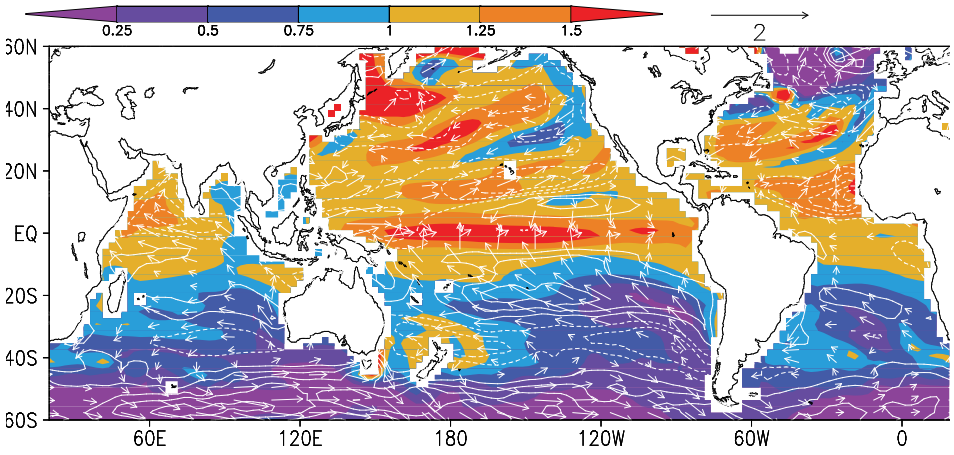

Figure 1.1. SST warming (°C) from 2000 to 2050 under the A1B emission scenario, along with changes in wind velocity (arrows in m/s) and scalar wind speed (white contours). All values are annually averaged. The Pacific warming features an equatorial peak. Warming is greater in the Northern than the Southern Hemisphere, consistent with hemispheric contrast in wind speed.

(NCAR), and A.T. Wittenberg (GFDL), 2010: Global warming pattern formation: Sea surface temperature and rainfall. *J. Climate*, **23**, 966–986. IPRC-632]

Variability and change in the sea surface temperature threshold for convection over tropical oceans

Numerous studies have discussed the existence of a tropical ocean sea surface temperature (SST) threshold in the vicinity of 26°C –28°C, below which atmospheric deep convection is rarely observed and above which deep convection is common. In this study, the SST threshold for convection is shown not to be a static quantity but exhibits substantial variability on interannual and longer timescales. The variability of both the annual tropical mean SST and SST threshold for convection were examined over the past 30 years in the Extended Reconstruction Sea Surface Temperature (ERSST) and the Climate Prediction Center Merged Analysis of Precipitation (CMAP) datasets (Figure 1.2a). The SST threshold was calculated based on the assumption that precipitation rate can be modeled as a linear function of SST above a threshold. Figure 1.2a demonstrates that the SST threshold varies in tandem with the tropical mean SST, with a correlation coefficient of 0.88 between them. Both the tropical mean SST and SST convection threshold have undergone a statistically significant increase over the past 30 years.

It was hypothesized that the tight coupling between tropical mean SST and SST threshold relates to the strong relationship between tropical mean SST and upper tropospheric temperature through moist adiabatic lapse rate (MALR) adjustment. To test this idea, and to examine SST threshold variability in global climate models, the relationship between the SST threshold and the tropical mean 300 hPa temperature was examined in 10 IPCC AR4 models under the SRES A1B emissions scenario. Figure 1.2b shows that, consistent with the hypothesis, the SST threshold in the models is tightly coupled with the tropical upper tropospheric mean temperature. This result suggests that as the upper troposphere warms in response to MALR adjustment, the SST required to generate deep convection must also increase; thus the SST threshold for convection increases with both the tropical mean SST and upper tropospheric temperature. [N. Johnson and S.-P. Xie (IPRC)]

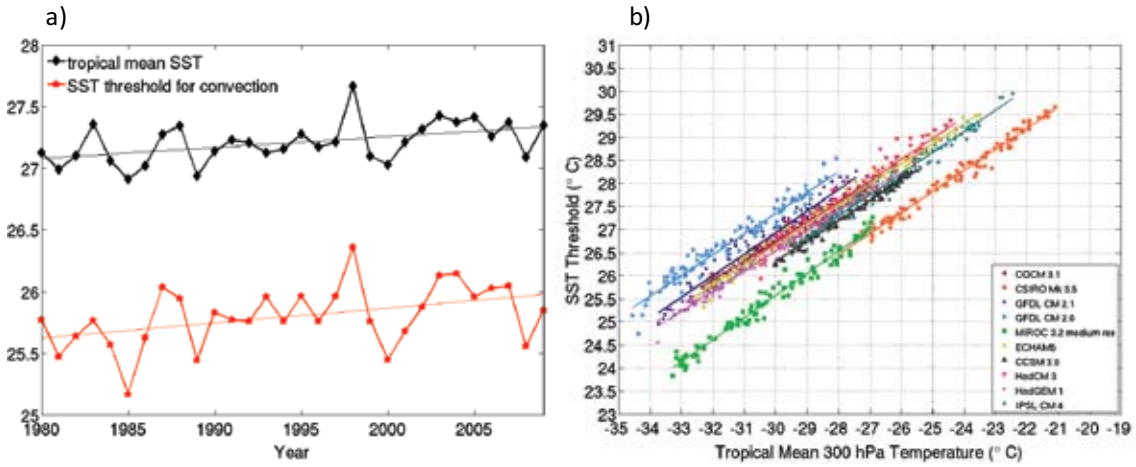

Figure 1.2. (a) Observed time series and linear trend lines from 1980 to 2009 for the annual tropical (20°S–20°N) mean SST (black line) and SST threshold for convection (red line). Both trends are statistically significant above the 95% confidence level based on a two-sided t-test. (b) Scatter plot of SST threshold versus tropical mean 300 hPa temperature with regression lines for the A1B simulations of each of 10 IPCC models.

Climate effects of the Indian Ocean

Work by IPRC scientists and their colleagues has suggested that ocean–atmosphere interactions in the tropical Indian Ocean (TIO) act to prolong the basin-wide warming in response to El Niño through the following summer, and force an anticyclonic circulation with suppressed rainfall over the subtropical western North Pacific (WNP). The subtropical anomalies are thought to force the Pacific–Japan pattern, extending the TIO influences to East Asia. In this study, this TIO teleconnection was tested in seasonal forecast experiments using SINTEX-F (Scale Interaction Experiment Global Ocean-Atmosphere Coupled GCM) modified and improved at JAMSTEC. Results from the control (CTL) run, in which the atmosphere and global ocean were fully interactive, were compared with a run in which the monthly sea surface temperature (SST) climatology was prescribed for the TIO between 25°S and 25°N (NoTIO run).

June through August composites from observations and 3-month lead in CTL minus NoTIO show robust atmospheric anomalies over the WNP (Figure 1.3) during summers following El Niño. Atmospheric anomalies in NoTIO were smaller by 50% over the Northwest Pacific and East Asia during summers following El Niño episodes (1983, 1987, 1992, 1998 and 2003). A wedge-like warm Kelvin wave propagates into the equatorial western Pacific (not shown), which, accompanied by low surface pressure centered on the equator, drives northwesterly winds on its northern flank due to friction. The resulting surface divergence suppresses atmospheric convection (shaded) in the subtropical WNP, and forms an anomalous anticyclonic circulation (vectors). The prediction skill (Anomaly Correlation Coefficient; ACC) scores are significantly higher and the predicted atmospheric variance is greater in the CTL than in the NoTIO run, confirming the TIO effect on WNP seasonal variations. Thus, using the fully coupled SINTEX F extends the useful (ACC>0.5) prediction of WNP anomalies by 1 to 2 months compared to results obtained with the NoTIO version. [J. S. Chowdary, S.-P. Xie (IPRC); J.-J. Luo (JAMSTEC); J. Hafner (IPRC); S. Behera, Y. Masumoto (JAMSTEC); and T. Yamagata (U. Tokyo): Predictability of Northwest Pacific climate during summer and the role of the tropical Indian Ocean. *Clim. Dyn.,* in press, IPRC-640]

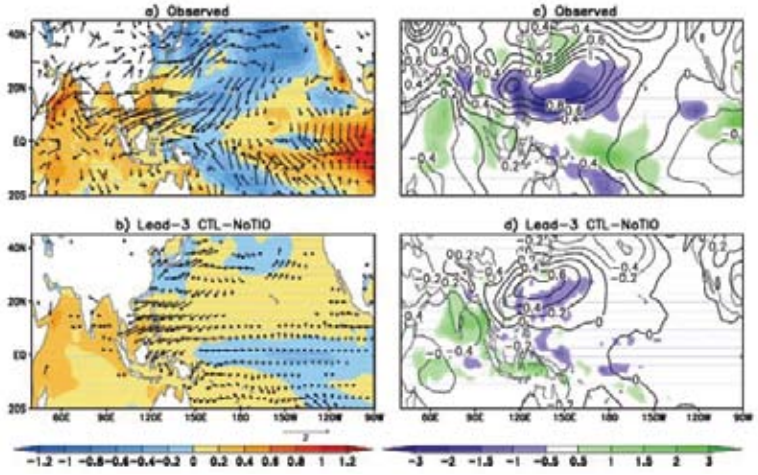

Figure 1.3. Composites of (a) observed SSTs (shaded;°C) and surface wind anomalies (vectors; above 0.3 m/s are displayed) during the summer following El Niño episodes (JJA(1)); (b) same as in (a) except for CTL minus NoTIO run for 3-month-lead prediction experiment; (c) and (d) same as in (a) and (b), but for precipitation (shaded; above 0.5 mm/day and below –0.5 mm/day are displayed) and sea level pressure anomalies (contours; hPa).

Decadal modulation of interannual Indo-Pacific climate variability

El Niño's influence on subtropical western North Pacific (WNP) climate appears to have strengthened after the widely recognized Pacific climate regime shift in the 1970s. This is manifested in well-organized atmospheric anomalies of suppressed convection and a surface anticyclone during the summer of the year that El Niño decays [June–August 1 (JJA1)], a season when equatorial Pacific sea surface temperature (SST) anomalies have dissipated. In situ observations and ocean–atmospheric reanalyses were used to investigate the mechanisms for this interdecadal change. During JJA1, the influence of the El Niño/Southern Oscillation (ENSO) on the WNP is indirect and mediated by SST conditions over the tropical Indian Ocean (TIO). Results of this study show that the interdecadal change in this influence is due to changes in the TIO response to ENSO (Figure 1.4).

Before the regime shift, ENSO variance is significantly smaller and El Niño decays earlier than after the regime shift. The southern TIO Rossby waves are weaker, as are the anti-symmetric wind pattern and North Indian Ocean warming during JJA1. Without TIO warming, atmospheric anomalies over the WNP fail to develop during JJA1 prior to the mid-1970s. An atmospheric GCM hindcast forced with observed SST since 1950 reproduces the decadal strengthening of the teleconnection between ENSO and the Indo-western Pacific. [Xie, S.-P. (IPRC), Y. Du (South China Sea Institute of Oceanology, CAS), G. Huang (Institute of Atmospheric Physics, CAS), X.-T. Zheng (Ocean University of China), H. Tokinaga (IPRC), K. Hu (Institute of Atmospheric Physics, CAS), and Q. Liu (Ocean University of China), 2010: Decadal shift in El Niño influences on Indo-western Pacific and East Asian climate in the 1970s. *J. Climate*, in press; and G. Huang, K. Hu (Institute of Atmospheric Physics, CAS); and S.-P. Xie (IPRC): Strengthening of the tropical Indian Ocean–Northwest Pacific teleconnection since the mid-1970s: An atmospheric GCM study, submitted]

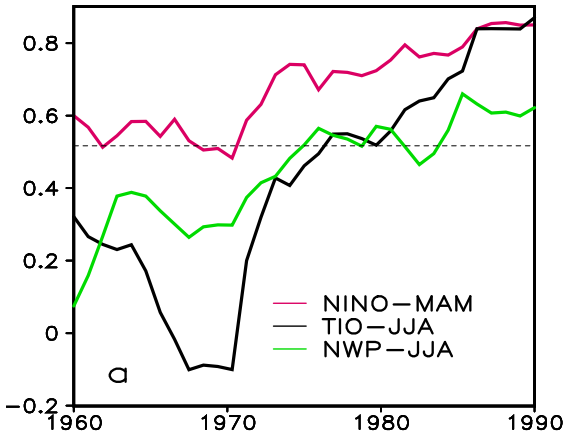

Figure 1.4. The 21-year running correlation between ENSO and climate indices in the El Niño-decay year as a function of time: Niño3.4 SST during March–May, tropical Indian Ocean SST and sea level pressure in the subtropical western North Pacific during June–August.

Season-dependent Indian Ocean SST forcing during an El Niño year

To study the dominant modes of the East Asian monsoon variability, a season-reliant Empirical Orthogonal Function (S-EOF) analysis was applied to seasonal-mean rainfall over East Asia for the period of 1979–2004. The diagnosis of upper-level velocity potential and mid-level vertical motion fields revealed a season-dependent tropical Indian Ocean (TIO) sea surface temperature (SST) forcing. Although the IO basin warming sets up in boreal winter during the El Niño mature phase, its impact on the Western North Pacific (WNP) anomalous anticyclone is limited to that season. Only during the El Niño decaying

summer does the Indian Ocean basin-wide warming impact the WNP anticyclone through Kelvin wave induced anticyclonic shear vorticity and associated boundary layer moisture divergence. [B. Wu, T. Zhou (Institute of Atmospheric Physics, CAS) and T. Li (IPRC), 2009a: Seasonally evolving dominant interannual variability modes of East Asian Climate. *J. Climate*, **22** (11), 2992–3005, IPRC-601]

Local and remote effects on the Western North Pacific anticyclone

The role of sea surface temperature (SST) anomalies in the WNP and in the tropical Indian Ocean (TIO) in maintaining the anomalous WNP anticyclone during El Niño decaying summer was compared in a suite of atmospheric general circulation model experiments. The results indicate that the WNP anticyclone is maintained by the combined effect of the local forcing of a negative SST anomaly in the WNP and the remote forcing of a basin-wide warming in the TIO. The effect of the local SST anomaly forcing is greater in early summer; the remote TIO forcing effect is stronger in late summer (see atmospheric general circulation simulation results in Figure 1.5). [B. Wu (Institute of Atmospheric Physics, CAS), T. Li (IPRC), and T. Zhou (Institute of Atmospheric Physics, CAS), 2010: Relative contributions of the Indian Ocean and local SST anomalies to the maintenance of the western North Pacific anomalous anticyclone during El Niño decaying summer. *J. Climate*, in press, IPRC-684].

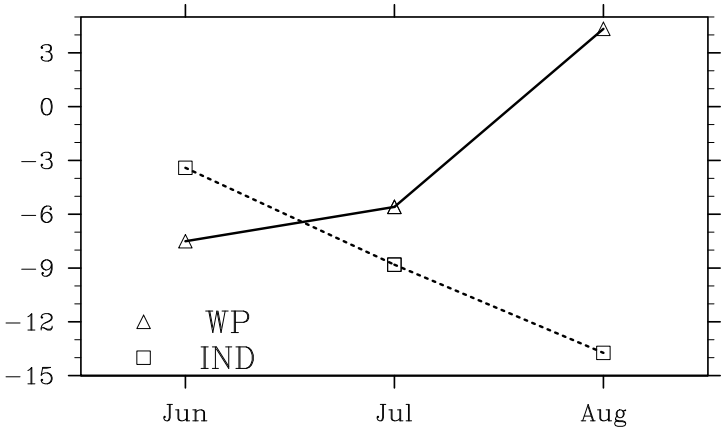

Figure 1.5. Atmospheric GCM simulations of the evolution of area-averaged vorticity anomalies (units: $10^{-6}m^2/s$) over the region of 10–35°N, 120–160°E during the El Niño decaying summer. "WP" is a run with the observed SST anomaly forcing over 120–180°E, 5–30°N. "IND" is a run with the observed SST anomaly forcing north of 30°S over tropical Indian Ocean.

Western North Pacific circulation patterns in El Niño and La Niña winters

The asymmetry in the western North Pacific (WNP) circulation patterns between mature El Niño and La Niña winters was examined. The center of the WNP anomalous cyclone (WNPAC) during La Niña lies further west than the WNPAC during El Niño (Figure 1.6). Two factors, the longitudinal shifting of El Niño and La Niña anomalous heating and local WNP SST anomaly amplitude, may contribute to this asymmetric response. Precursors of El Niño and La Niña onset were also investigated. The ENSO onset is governed by two different types of positive feedback processes over the western Pacific. The first type involves the interaction between interannual and higher frequency winds. The second type involves the positive air–sea feedback among the westerly, SST and zonal-mean thermocline anomalies. [B. Wu (Institute of Atmospheric Physics, CAS), T. Li (IPRC), and T. Zhou (Institute of Atmospheric Physics, CAS), 2010b: Asymmetry of atmospheric circulation anomalies over the western North Pacific between El Niño and La Niña. *J. Climate*, in press, IPRC-683. And J. S. Kug (Korea Ocean Research and Development Institute); K.P. Sooraj, T. Li (IPRC); F.-F. Jin (U Hawaii);

and I.-S. Kang (Seoul National University), 2010: Precursors of the El Niño/La Niña onset and their inter-relationship. *J.Geophy.Res*., in press]

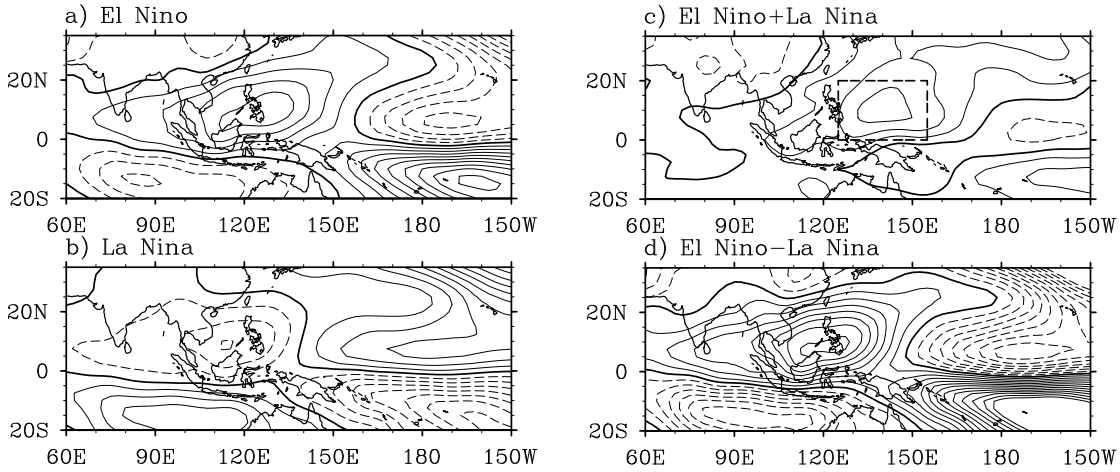

Figure 1.6. Composite of Deccember–February mean 850hPa streamfunction anomalies for (a) nine El Niño events and (b) nine La Niña events in the past 50 years (Units $10^6 m^2/s$). (c) Asymmetric component estimated from the sum of (a) and (b). (d) Symmetric component estimated from the difference of (a) and (b). The solid lines denote positive values and the dashed lined denote negative ones. The contour interval is 0.5.

Meiyu-Baiu dynamics

The rainy Meiyu-Baiu season is associated with a zonally elongated rainband stretching over central China and Japan and typically lasts from June to mid-July. Work featured in last year's report showed that the westerly jet plays an important role in the formation of the Meiyu-Baiu rainband. To follow up on this study, the warm advection mechanism thought to be responsible for the rainband was evaluated by studying the interannual variability of the Meiyu-Baiu rainfall. Singular value decomposition (SVD) analysis, applied to precipitation and 500 hPa horizontal advection of temperature, showed that anomalies in mid-tropospheric temperature advection (Figure 1.7b) are indeed related to precipitation anomalies in the vicinity of the Meiyu-Baiu rainband (Figure 1.7a), suggesting that the former induces the latter through adiabatically driven anomalous vertical motion (Figure 1.7c–d). In addition, teleconnection patterns such as the Pacific–Japan pattern can induce the precipitation anomalies downstream of the westerly jet by anomalous temperature advection. [Y. Kosaka and S.-P. Xie (IPRC)]

Air-sea interactions over ocean fronts

Earlier studies of the effects of the Gulf Stream on the overlying atmosphere have been followed up with additional modeling and observational studies. The modeling study showed that the Gulf Stream has a strong effect on convective rainfall but not very much on stratiform rain. The observational results show a pronounced seasonal cycle in the rainbelt that hugs the Gulf Stream, with the associated latent heating trapped in the lower troposphere in winter but extending high into the upper troposphere during summer (Figure 1.8). [S. Minobe (Hokkaido University); S. M. Miyashita, A. Kuwano-Yoshida (JAMSTEC); H. Tokinaga, S.-P. Xie (IPRC): Atmospheric response to the Gulf Stream: Seasonal variations, *J. Climate*, in press, IPRC-671. And A. Kuwano-Yoshida (JAMSTEC), S. Minobe (Hokkaido University); S.-P. Xie (IPRC): Precipitation response to the Gulf Stream in an atmospheric GCM, submitted]

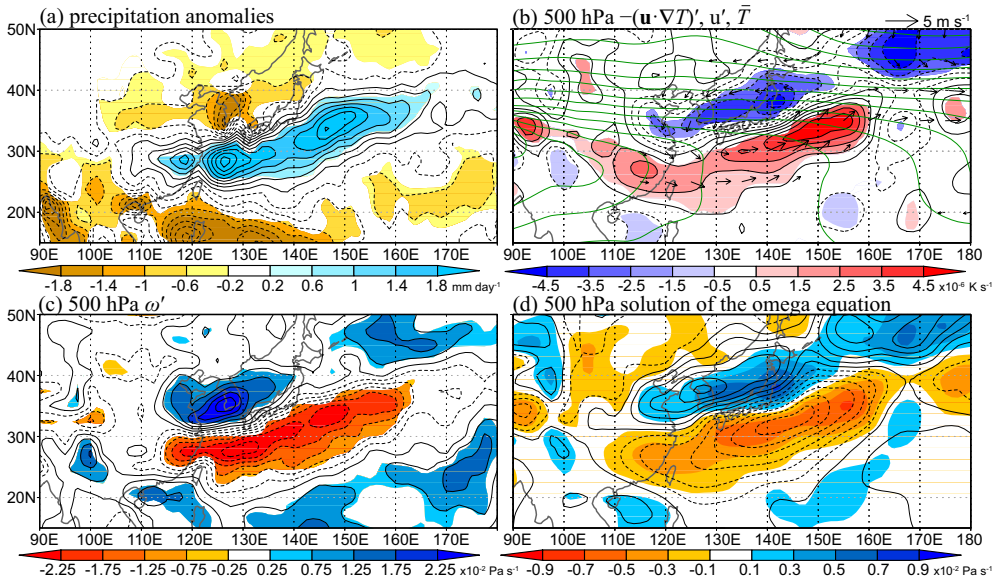

Figure 1.7. Regressed anomalies based on SVD1 obtained for the interannual covariance between precipitation and 500 hPa horizontal temperature advection over 20°–45°N, 110°–170°E during the Meiyu-Baiu season (June 15–July 14). Black contours indicate anomalies in (a) precipitation, (b) 500 hPa horizontal advection of temperature, and (c) 500 hPa vertical p-velocity, with shading, if significant, at the 90% confidence level. Arrows and green contours in (b) indicate regressed horizontal wind anomalies and climatological-mean temperature (with 1 K interval), respectively, at the 500 hPa level. (d) 500 hPa vertical p-velocity anomalies diagnosed with the linearized omega equation with regressed anomalies for SVD1 but without diabatic heating anomalies. The diagnosis is conducted with both the temperature and vorticity advection anomalies (contours) and with only the temperature advection anomaly (shading).

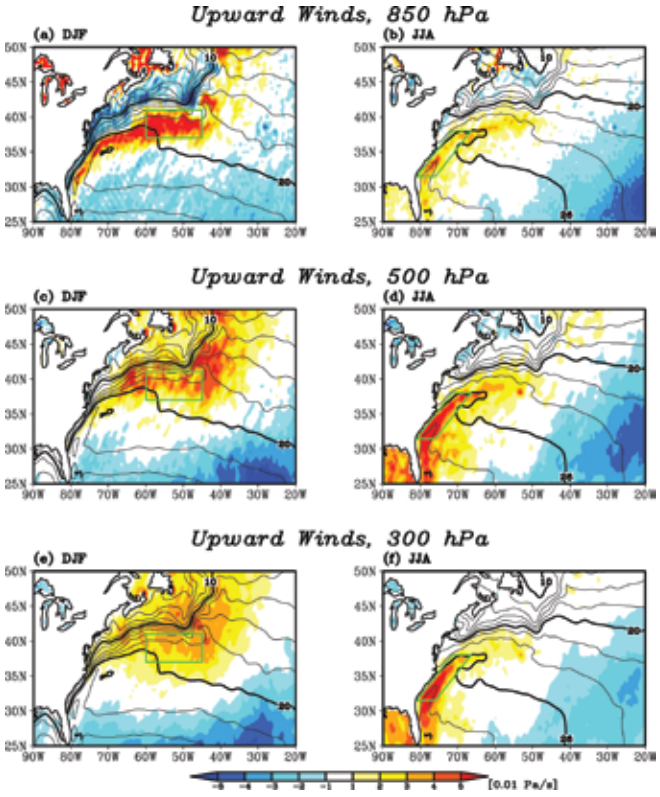

Figure 1.8. Upward wind velocities at 850 hPa (top), 500 hPa (middle) and 300 hPa (bottom) (10^{-2} Pa/s, positive upward). Rectangles indicate the analysis regions for Gulf Stream proper (left panels) and Florida Current (right panels).

The Kuroshio south of Japan shifts between along- and off-shore paths. Both paths are quasi-steady and typically last several years. In the summer of 2004, the Kuroshio took a large meander path south of Japan for the first time since 1991, and this large meander persisted until the next summer. Satellite observations and numerical model simulations were used to study the effect of this large meander event on the atmosphere. The large meander left a cool water pool between the Kuroshio and the Japan Coast that was 2°–3°C colder than the surroundings during winter and spring. Over the cool water pool, wind speed, cloud water, and precipitation were reduced (Figure 1.9). [H. Xu (Nanjing University of Information Science and Technology); H. Tokinaga, and S.-P. Xie (IPRC): Atmospheric effects of the Kuroshio large meander during 2004–05, *J. Climate*, in press]

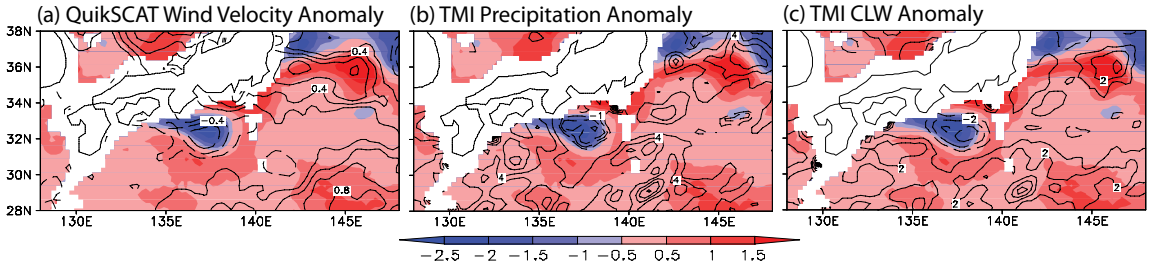

Figure 1.9. Seasonal (December–February in 2004/2005) mean anomalies of (a) QuikSCAT wind velocity (contours at 0.2 m/s intervals), (b) TMI precipitation (contours at 2 (0.5) mm/day intervals for solid (dashed) contours), and (c) TMI column integrated cloud liquid water content (contours at 10^{-2} mm intervals). The December–February mean TMI SST anomalies are plotted as shading.

The influence on the overlying atmosphere of the oceanic fronts in the Kuroshio and Oyashio Extension (KOE) region was investigated by comparing two atmospheric regional model hindcast experiments for the 2003/04 cold season: one with the observed fine-scale frontal structures in sea surface temperature (SST) prescribed at the model lower boundary (CNTL experiment) and the other with an artificially smoothed SST distribution (SMTH experiment). The comparison reveals the local sharp meridional gradient of heat and moisture turbulent fluxes and surface air temperature (SAT) across the oceanic frontal zone, which favors storm-track development both in winter and spring (Figure 1.10). The

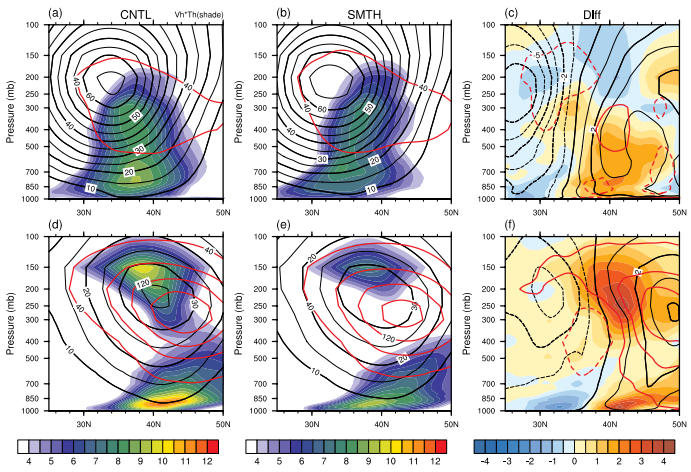

Figure 1.10. Meridional sections of poleward eddy heat flux (K m/s; color shading as indicated in the color bar legends) and the variance of the meridional wind velocity (red contours with intervals of 40 m^2/s^2) based on zonal averaging over the KOE region (145°E–180°) simulated for winter in the (a) CNTL and (b) SMTH experiments, and (c) their difference [i.e., (a) minus (b)]. The corresponding distributions of the mean westerly wind speed are superposed with black contours (every 5 m/s for the CNTL and SMTH experiments, and every 1 m/s for their difference; every other contour is thickened, and negative contours are dashed). (d) to (f) Same as in (a) to (c), respectively, but for spring.

influence of storm-track activity on the time-mean distribution of heat and moisture from the ocean was found to have a distinct seasonal dependency. [B. Taguchi, H. Nakamura, M. Nonaka (JAMSTEC); and S.-P. Xie (IPRC), 2009: Influences of the Kuroshio/ Oyashio Extensions on air-sea heat exchanges and storm-track activity as revealed in regional atmospheric model simulations for the 2003/04 cold season. *J. Climate*, **22** (24), 6536–6560, IPRC-633]

Low-frequency variations of the Kuroshio Extension

The connections between low-frequency variations in the intensity of the recirculation gyres of the Kuroshio Extension (KE) and decadal variations of the KE jet induced by the basin-wide wind change were investigated. The results show that these quantities are highly correlated and, specifically, that the change in the northern recirculation gyre is explained by the turbulent Sverdrup balance suggestive of eddy feedback (Figure 1.11). [B. Taguchi (JAMSTEC); B. Qiu (U. Hawaii); M. Nonaka, H. Sasaki (JAMSTEC); N. Schneider, and S.-P. Xie (IPRC): Decadal variability of the Kuroshio Extension: Mesoscale eddies and recirculations. submitted]

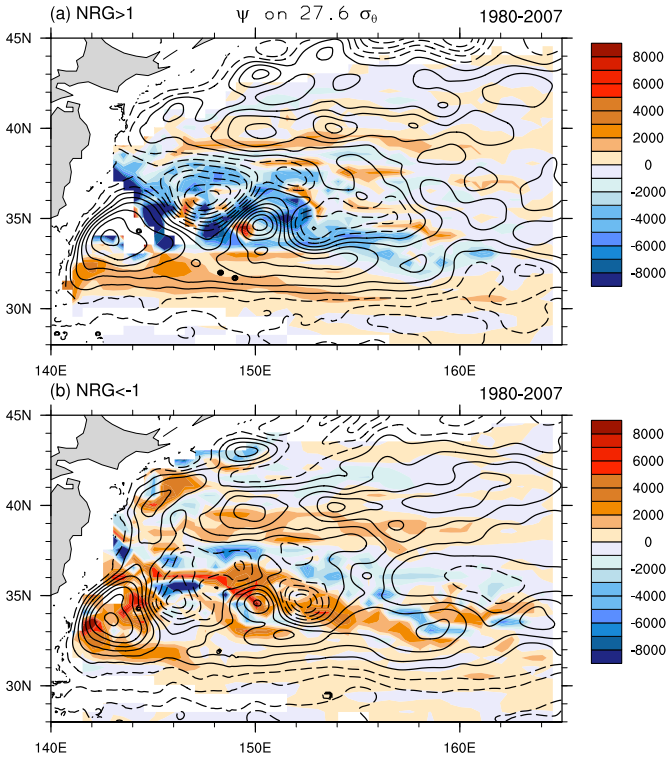

Figure 1.11. Composite maps of the mid-depth stream intensity on the 27.6 σ_θ isopycnal for the Kuroshio Extension Northern Recirculation Gyre (NRG) from the OFES hindcast (contour interval is 1,000 m^2/s) and from the estimated turbulent Sverdrup balance of convergent eddy potential vorticity flux (color shade), for the period 1980–2007. A strong NRG composite is computed from periods in which the NRG intensity is on average greater than one standard deviation; the weak NRG composite is computed from periods in which the NRG intensity is less than minus one standard deviation.

Simulating the Hawaiian Lee Countercurrent

OFES integrations were analyzed to evaluate the simulation of the Hawaiian Lee Countercurrent. The results show that OFES simulates the seasonal cycle of the Hawaiian Lee Countercurrent well (Figure 1.12) and that this countercurrent can be understood as a response to the seasonal changes in the strength of the southeast trade winds as they impinge on mountains of Hawaii. [H. Sasaki (JAMSTEC); S.-P. Xie (IPRC); B. Taguchi, M. Nonaka, and Y. Masumoto (JAMSTEC): Seasonal variations of the Hawaiian Lee Countercurrent induced by the meridional migration of the trade winds. *Ocean Dynamics*, in press, IPRC-639]

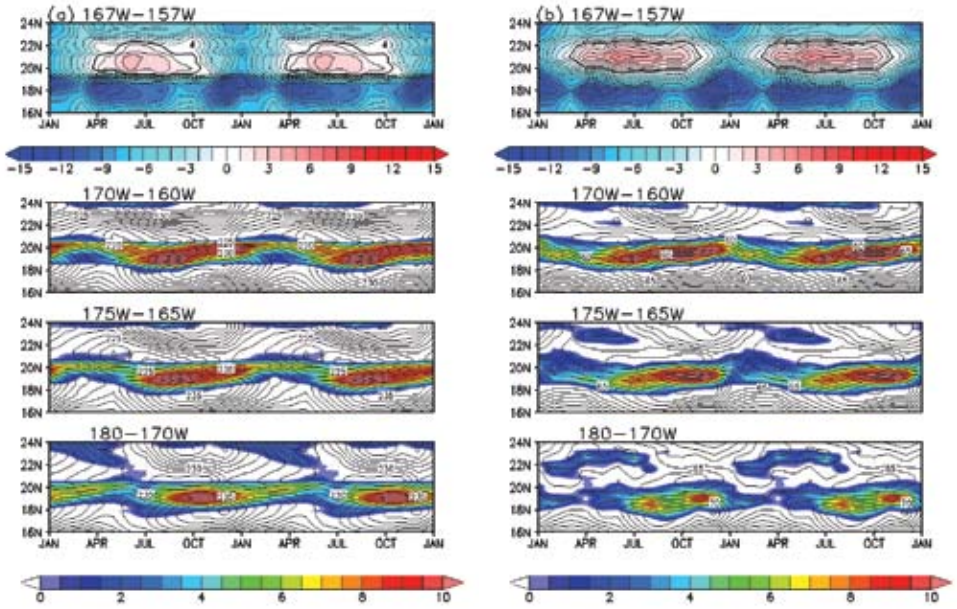

Figure 1.12. Left panels: Seasonal variations of monthly climatology of (top) QuikSCAT surface wind stress curl (10^{-8} N/m^3) with the 0.5° horizontal resolution averaged between 167°W and 157°W, and of (lower three panels) sea surface height (contour, cm) and the geostrophic zonal current (color, cm/s) based on AVISO satellite observation averaged (top-most of the three panels) between 170°W and 160°W, (middle) between 175W° and 165°W, and (bottom) between 180° and 170°W. Right panels: Same as the left panels but wind stress curl is based on QuikSCAT satellite observation with the 1° horizontal resolution and geostrophic zonal current and sea surface height are based on the OFES QS run.

Response of Indian Ocean Dipole to increasing greenhouse gases

The response of the Indian Ocean dipole (IOD) to increasing greenhouse gas concentrations was investigated by comparing coupled model present-day simulations with those that include a projected increase in greenhouse gas concentrations. The increasing greenhouse gas simulation shows the Walker circulation weakening, which leads to easterly wind anomalies and thermocline shoaling in the equatorial Indian Ocean. Although under greenhouse forcing, the thermocline feedback intensifies, the IOD variance surprisingly does not increase (Figure 1.13). The zonal wind anomalies associated with the IOD weaken

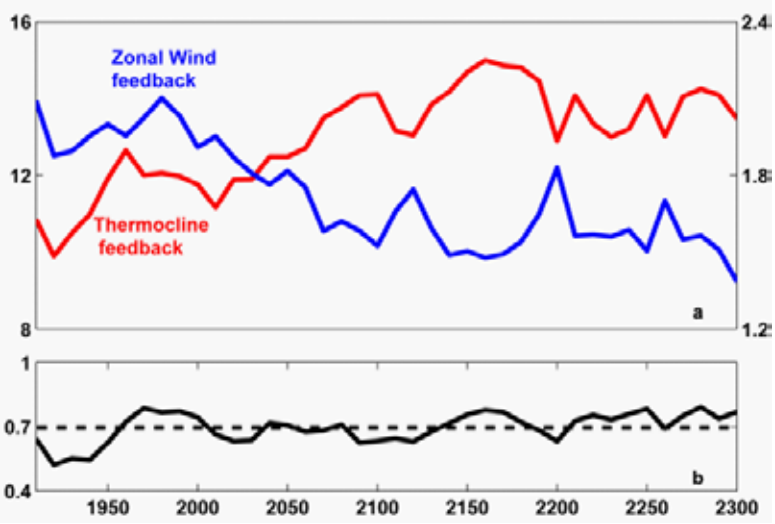

Figure 1.13. Fifty-year running time series for August through November in the global warming run: (a) thermocline (in red, °C/m) and zonal wind (in blue, m/s/K) feedback parameters in the eastern equatorial Indian Ocean (EEIO); (b) standard deviation (°C) of interannual SST variability in EEIO.

due to increased static stability of the troposphere with global warming. The fact that IOD variance in the model does not increase suggests that the apparent intensification of IOD activity during recent decades is likely to be either a part of natural, chaotic variation of the ocean–atmosphere system or a response to climate forcings other than those associated with increasing greenhouse gas concentrations. [X.-T. Zheng (South China Sea Institute of Oceanology, CAS), S.-P. Xie (IPRC), G. A. Vecchi (GFDL), Q. Liu (South China Sea Institute of Oceanology, CAS), and J. Hafner (IPRC), 2010: Indian Ocean dipole response to global warming: Analysis of ocean-atmospheric feedbacks in a coupled model. *J. Climate*, **23** (5), 1240–1253. IPRC-638]

Wind effects on past and future sea-level rise

Global sea-level rise due to the thermal expansion of the warming oceans and freshwater input from melting glaciers and ice-sheets is threatening to inundate low-lying islands and coastlines worldwide. In recent years, global mean sea level has risen 3.1 +/-0.7 mm/year with an accelerating tendency. However, the magnitude of recent decadal sea-level trends has a large geographic dependence, attaining values of up to 10 mm/year in some areas of the western tropical Pacific. Identifying the causes of recent regional sea-level trends and understanding the patterns of future projected sea-level change is of crucial importance. Results from a simplified dynamical ocean model forced with historical observed winds suggest that the regional features of recent decadal and multidecadal sea-level trends in the tropical Indo-Pacific are attributable to changes in the prevailing wind-regimes. Furthermore it was demonstrated that within an ensemble of ten state-of-the art coupled general circulation models, forced by increasing atmospheric CO_2 concentrations over the next century, wind-induced redistributions of upper-ocean water play a key role in establishing the spatial characteristics of projected regional sea-level rise (Figure 1.14). Wind-related changes in near-surface mass and heat convergence near the

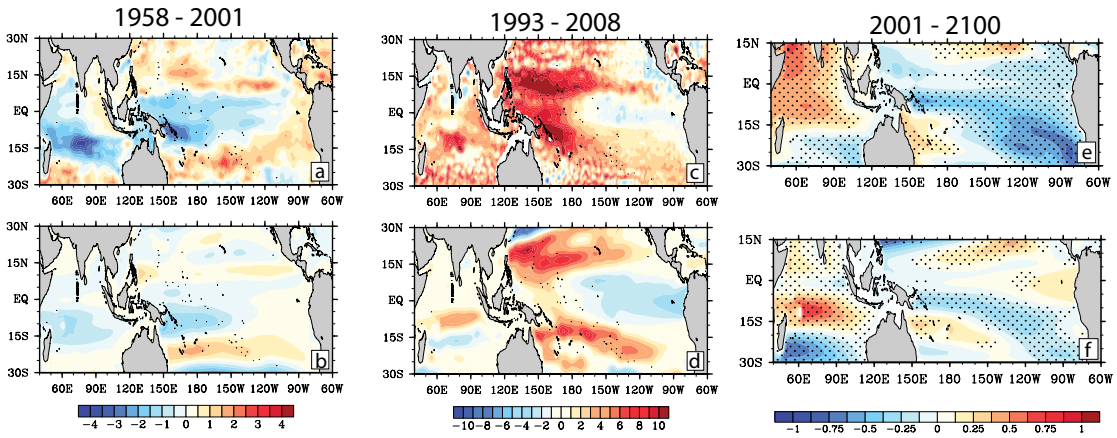

Figure 1.14. Linear sea-surface height trends in mm/year: for 1958–2001 (a) in ocean re-analysis data and (b) as simulated by the shallow water model forced by ERA40 winds; for 1993–2008 (c) in satellite altimeter-data and (d) as simulated by the shallow water model forced by ECMWF operational winds; for 2001–2100 (e) as derived from a 14-member ensemble of coupled GCM simulations forced with greenhouse gas concentrations following the A1B emission scenario (where the Indo-Pacific spatial average between 30°S–30°N has been subtracted and stippled areas indicate high agreement among models); and (f) as simulated by the shallow water model forced by wind from the A1B multi-model coupled GCM ensemble (stippled areas indicate high agreement among models).

Solomon Islands, Tuvalu, Kiribati, the Cook Islands and French Polynesia oppose, but cannot offset the regional signal of global mean sea-level rise. [Timmermann, A., S. McGregor (IPRC); and F.-F. Jin (U Hawaii), 2010: Wind effects on past and future regional sea-level trends in the southern Indo-Pacific, *J. Climate*, in press]

Semi-annual cycle in the winds and currents of the equatorial Indian Ocean

The semi-annual development of a westward equatorial ocean jet in the Indian Ocean is well known. It is thought to be a response to wind variations of the same frequency. In this study the origin of the pronounced semi-annual cycle in equatorial zonal wind was investigated. It was found that the semi-annual cycle is driven by the equatorward advection of easterly momentum, which peaks twice a year as the southwest and northeast monsoons blow across the equator. This semi-annual zonal wind peaks in the middle of the equatorial Indian Ocean basin, a structure that is optimal for driving the semi-annual ocean jet (Figure 1.15). [T. Ogata and S.-P. Xie (IPRC)]

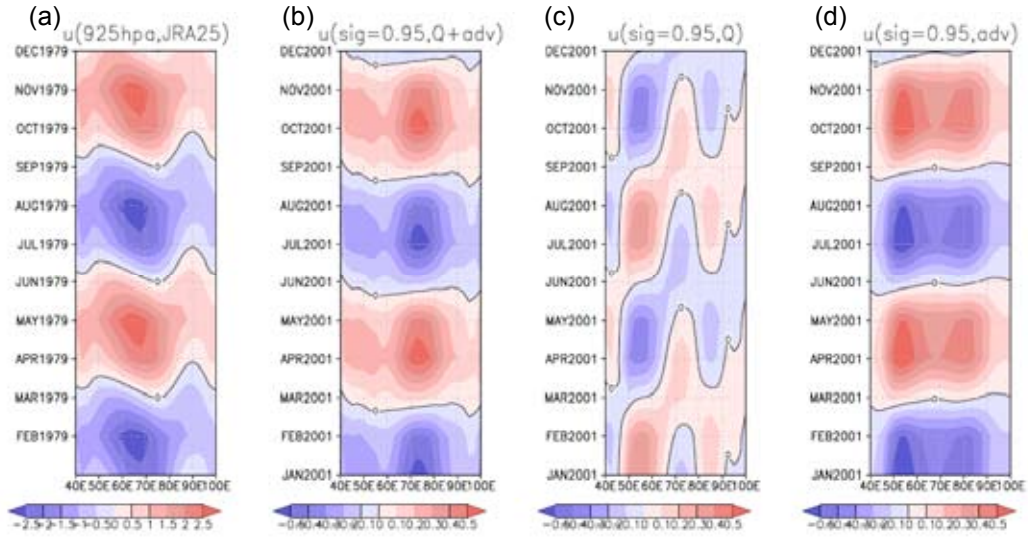

Figure 1.15. Longitude-time sections of the zonal surface wind on the equator: (a) JRA2 reanalysis at 925 hPa, (b) model response to the heating and momentum forcing due to the advection term at the lowest level (sigma=0.95), (c) model response to heating only, (d) model response to momentum forcing only.

Yellow Sea fog

This study investigated the mechanisms for the abrupt onset of fog in the Yellow Sea in April and its abrupt basin-wide disappearance in August (Figure 1.16 left panel). Such abrupt changes cannot be explained simply by the gradual changes in solar radiation. From March to April, a temperature inversion forms in a layer 100–350 m over the northwestern Yellow Sea, and the prevailing surface winds switch from northwesterly to southerly; both changes are favorable to advection fog. A land–sea contrast is established in April, with the land warming up much faster than the ocean. The prevailing west-southwesterlies at 925 hPa advect warm, continental air to form an inversion over the western Yellow Sea. The land–sea differential warming also leads to the formation of a shallow anticyclone over the cool Yellow and northern East China Seas in April. The southerlies on the west flank of this anticyclone

advect warm and humid air from the south, causing the abrupt fog onset along the China coast. The end of Yellow Sea fog is associated with a shift in the prevailing winds from southerly to easterly from July to August (Figure 1.16 right panel). The August wind shift over the Yellow Sea is part of a large-scale change in the East Asian–western Pacific monsoons, characterized by enhanced convection over the subtropical western North Pacific and the resulting teleconnection into the midlatitudes, known as the western Pacific–Japan pattern. Back trajectories for foggy and fog-free air masses support the results from the climatological analysis.[S.-P. Zhang (Ocean University of China); S.-P. Xie (IPRC); Q.-Y. Liu, Y.-Q., Yang (Ocean University of China); X.-G. Wang (Qingdao Meteorological Bureau); and Z.-P. Ren (Ocean University of China), 2009: Seasonal variations of Yellow Sea fog: Observations and mechanisms. *J. Climate*, **22** (24), 6758–6772. IPRC-611]

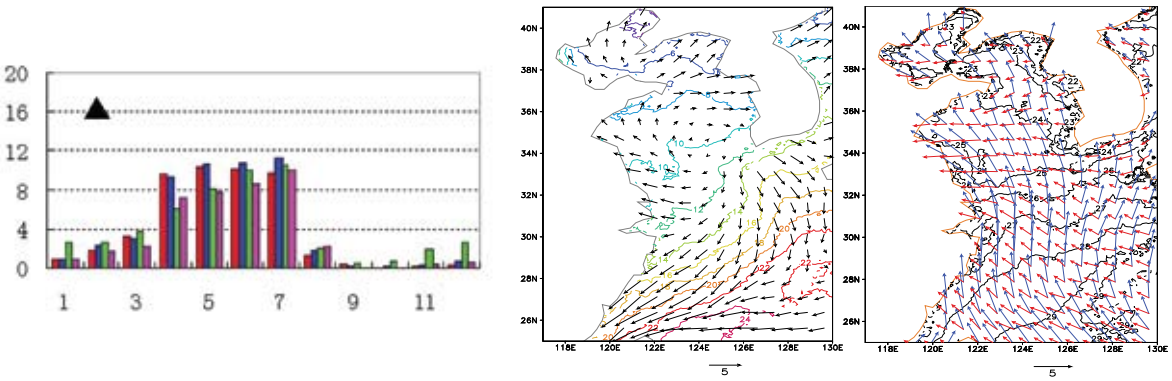

Figure 1.16. Left panel: Fog days at four stations in the Northwest Yellow Sea as a function of calendar month. Two right panels: Surface wind (m/s) and SST (°C) at the onset of the northwest Yellow Sea fog season in April: (left) in July (blue arrows) and (right) August (red) when the fog season ends.

Intraseasonal variability in the South China Sea

Intraseasonal sea surface height (SSH) variability and associated eddy energy in the South China Sea were studied in satellite observations and in an eddy-resolving, global ocean general circulation model. In both model hindcast and satellite observations, a conspicuous minimum variance in SSH occurs along the continental break between the shallow shelf and deep basin (Figure 1.17). Strong intraseasonal

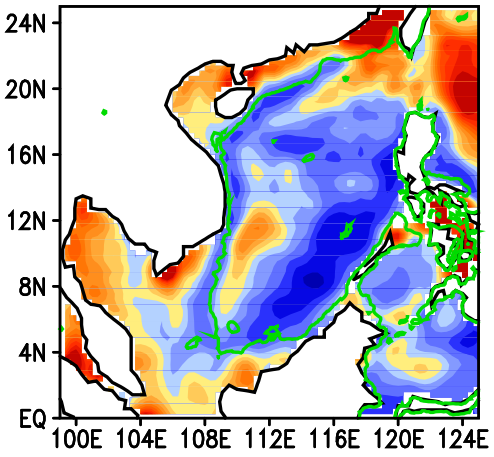

Figure 1.17. Annual-mean standard deviation of intraseasonal variability in sea surface height (color shade, in cm), along with 100 m bathymetry (green line).

variability (ISV) exists in the northern continental shelf, the Gulf of Thailand, and along two bands in the deep basin, with the northern band located west of Luzon Strait and the southern one southeast of Vietnam. The intraseasonal variability in SSH exhibits clear seasonality. During active seasons, the intraseasonal variability in the deep water, high-variance bands displays robust propagation in the direction of the mean flow. Low correlation between observations and model hindcast suggests the importance of dynamical instabilities for the intraseasonal variability in the deep basin, in agreement with an energetics analysis. An exception is along the Vietnam offshore jet during summer, where intraseasonal variability is forced by wind curl created by the obstruction of the Annam Cordillera. In shallow waters, especially in the Gulf of Thailand, intraseasonal variability in SSH is dominated by the barotropic response to intraseasonal wind stress forcing. The agreement between altimetry and the model simulation in the Gulf of Thailand demonstrates the ability of satellite altimeters to observe SSH variability in shallow shelves in the presence of weak tides. [W. Zhuang (South China Sea Institute of Oceanology, CAS); S.-P. Xie (IPRC); D. Wang (South China Sea Institute of Oceanology, CAS); B. Taguchi, H. Aiki, and H. Sasaki (JAMSTEC): Intraseasonal variability in sea surface height over the South China Sea. *J. Geophys. Res.-Oceans*, in press, IPRC-658]

North Pacific subduction rate

The subduction of North Pacific waters is part of the subtropical overturning cell (STC) that transports heat and salt from the subtropics to the equator and is believed to play an important role in the decadal variability of El Niño and the Southern Oscillation (ENSO). Studies of the STC have focused on the variability of the gyre circulation, particularly on the equatorward flow in the thermocline. Neither the variability of water subducting in the subtropics, nor the subduction rate of North Pacific waters has been well documented, though changes in the properties of these water masses are widely recognized.

Based on a global eddy-resolving general circulation model, the decadal variability in the North Pacific subduction rate was calculated. The North Pacific subduction rate was found to correspond well to phases of the Pacific Decadal Oscillation (PDO), with the correlation between the two time series exceeding 0.80 after the climate shift in the mid-1970s. This decadal variability in subduction rate is consistent with the previously described variability in sea surface temperature, surface wind, and surface heat flux (Figure 1.18). Changes in evaporative cooling associated with the Aleutian Low seem to be a key factor influencing this decadal signal. [T. Qu, and Chen, J. (IPRC), 2009: A North Pacific decadal variability in subduction rate. *Geophys. Res. Lett*, **36**, L22602, doi:10.1029/2009GL040914, IPRC-641]

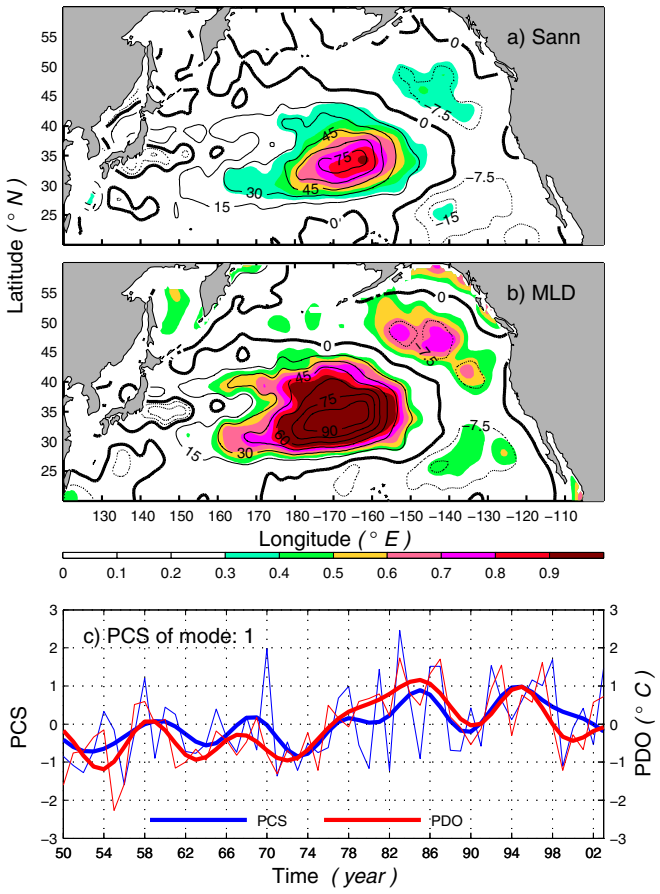

Figure 1.18. Patterns (contours) and fraction of explained variance (color) of the leading combined EOF mode of (a) subduction rate (m/yr) and (b) winter MLD (m) anomalies in the North Pacific. (c) Time series of the leading mode (blue) and PDO index (red). Heavy lines denote the time series smoothed by a 7-year low-pass filter.

Chapter 2: REGIONAL AND SMALL-SCALE CLIMATE PROCESSES AND PHENOMENA

Modeling interannual variations in Eastern Pacific clouds

Better understanding of the processes and mechanisms driving the interannual variability of low-level clouds in the Eastern Pacific could help to reduce uncertainties associated with simulations of these clouds by current climate models and give more confidence in climate-change projections. An analysis of the patterns and anomalies of clouds in the tropical and subtropical Eastern Pacific requires long time series. The IPRC regional atmospheric model (iRAM) has now been integrated continuously for a 28-year period from 1982 through 2009 using NCEP reanalysis data and NOAA SSTs as boundary conditions as well as observed monthly mean carbon dioxide concentrations as input for the radiation scheme. This period covers most of the era of available satellite measurements. The simulated interannual variability of low-level clouds is compared to satellite observations (Figure 2.1). Cloud responses to changes in the local thermal structure of the atmosphere and in the large-scale circulation are being analyzed. [A. Lauer, Y. Wang, K. Hamilton (IPRC); and R. Bennartz (U. Wisconsin)]

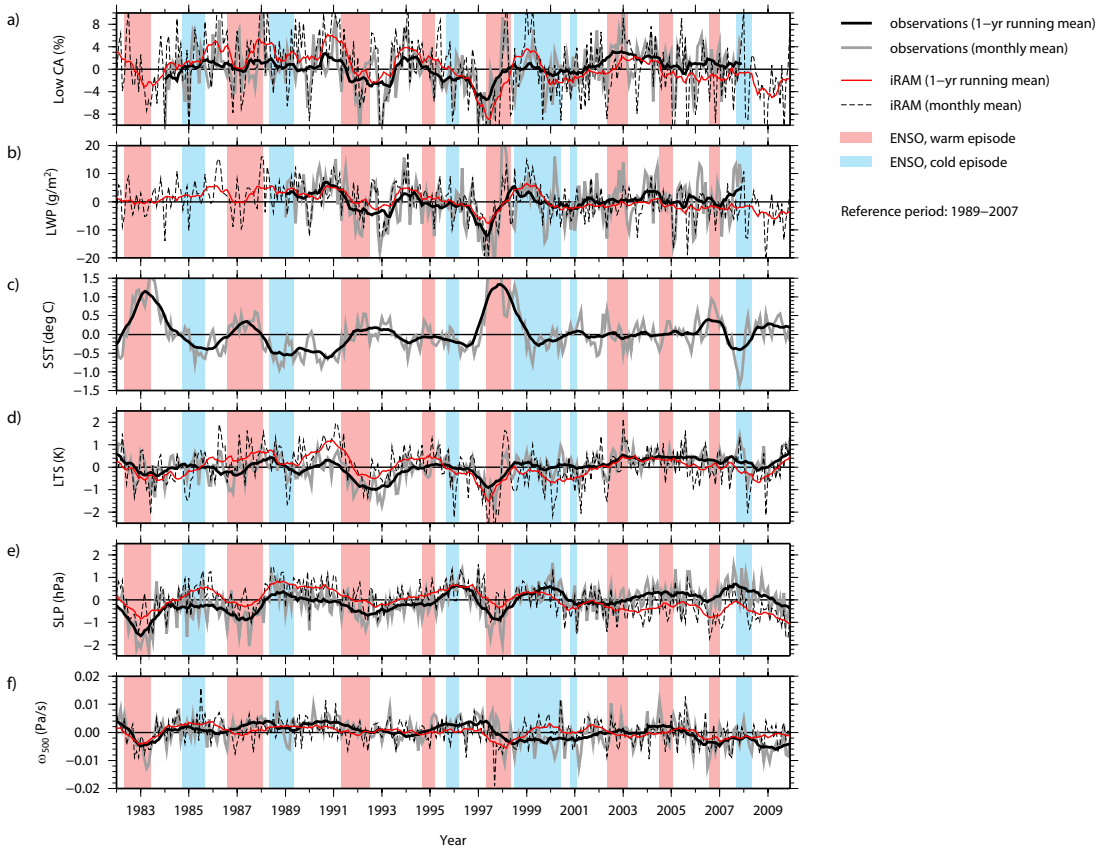

Figure 2.1. Time series of monthly mean anomalies in (a) low-level cloud amount (ISCCP), (b) liquid water path (U. Wisconsin satellite climatology), (c) sea surface temperature (NOAA analysis), (d) lower tropospheric stability, (e) sea level pressure, and (f) 500 hPa vertical velocity from NCEP Reanalysis data compared with results from iRAM. The figure shows monthly means as well as one-year running means averaged over the southeastern Pacific (100°W–75°W, 25°S–5°S). Warm and cold ENSO episodes are shaded in light red and light blue, respectively.

Modeling the lower troposphere in the Southeast Pacific: PreVOCA

The IPRC regional atmospheric model (iRAM) was used in the PreVOCA project. PreVOCA is a preliminary VOCALS study that assesses current atmospheric modeling of the subtropical eastern South Pacific, with a particular focus on the clouds and the marine boundary layer (MBL). Model results for the month of October 2006 were collected from 14 modeling centers and include results from operational forecast models, regional models, and global climate models. Forecast and global climate models produced daily forecasts, while most regional models were run continuously during the study period, initialized and forced at the boundaries with global model analyses. Results among the models, and between models and observations were compared from 40°S to the equator and from 110°W to 70°W, roughly corresponding to the subtropical Pacific coastal region of South America. Model monthly mean surface winds agree well with QuikSCAT observed winds, and the models agree fairly well in showing weak large-scale subsidence near the coast. However their geographic patterns of cloud fraction differ greatly, with only a few models agreeing well with MODIS observations. Compared with satellite products, most models also underestimate the MBL depth by several hundred meters in the eastern part of the study region (Figure 2.2) and the diurnal cycle of liquid water path at the 85°W, 20°S stratus buoy site. Furthermore, the models underestimate the low cloud fraction during all parts of the diurnal cycle compared to surface-based climatologies. [M. C. Wyant (U. Washington) et al.: The PreVOCA Experiment: Modeling the lower troposphere in the Southeast Pacific, *Atmospheric Chemistry and Physics*, submitted]

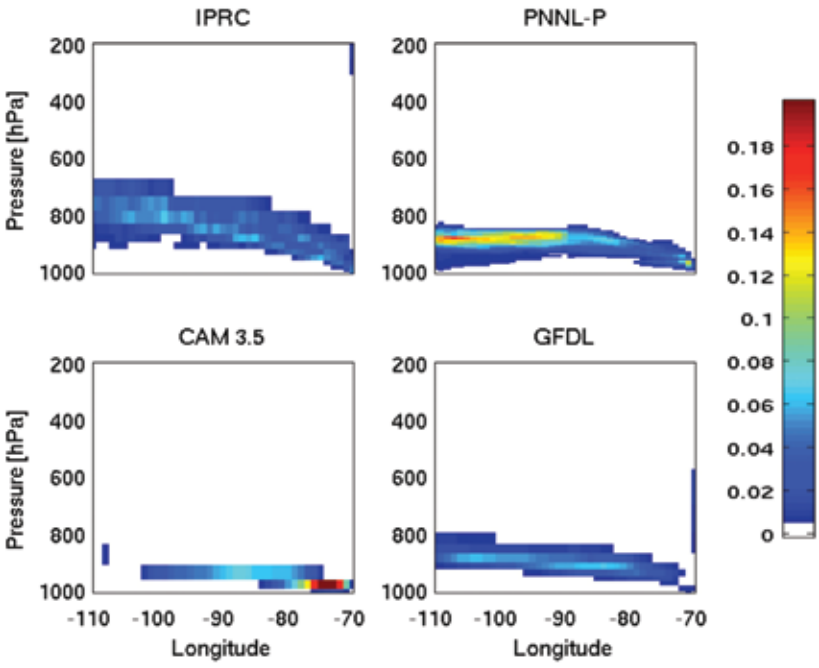

Figure 2.2. For October 2006, 20°S cross-sections of model mean liquid water content (g/kg) in several of the models that are participating in PreVOCA model intercomparison project.

Cloud sensitivity to global warming

Current climate models exhibit a wide range of global climate sensitivity. Cloud radiative feedbacks have been identified as a significant source of the large spread of climate sensitivities among the models and thus of projections of the temperature response to imposed anthropogenic climate forcings. The Eastern Pacific

is of particular interest because of the two large stratocumulus decks in this region. Even slight changes in the properties of these clouds could have important implications for the radiation budget and climate. The sensitivity of clouds over the Eastern Pacific to global warming has been studied with the IPRC Regional Atmospheric Model (iRAM), applying the pseudo-global-warming method. Several 10-year model runs have been performed for different warming scenarios suggesting a high sensitivity of marine stratocumulus clouds to global warming and an overall positive cloud-climate feedback in the Eastern Pacific region (Figure 2.3). Cloud-climate feedbacks from the IPCC AR-4 models averaged over the iRAM model domain are less than the value obtained from comparable iRAM simulations. As the cloud feedback in the entire tropics/subtropics in the AR-4 models is strongly correlated to that in the Eastern Pacific region, and because the cloud feedback largely determines global climate sensitivity, the results from iRAM suggest support for the high end of current estimates of climate sensitivity. [A. Lauer, K. Hamilton, Y. Wang (IPRC); V. Phillips (U. Hawaii); and R. Bennartz (U. Wisconsin): The impact of global warming on marine boundary layer clouds over the Eastern Pacific – A regional model study, *J. Climate,* accepted]

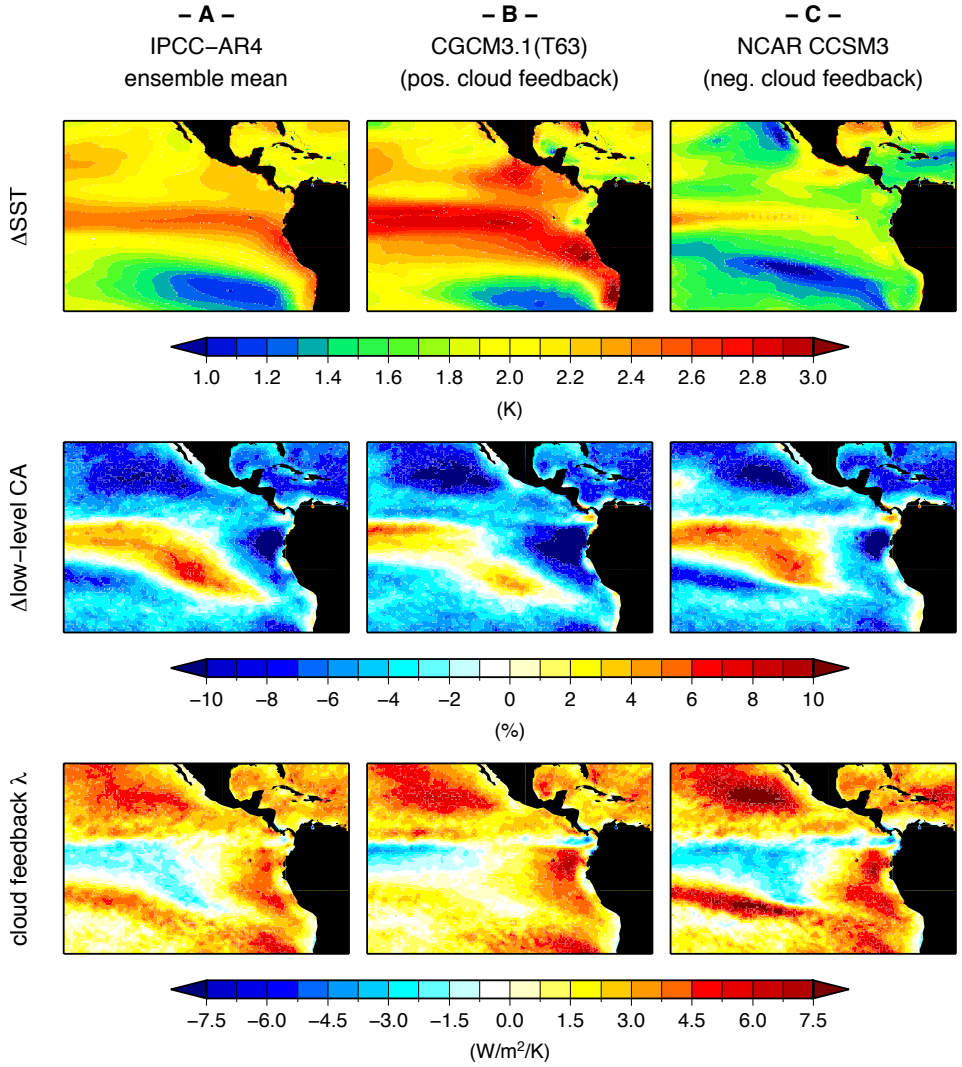

Figure 2.3. Top: The imposed global warming signals in sea surface temperatures (ΔSST) for 3 global warming cases; middle: ten-year-average changes in low-level cloud amount (ΔCA); bottom: cloud feedback parameter (λ).

Incorporation of cloud microphysics in a convection parameterization

The convection scheme currently used in the IPRC Regional Atmospheric Model has been modified by including the double-moment cloud microphysics that had already been applied to grid-scale clouds. The new implementation tracks an air parcel from cloud base to cloud top, calculating supersaturation, aerosol activation and all relevant microphysical processes such as droplet growth, precipitation formation or ice formation. The improved representation of cumulus clouds will be applied to study shallow convection in the trade wind regime. [A. Lauer, Y. Wang, K. Hamilton (IPRC); and V. Phillips (U. Hawaii)].

Observed characteristics of hail size in four regions in China during 1980–2005

The climatology and long-term trends in the hail size in four regions of China were documented for the period of 1980–2005 using the maximum-hail-diameter (MHD) data from the Meteorological Administrations of Xinjiang Uygur Autonomous Region (XUAR), Inner Mongolia Autonomous Region (IMAR), Guizhou Province, and Hebei Province. The reported MHD in the four regions is mostly around 10 mm. Guizhou (in Southwest China) has the largest proportion of severe hail (MHD greater than 15 mm) among the four regions. Severe hailstorms occur in Southwest China mainly between February and June, while in North China they occur in summer (from May to August) with the peak in June. During the period studied, the hail sizes recorded in severe hailstorms show a slight downward trend in Guizhou and IMAR, an upward trend in Hebei, and little trend in XUAR. However, none of the trends is statistically significant. Results from sensitivity experiments using a one-dimensional numerical model show that hail size is sensitive to the freezing level height, the maximum updraft, and column cloud liquid water. [B. Xie, Q.-H. Zhang (Peking University); and Y. Wang (IPRC), *J. Climate*, submitted]

Theory of tropical cyclone Maximum Potential Intensity (MPI)

A tropical cyclone (TC) can be viewed as a heat engine that converts heat energy extracted from the ocean into the kinetic energy of the TC. The kinetic energy eventually dissipates because of surface friction. Since the energy production rate is a linear function and the frictional dissipation rate is proportional to the third power of surface wind speed, the dissipation rate is at first generally lower than the production rate but increases more quickly than the production rate as the storm intensifies. When the dissipation rate reaches the production rate, the TC cannot intensify further. Emanuel hypothesized that a TC achieves its maximum potential intensity (E-MPI) when the surface frictional dissipation rate balances the energy production rate near the radius of maximum wind (RMW). Although the E-MPI agreed well with the maximum intensity of numerically simulated TCs in earlier axisymmetric model studies, the balance hypothesis near the RMW has not been evaluated systematically. This study shows that in a numerically simulated mature TC the frictional dissipation rate is about 25% larger than the energy production rate near the RMW, but lower than the energy production rate outside the eyewall. This finding implies that the excess frictional dissipation under the eyewall should be partially balanced by the energy production outside the eyewall and that the local balance hypothesis underestimates the TC maximum intensity. Budget analyses of Lagrangian and control volume equivalent potential temperature both demonstrate that the energy gained by boundary layer inflow of air due to surface

entropy fluxes outside the eyewall, and before interaction with the eyewall, contributes significantly to the energy balance in the eyewall through the lateral inward energy flux (Figure 2.4). This contribution to energy was supported by a sensitivity experiment in which the surface entropy fluxes beyond a radius of 30–45 km were eliminated. This elimination led to a 13.5% reduction in the maximum sustained near-surface wind speed and in the size of the model TC. [Y Wang and J. Xu (IPRC), 2010: Energy production, frictional dissipation, and maximum intensity of a numerically simulated tropical cyclone. *J. Atmos. Sci*., **67**, 97–116, IPRC-621]

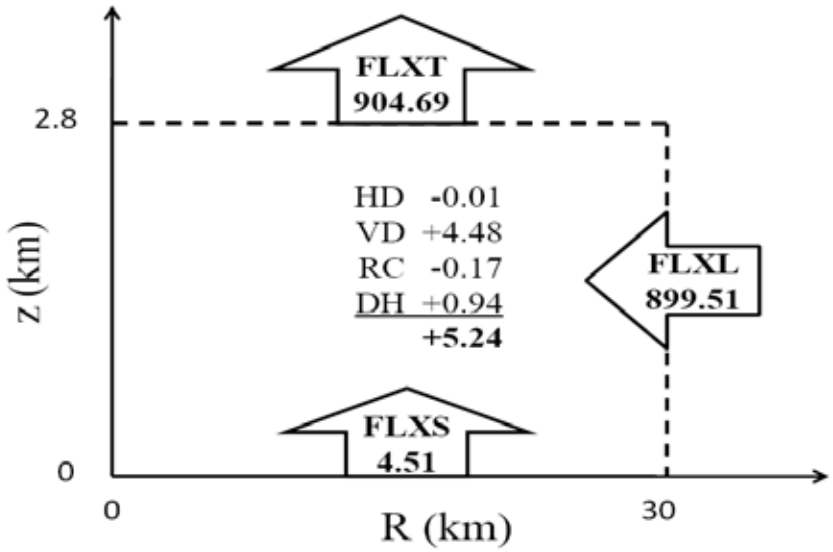

Figure 2.4. Results for a cylindrical control volume entropy budget averaged between 144 h and 192 h of simulation. Shown are the lateral inward entropy flux across a 30-km radius (FLXL), the upward entropy flux at the top (2.8 km above the sea surface) of the cylinder (FLXT), and the surface entropy flux at the base of the cylinder (FLXS). Given are also the entropy changes due to horizontal diffusion (HD), vertical mixing (VD), radiative cooling (RC), and dissipative heating (DH). Note that the vertical mixing (VD) includes the surface entropy flux (FLXS) already. The unit is 10^9 K kg/s. The total volume-integrated entropy in the cylinder experienced some small fluctuations around 267.5×10^{13} K kg between 266.6×10^{13} and 268×10^{13} K kg during this time period.

Dependence of tropical cyclone inner-core size and intensity on the radial distribution of surface entropy flux

The surface entropy flux is critical to the development and maintenance of a tropical cyclone (TC). However, it is unclear how sensitive the inner-core size and intensity of a TC are to the radial distribution of the surface entropy flux underneath the TC. Such sensitivity was examined using the multiply nested, fully compressible, nonhydrostatic TC model developed at the IPRC, the TCM4. In a simulated TC, the effect of the surface entropy flux at different radial ranges on the inner-core size and intensity was evaluated by artificially eliminating the surface entropy fluxes at different radial ranges. Consistent with recent findings from axisymmetric models, the entropy flux in the eye region of a TC is found to contribute little to the storm's intensity, but it plays a role in reducing the radius of maximum wind (RMW). Although surface entropy fluxes under the eyewall contribute greatly to storm intensity, those outside the eyewall up to a radius of about 2–2.5 times the RMW are also important. Further away from

the core, the surface entropy fluxes are crucial to the growth of the storm's inner-core size but can reduce its intensity. The surface entropy fluxes outside the inner core are critical to maintaining high convective available potential energy (CAPE) outside the eyewall and thus to maintaining active spiral rainbands. The latent heat released in these rainbands increases the storm's inner-core size. A positive feedback was identified that explains changes in the RMW and the inner-core size in the different simulation experiments (Figure 2.5). [J. Xu and Y. Wang (IPRC): Sensitivity of tropical cyclone inner core size and intensity to the radial distribution of surface entropy flux, *J. Atmos. Sci.,* IPRC-667, in press]

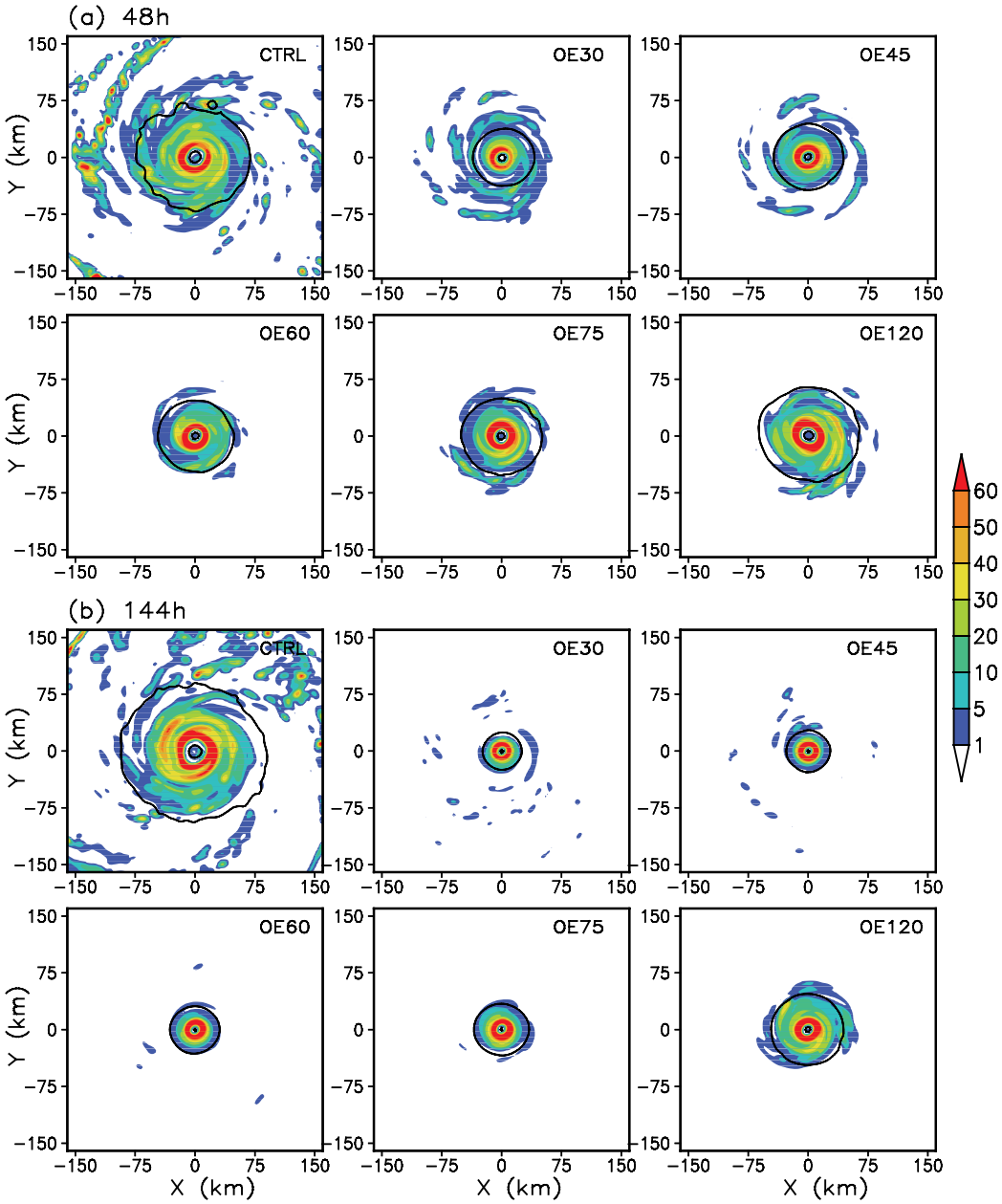

Figure 2.5. The plan view of the rain rate (mm/h) in the model tropical cyclones for the control experiment (CTRL) (a) after 48 h of simulation and (b) after 144 h of simulation. The remaining panels show the respective rain rates for experiments with surface entropy flux removed beyond a radius of 30 km (OE30), 45 km (OE45), 60 km (OE60), 75 km (OE75), and 120 km (OE120). Contours show the 25.7 m/s isotach at the lowest model level.

Sensitivity of the simulated tropical cyclone inner-core size to the initial vortex size

The multiply nested, fully compressible, nonhydrostatic tropical cyclone model (TCM4) was used to examine and understand the sensitivity of the inner-core size of a simulated tropical cyclone (TC) to its initial vortex size. The results show that although at the mature stage the simulated TC intensity depends weakly on the initial vortex size for its general characteristics, the simulated TC inner-core size is largely determined by the initial vortex size. The initial vortex size is critical to both the energy input from the ocean and the effectiveness of the inward angular momentum transport by the transverse circulation driven by eyewall convection and diabatic heating in the spiral rainbands. Strong outer winds in an initially large storm lead to large entropy fluxes and to a large radial extent outside the eyewall, favoring the development of active spiral rainbands (Figure 2.6). Latent heat released in the spiral rainbands increases the low-level radial inflow and accelerates the tangential winds outside the eyewall. This leads to an outward expansion of tangential wind fields and thus increases the inner-core size of the simulated storm. In an initially small storm the weaker outer winds and smaller surface entropy fluxes outside the eyewall are accompanied by less active spiral rainbands, and thus the inner-core size increases more slowly. The extent to which the inward transport of absolute angular momentum leads to an increase in tangential winds outside the eyewall is largely determined by the radial extent of the vertical absolute vorticity, which is shown to be higher in a large vortex. The relative importance of initial vortex size and environmental relative humidity to TC inner-core size was also evaluated. The inner-core size of the simulated storm at the mature stage was found to depend more heavily on initial vortex size than on initial relative humidity of the environment. [J. Xu and Y. Wang (IPRC), submitted]

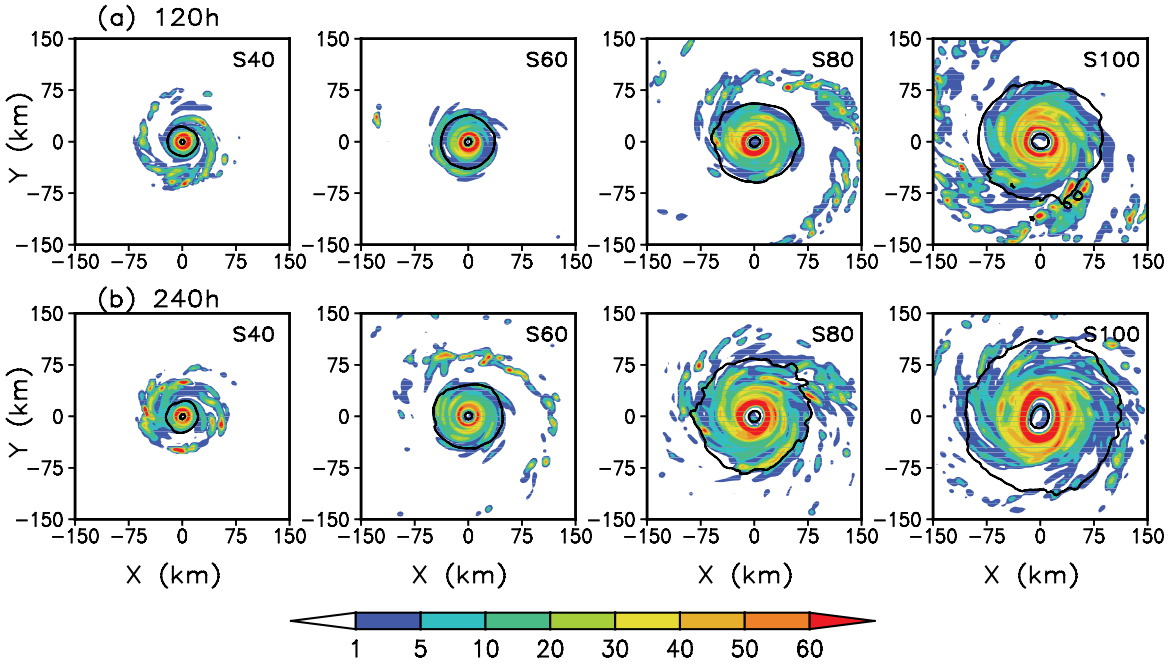

Figure 2.6. The plan view of the rain rate (mm/h) at the surface after (a) 120 h and (b) after 240 h in simulations experiments with different initial radius of maximum wind (RMW) of the vortex. S40, S60, S80, and S100 represent respectively initial RMW of 40, 60, 80, and 100 km. Contours show the isotaches of 25.7 m/s at the lowest model level.

Effect of vertical shear on tropical cyclone intensity and structure change

Analyses of the best-track data of tropical cyclones (TCs) in the North Atlantic and the NCEP/NCAR reanalysis during 1981–2008 show that TC intensity change and vertical wind shear (VWS) are generally negatively correlated, indicating that VWS has an overall negative effect on TC intensity. VWS has a strong impact on the deep layer of slow-moving, and low-latitude TCs, while it exerts a strong effect on the mid-lower troposphere of weak, fast moving, and high latitude TCs. Furthermore, overall easterly shear, especially in the mid- to lower-troposphere, has considerably weaker effects on TC intensity than westerly shear because part of the easterly shear could be offset by the beta-induced northwesterly shear. [Z.-H. Zeng (Institute of Atmospheric Physics, CAS), Y. Wang (IPRC), and L.-S. Chen (Chinese Academy of Meteorological Sciences), 2010: A statistical analysis of vertical shear effect on tropical cyclone intensity change in the North Atlantic, *GRL*, **37**, L02802, 6 PP., doi:10.1029/2009GL041788]

In another study, the effects of environmental vertical wind shear (VWS) on the intensity and rainfall asymmetries in Tropical Storm (TS) Bilis (2006) were analyzed using the following data products: TRMM/TMI estimated surface rainfall data, the QuikSCAT wind fields, 850 hPa and 200 hPa winds of the NCEP/NCAR reanalysis, the precipitation data at 5-minute intervals from automatic weather stations over mainland China, and the best track data of TS Bilis. The results show that the simultaneous and 6 h lagged correlation coefficients between VWS and storm intensity (the minimum central sea level pressure) are 0.59145 and 0.57438 ($p<0.01$), respectively. The averaged VWS was found to be about 11 m/s and the shear suppressed intensification of Bilis. The precipitation in Bilis was highly asymmetric (Figure 2.7). The azimuthally averaged rainfall rate in the partial eyewall, moreover, was smaller than that in a major outer rainband. As the storm intensified, the major rainband showed an unusual outward

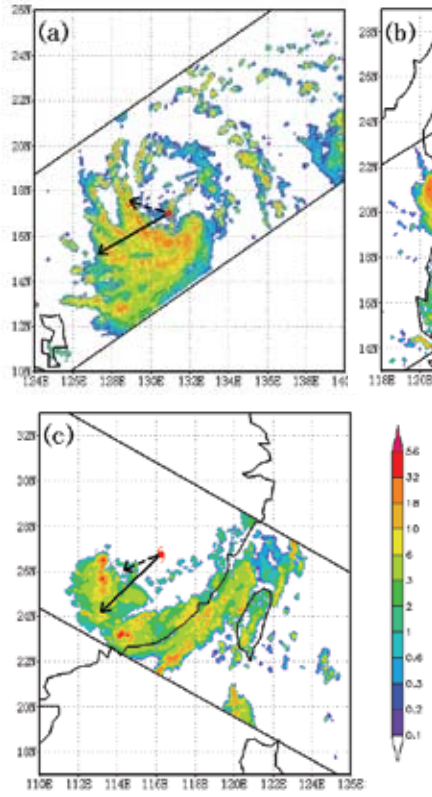

Figure 2.7. TRMM/TMI estimated surface rainfall rate (mm/h). The solid arrow denotes the vertical wind shear direction, the dashed arrow indicates the motion direction of Tropical Storm Bilis: (a) 1323–1326 UTC 10 July 2006, (b) 1309–1312 UTC 12 July 2006, (c) 1927–1930 UTC 14 July 2006.

propagation. Consistent with previous modeling studies, heavy rainfall generally occurred downshear to downshear-left of the VWS vector both near and outside the eyewall, showing a strong wavenumber-one asymmetry, which was amplified as the VWS increased. [J. Yu, (Nanjing University of Information Science and Technology), Z.-M. Tan (Nanjing University), and Y. Wang (IPRC), submitted]

Real-case typhoon genesis and rainfall simulations

The genesis of Typhoon Prapiroon (2000) in the western North Pacific (WNP) was simulated to understand the role of Rossby wave energy dispersion of a pre-existing tropical cyclone (TC) on the subsequent genesis of Prapiroon. Two experiments were conducted. In the control experiment (CTL), the circulation of the previous Typhoon Bilis and its wave train were retained in the initial conditions. In the sensitivity experiment, the circulation of Typhoon Bilis was removed using a spatial filtering technique, but its wave train in the wake was kept. The comparison between these two numerical simulations demonstrates that the pre-existing Typhoon Bilis impacted the subsequent TC genesis both directly and indirectly. [X. Ge, T. Li (IPRC); and M. S. Peng (Naval Research Laboratory), 2010: Cyclogenesis simulation of Typhoon Prapiroon (2000) associated with Rossby wave energy dispersion. *Mon. Weath. Rev.*, **138**, 42–54, IPRC-623]

Despite being only category-2 intensity, Typhoon Morakot in 2009 produced record rainfall in Taiwan. A cloud-resolving model was used to simulate this extreme rainfall event in order to understand the dynamic and thermodynamic processes behind this event. Figure 2.8 shows the simulated rainfall with and without the Taiwan terrain. The numerical results indicate that it was the interaction among the TC, a monsoon gyre, and the local terrain that led to this extreme rainfall event. [X. Ge, T. Li, S. Zhang (IPRC); and M. S. Peng (Naval Research Laboratory), 2010: What causes the extremely heavy rainfall in Taiwan during Typhoon Morakot (2009)? *Atmos. Sc. Lett.*, **11** (1), 46–50, IPRC-650]

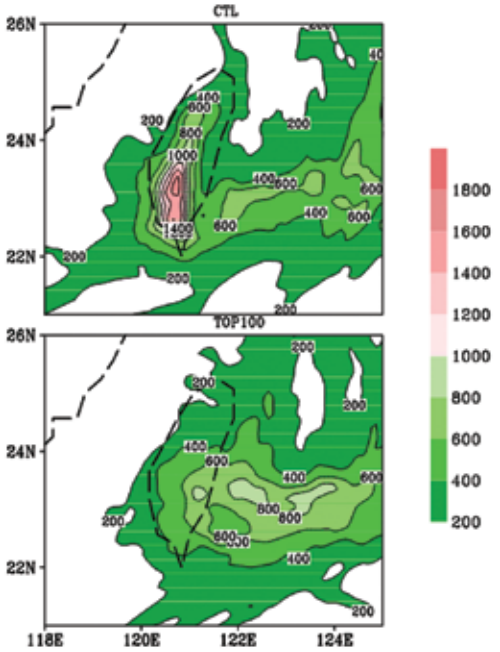

Figure 2.8. Simulated accumulated Morakot rainfall (in mm) during 108 h: (top panel) CTL experiment includes the Taiwan topography; (bottom panel) in the TOP100 experiment, the topography of Taiwan is set to a maximum of 100 m.

Mindoro Strait and Sibutu Passage transports

Studies of marginal sea circulation in the Asia–Pacific region have revealed the existence of a South China Sea (SCS) throughflow (SCSTF), which involves inflow of cold, salty water through the deep Luzon Strait and outflow of warm, fresh water through the shallow Karimata and Mindoro Straits (Figure 2.9). Balanced by an excess of precipitation over evaporation in the SCS, the SCSTF acts as a heat and freshwater conveyor and is believed to play an important role in the region's climate. Due to the complicated topography and highly variable nature of the circulation, direct measurements of the SCS strait transports have proven to be difficult. In this study a new method is proposed that allows the SCS strait transports to be estimated from remotely sensed sea surface height and ocean-bottom-pressure. This method has provided the first "observational" estimate of the Mindoro Strait transport. As the high-resolution satellite data become available, this method can be a reliable monitoring system for strait transports in the SCS and possibly over the global ocean. [T. Qu (IPRC) and Y.T. Song (NASA JPL), 2009: Mindoro Strait and Sibutu Passage transports estimated from satellite data. *Geophys. Res. Lett.*, **36**, L09601, doi:10.1029/2009GL037314. IPRC-604]

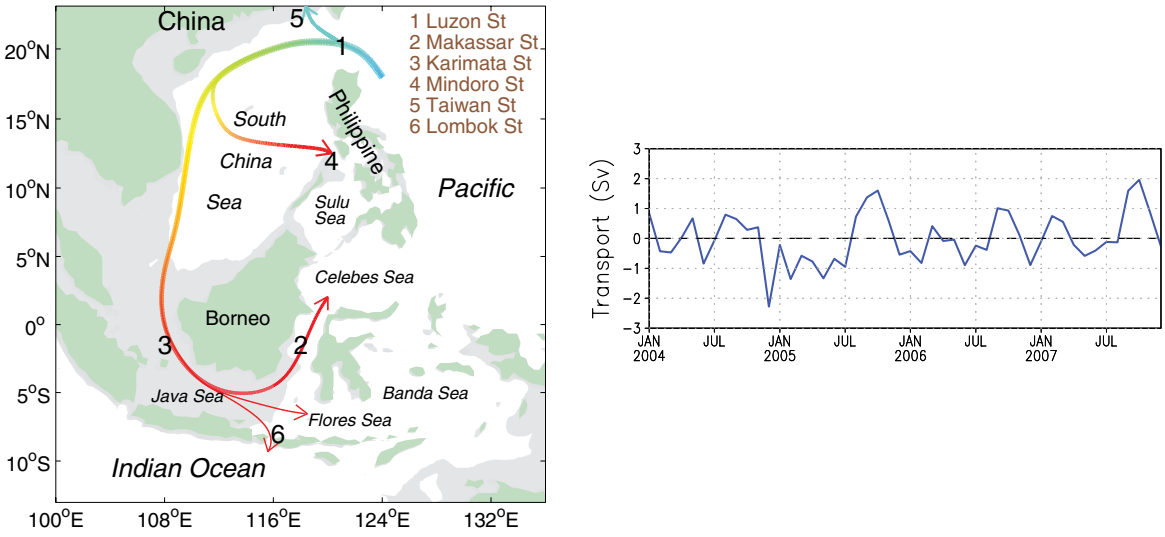

Figure 2.9. Left: A schematic diagram of the South China Sea throughflow (SCSTF); right: Variability of SCSTF across the Mindoro Strait estimated from satellite data. The annual mean value of 2.4 Sv has been subtracted before plotting.

Processes responsible for extended monsoon breaks

An observational and modeling study of the South Asian summer monsoon dry (break) and wet (active) phases was conducted. Break monsoon periods are defined as follows: at least three consecutive days when the area-averaged rainfall over central India is less than one standard deviation from its long-term mean. A diagnosis of observed daily rainfall shows that short breaks (breaks of 3 days or less) and extended breaks (breaks persisting for 7 days or longer) are more frequent than breaks of 4 to 6 days. Diagnostics from both observations and coupled model runs indicate that well before the start of extended breaks over central India, enhanced rainfall and associated ascending motion are noticeable over the tropical western Pacific (Figure 3.1a). During extended breaks, however, rainfall increases over the equatorial Indian Ocean (Figure 3.1c). The diagnostics suggest that the enhanced rainfall over the west Pacific induces a Rossby wave to the west that initiates an extended break through advection of cold and dry air in the upper- and mid-tropospheric levels respectively. The persistence of dry periods, however, is maintained by anomalous descending motion forced by the enhanced convection over the equatorial Indian Ocean. [V. Prasanna and H. Annamalai (IPRC)]

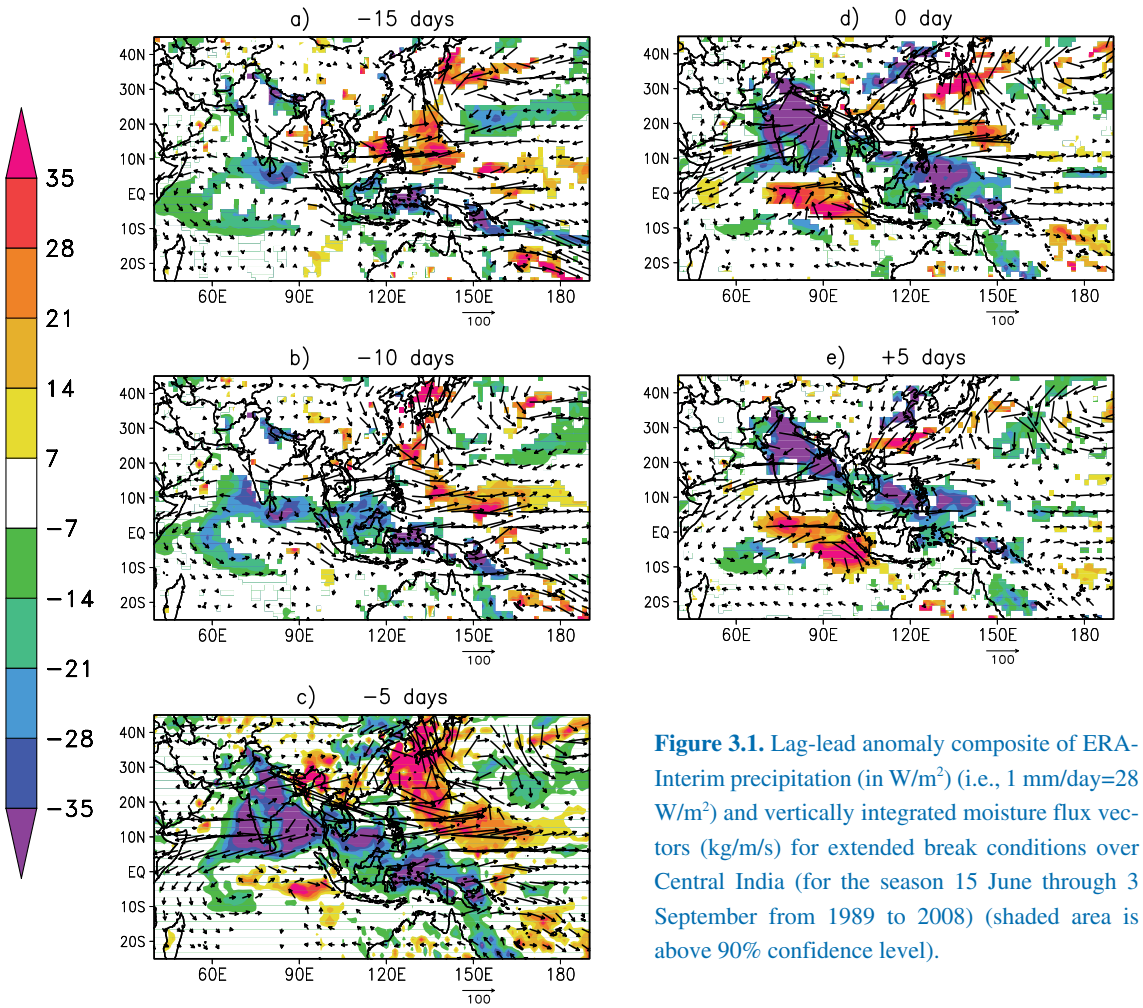

Figure 3.1. Lag-lead anomaly composite of ERA-Interim precipitation (in W/m^2) (i.e., 1 mm/day=28 W/m^2) and vertically integrated moisture flux vectors (kg/m/s) for extended break conditions over Central India (for the season 15 June through 3 September from 1989 to 2008) (shaded area is above 90% confidence level).

Spring NAO and East Asian summer monsoon

Forecasting the East Asian summer monsoon (EASM) is one of the most challenging and important tasks in climate prediction. Observations and numerical experiments both show that the circulation associated with the North Atlantic Oscillation (NAO) in spring (April–May) can induce a tripole sea surface temperature (SST) pattern in the North Atlantic that persists into summer and excites downstream the development of sub-polar teleconnections across northern Eurasia. These teleconnections raise (or lower) the pressure over the Ural Mountain and the Okhotsk Sea; the pressure changes over the Okhotsk Sea strengthen (or weaken) the East Asian subtropical front, i.e., Meiyu-Baiu, leading to a strong (or weak) EASM. An empirical model was developed to predict the EASM strength by including both ENSO and spring NAO indices. The hindcast for the 1979–2006 period shows a prediction skill that is comparable to results with a 14 multi-model ensemble hindcast (Figure 3.2). Since all these predictors can be readily monitored in real time, this empirical model provides a real-time forecast tool. [Z. W. Wu (UH), B. Wang (IPRC), and J. P. Li (Institute of Atmospheric Physics, CAS), 2009: An empirical seasonal prediction model of the East Asian summer monsoon using ENSO and NAO. *J. Geophys. Res.*, **114**, D18120, doi:10.1029/ 2009JD011733, IPRC-677].

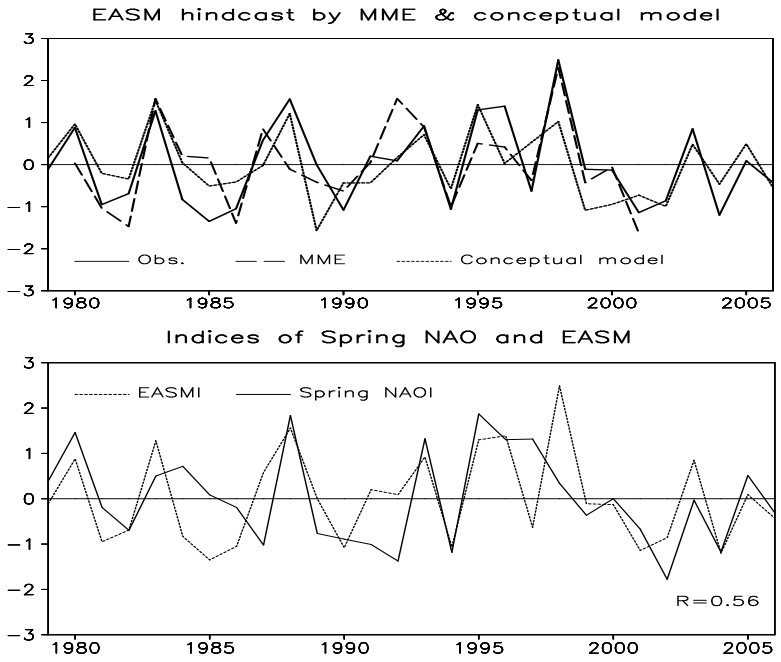

Figure 3.2. Upper panel: East Asian summer monsoon intensity index (EASMI) and the previous spring NAO index (NAOI) for the 1979–2006 period. For ease of comparison, the NAOI sign is reversed. Correlation coefficient r=0.56. Lower panel: The strength of the EASM in observations and in the hindcasts of the conceptual model and of the ensemble mean of 14 state-of-the-art dynamical models.

Moist teleconnection between equatorial Pacific SST and South Asian monsoon

To elucidate the precursors of extreme dry monsoons over southern Asian, atmospheric circulation and sea surface temperature patterns were analyzed during the developing phase of El Niño in 20th century integrations conducted with the coupled GFDL_CM2.1 model and in experiments performed with the atmospheric component of this model, AM2.1. The moisture and moist static energy budgets were calculated to identify moist teleconnections. When warm SST anomalies are prescribed in the equatorial Pacific, AM2.1 produces anomalous westerlies (Figure 3.3a), moisture convergence (Figure 3.3b), and

evaporation (Figure 3.3d), leading to increased rainfall in the equatorial Pacific and drought over the South Asian monsoon region. Concentrated easterly anomalies along the equatorial Indian Ocean extend into Africa (Figure 3.3a). These easterlies are interpreted as a Kelvin wave response to the equatorial Pacific increase in rainfall and also partly as a Rossby wave response to the drought over the Asian summer monsoon region. The decrease in monsoon precipitation appears to be induced by two processes. First, the easterly wind anomalies, due to Ekman pumping, lead to anticyclonic vorticity over the northern Indian Ocean, promoting dry air advection from the north to the monsoon region (Figure 3.3c). Second, the Southern Hemisphere anticyclonic circulation opposes the cross-equatorial monsoon flow (Figure 3.3a), resulting in less evaporation (Figure 3.3d) and less rainfall (Figure 3.3a) in the northern Indian Ocean. Thus in the models the interaction between equatorial waves and moist processes sets up a teleconnection causing the drought over South Asia that persists into the summer. [P.A. Pillai and H. Annamalai (IPRC)]

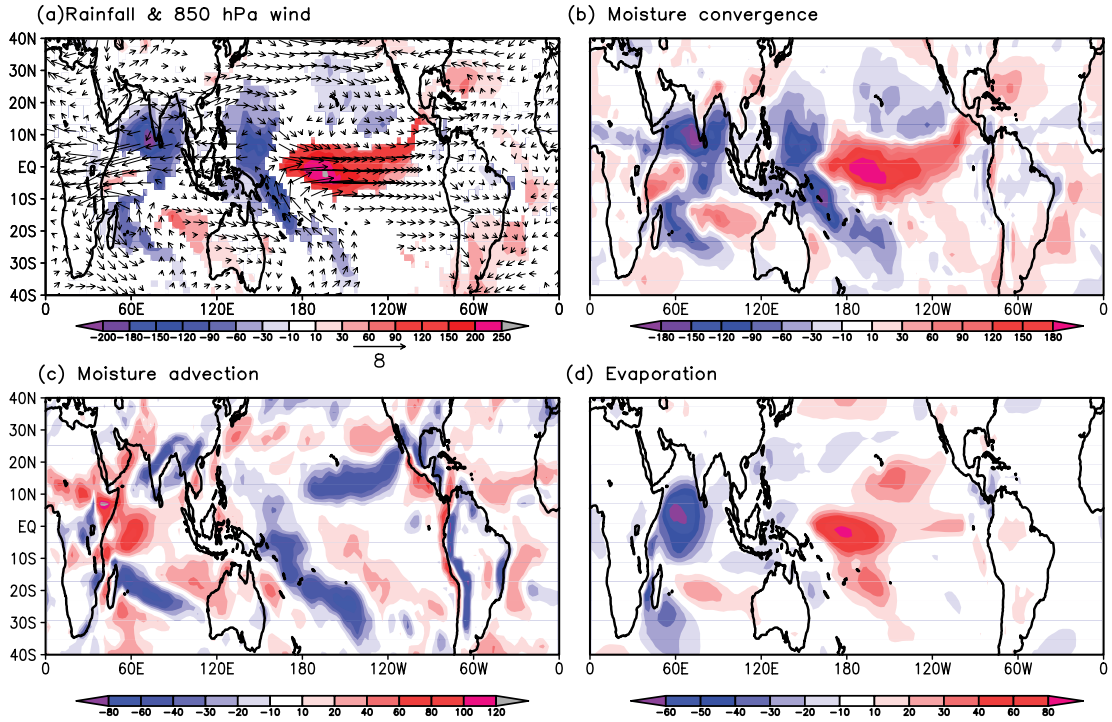

Figure 3.3. April–May moisture budget terms in AM2.1 ensemble mean simulations during severe weak monsoon anomalies in years of developing El Niño: (a) Precipitation (shaded) and 850 hPa wind (vector); (b) vertically integrated moisture convergence; (c) vertically integrated moisture advection; and (d) evaporation. Except for wind (m/s), the terms are in W/m^2: note different color scales.

Coupled model prediction of the western North Pacific – East Asian summer monsoon

The potential for predicting western North Pacific – East Asian summer monsoon (WNP–EASM) precipitation and circulation one or two seasons ahead was investigated using retrospective forecast data for the 26-year period of 1981–2006 from two operational coupled models: the NCEP Climate Forecast System (CFS) and the BMRC Predictive Ocean–Atmosphere Model for Australia (POAMA). Although both coupled models have difficulty predicting summer mean precipitation anomalies over the region of interest for even a 0-month lead forecast, they are capable of predicting zonal wind anomalies at 850

hPa several months ahead and, consequently, satisfactorily predict summer monsoon circulation indices for the EA region (EASMI) and for the WNP region (WNPSMI). It is noteworthy that current coupled models have difficulty capturing the interannual variability component of the WNP–EASM system, which is not correlated with typical ENSO variability. To improve the long-lead seasonal prediction of WNP–EASM precipitation, a statistical post-processing method was developed based on the multiple linear regression method. The method uses the Multi-Model Ensemble predictions of the EASMI and of the WNPSMI as predictors. This statistical post-processing improves the forecast skill for the summer mean precipitation over most of the WNP–EASM region at all forecast lead times (Figure 3.4). [S.-S. Lee (Pusan National University), J.-Y. Lee (IPRC), K.-J. Ha (Pusan National University), B. Wang (IPRC), and J. Schemm (NCEP Climate Prediction Center): Deficiencies and possibilities for long-lead coupled climate prediction of the western North Pacific–East Asian summer monsoon. *Climate Dynamics*, in press, IPRC-697]

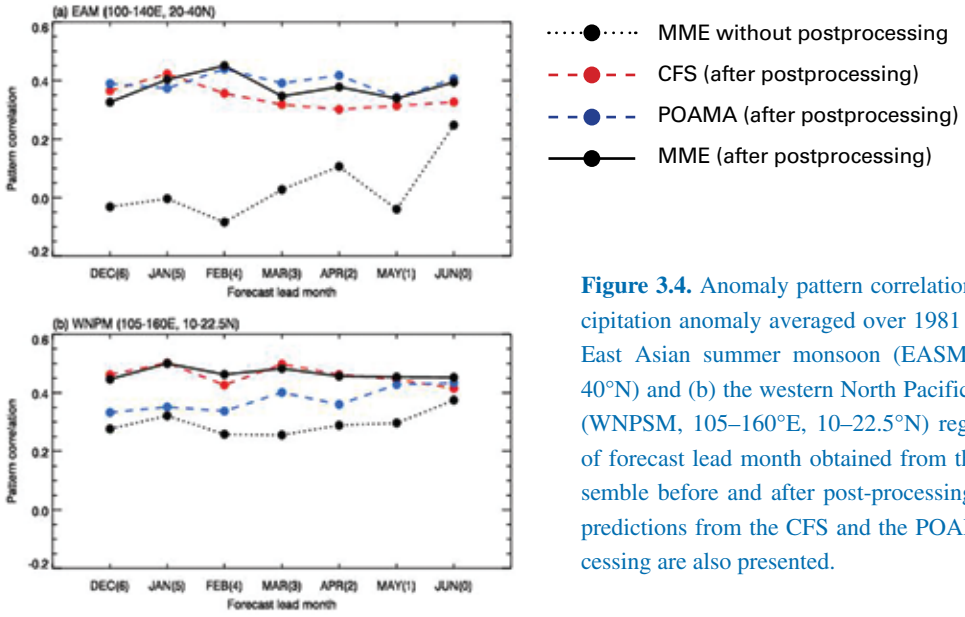

Figure 3.4. Anomaly pattern correlation skill for JJA precipitation anomaly averaged over 1981 to 2006 for (a) the East Asian summer monsoon (EASM, 100–140°E, 20–40°N) and (b) the western North Pacific summer monsoon (WNPSM, 105–160°E, 10–22.5°N) regions as a function of forecast lead month obtained from the multi-model ensemble before and after post-processing. For comparison, predictions from the CFS and the POAMA after post-processing are also presented.

Drying trends over South Asia: Are they due to Global Warming?

The seasonal-mean (June through September) rainfall associated with the Asian summer monsoon is critical for the water supply in the world's most densely populated region. A simple running mean of the observed all-India rainfall index (widely used as a measure of the strength of the South Asian summer monsoon) shows multi-decadal variability with shifts to drier or wetter periods about every 30 to 40 years. The expected shift to a stronger monsoon during the1990s, however, did not occur. All available observations as well as modeling results capture the current drying pattern over South Asia and the increasing rainfall over tropical west Pacific.

To understand the circulation changes causing this eastward shift of monsoon rainfall, a 5-member ensemble experiment was conducted with the GFDL atmospheric general circulation model (AM2.1), forced with the observed monthly incremental SST trend for the period 1951–2000. The forcing regions included: (i) tropical west Pacific; (ii) Indo-Pacific warm pool, and (iii) global tropics. Results were

compared with a 50-year control integration using seasonally varying climatological SST. Figure 3.5a shows the precipitation response to SST warming over the tropical Indo-Pacific warm pool. The drying pattern over South Asia and increased rainfall over the tropical west Pacific are well captured (boxed areas). While moisture convergence and precipitation dominate the moisture budget (Figure 3.5a and b), contributions from moisture advection (Figure 3.5c) and evaporation (Figure 3.5d) are substantial over South Asia and the tropical west Pacific. Contributions from temperature advection, sensible heat, and net radiative flux into the atmosphere are marginal over South Asia and the tropical west Pacific. The principal mechanism for the drying trends over India appears to be the rainfall increase over the tropical west Pacific, which forces a Rossby wave response with descending motion to the west. Because the SST warming over the tropical west Pacific during the last 5 to 6 decades is thought to be mostly due to an increase in human-generated greenhouse gases, the current drying trend over South Asia is also very likely such a response. [H. Annamalai, Jan Hafner, K.P. Sooraj, and P. Pillai (IPRC): Drying trends over South Asia: Is it Due to Global Warming?]

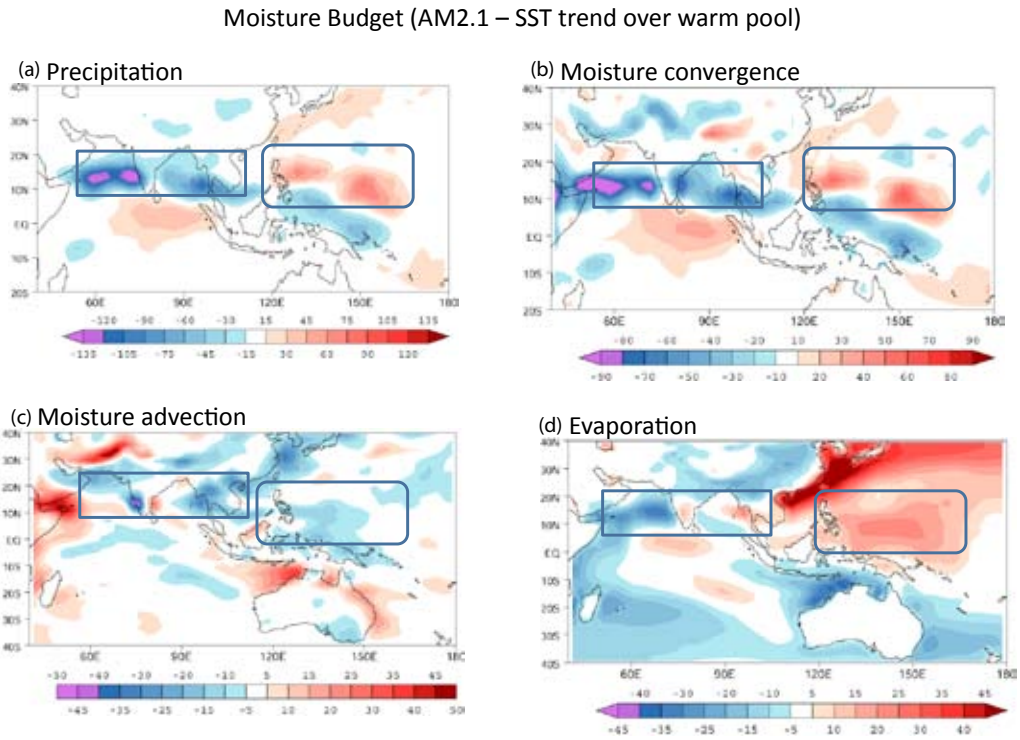

Figure 3.5. Dominant terms of the moisture budget from AM2.1 experiment forced with SST trend over the Indo-Pacific warm pool: (a) precipitation; (b) vertically integrated moisture convergence; (c) vertically integrated horizontal moisture advection; (d) evaporation. Units are in W/m^2.

Origin of the quasi-biweekly oscillation

The origin of the quasi-biweekly oscillation (QBWO) in boreal spring over the tropical Indian Ocean was investigated using 27-year daily OLR and the NCEP/NCAR reanalysis data. It is found that a few days prior to the onset of local convection in the eastern equatorial Indian Ocean, ascending motion appears in the boundary layer. Based on the diagnosis of the zonal momentum equation, a boundary-layer

triggering mechanism is proposed. The cause of the boundary-layer convergence is attributed to the downward transport of the background mean easterly momentum by the perturbation of the vertical motion during the preceding suppressed convective phase. The generated barotropic easterly wind further causes free-atmospheric divergence and thus boundary-layer convergence. The result suggests that the local process, rather than the eastward propagation of the disturbance from the western tropical Indian Ocean, is essential for the phase transition of the QBWO convection over the eastern equatorial Indian Ocean. [M. Wen (Chinese Academy of Meteorological Sciences), T. Li (IPRC); R. Zhang, and Y. Qi (Chinese Academy of Meteorological Sciences), 2010: Structure and origin of the quasi-biweekly oscillation over the tropical Indian Ocean in boreal spring. *J. Atmos. Sci.*, in press]

Climate impact on global storm days

Existing studies of the possible effects of global warming on tropical cyclone (TC) activity focus mostly on regional variations in the number and intensity of TCs. This study proposes a new, complementary metric, tropical storm days (TSD), to measure global climate variation and change in TC activity. The TSD metric provides integrated information about TC tracks, life spans, and areas of impacts. The metric is based on a consistent and reliable global "best track" record over the past 44 years (1965–2008) and is suitable for detecting long-term trends (Figure 3.6). A maximum covariance analysis of TSD and SST reveals that the rise in temperature of about 0.5°C in the tropics has so far not significantly affected the global number of tropical storm days, albeit regional upward trends are seen over the North Atlantic and the Indo-Pacific warm pool (17.5°S–10°N, 70–140°E). However, during the "tropical cyclone year" (from June 1 to the next May 31), unexpected large amplitude fluctuations were found in TSD, which are related to the occurrence of El Niño and a positive phase of the Pacific Decadal Oscillation (PDO). [B. Wang (IPRC), Y. Yang (OAC), Q.-H. Ding (IPRC), Hiroyuki Murakami (AESTO), and Fei Huang (OAC): Climate control of the global tropical storm days (1965–2008), *GRL*, in press]

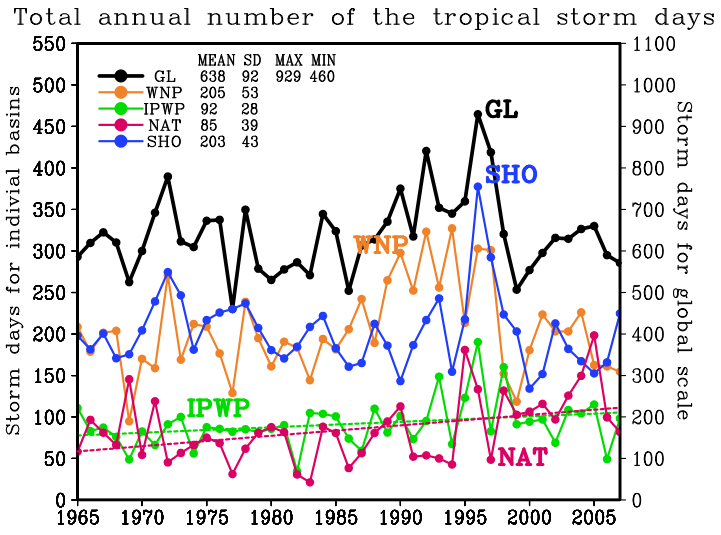

Figure 3.6. The total number of tropical storm days (TSD) from June 1 to the next May 31 for each "tropical cyclone year" from 1965–2008. The TSD in the global domain (GL), western North Pacific (WNP), and Southern Hemisphere oceans (SHO) show no trends over the 44-year period but large year-to-year variability driven by ENSO. The TSD in the North Atlantic (NAT) and Indo-Pacific Warm Pool (IPWP, 17.5°S–10°N, 70°E–140°E) show significant trends possibly associated with global warming. The axis at left is for individual basins (regions) and at right for the global total. The means and standard deviations, maximum and minimum values are shown in the legend.

Spatio-temporal (2-D) wavelet transform (STWT) applied to the MJO

The spatio-temporal (2-D) wavelet transform (STWT) is designed to detect significant, non-stationary, wave-propagation signals from a time–space domain. One of the major advantages of the STWT is its capability to localize the wave properties in both space and time, which facilitates study of interactions among multiple-scale disturbances by providing relevant information about energy concentration at a given time and location. To demonstrate how the STWT works, it was applied to an analysis of the multiscale structure of the Madden–Julian Oscillation (MJO), which had first been identified in the classic work of Tetsuo Nakazawa in the 1980s. All types of convectively coupled equatorial waves were identified. The results reveal the structural differences between the MJO and Kelvin waves and their different relationships with the embedded westward propagating inertio-gravity (WIG) waves (Figure 3.7). This difference may hold the key to understanding the difference in propagation speed between the MJO and Kelvin waves. [K. Kikuchi, and B. Wang (IPRC): Spatio-temporal wavelet transform and the multiscale behavior of the Madden–Julian Oscillation. *J. Climate*, in press, IPRC-664]

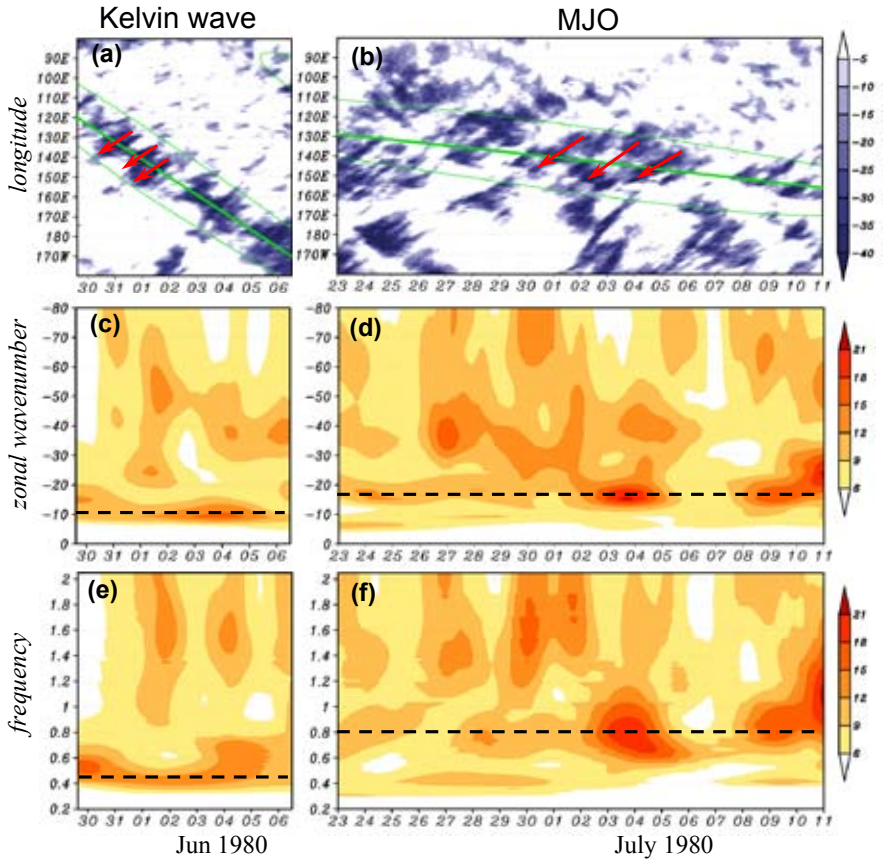

Figure 3.7. Spatio-temporal wavelet transform applied to identify the hierarchical structure of the MJO case studied by Nakazawa (1988). Upper two panels: Hovmöller diagram of infrared data (purple, in W/m^2); thick green lines indicate phase of the Kelvin wave and the MJO; thin green lines indicate –5 W/m^2 contours of each component; red arrows show some internal structures (WIG waves). Lower two panels: temporal variation of the most significant spectrum peaks of WIG waves averaged between the equator and 10°N as a function of (c and d) zonal wave number and (e and f) frequency. In panels (c–f) the power spectrum is normalized by the background spectrum of the global wavelet scalogram. Note, the value of 6.7 is significantly different from the background spectrum at the 99% confidence level.

Chapter 4: PALEOCLIMATE

The effect of topography-enhanced diapycnal mixing on oceanic and atmospheric circulation and marine biogeochemistry

An empirical topography-catalyzed diapycnal mixing scheme was incorporated into the Earth system model LOVECLIM, which includes a three-dimensional global model of the marine carbon cycle. This new addition to LOVECLIM allows study of the effect of topography-enhanced mixing on ocean physics and biogeochemistry, and the impact of ocean physics on the atmospheric circulation and sea ice. The mixing parameterization adopted here is the roughness diffusivity model (RDM) developed by Thomas Decloedt and Doug Luther (U. Hawai'i). Two model runs were conducted with two different parameterizations of vertical background diffusivity.

Results indicate that topography-enhanced mixing impacts the global oceanic and even the atmospheric circulation (demonstrated for the first time) as well as marine biogeochemistry. Increased diapycnal mixing weakens the stratification and strengthens the deep overturning cell and equatorial upwelling, leading to surface warming of the Southern Ocean and significant cooling in the low latitudes. These changes, in turn, have a series of cascading effects on the Walker circulation, equatorial divergence and upwelling, westerly winds in the Southern Hemisphere, water mass ages, ventilation, and the oxygen minimum zones.

A major implication of the study is that ocean topography significantly affects ocean mixing and this has major climatic consequences. A coupled model approach is necessary to reliably assess the global effects of diapycnal mixing parameterizations. [T. Friedrich, A. Timmermann (IPRC); T. Decloedt, D.S. Luther (U. Hawaii); A. Mouchet (U. Liege), 2010: The effect of topography-enhanced diapycnal mixing on ocean and atmospheric circulation and marine biogeochemistry, *Ocean Modeling*, to be submitted]

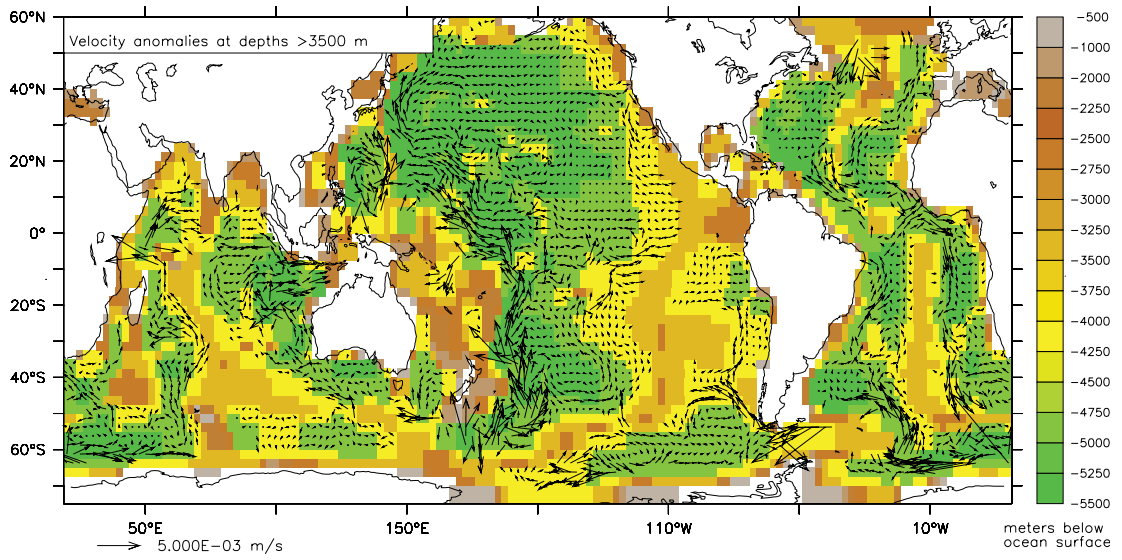

Figure 4.1. Model ocean topography (shaded) and difference in velocity (vectors) averaged over the lowest 3 levels (3300–5500 m) between the run with the RDM and the control run.

Development of ice-sheet/LOVECLIM coupling interface

To understand glacial inceptions and terminations, a comprehensive Earth system models is needed that can simulate carbon cycle responses and vegetation feedbacks as well as the interaction of the waxing and waning ice sheets with the atmospheric and oceanic circulation. The coupling of LOVECLIM with a thermomechanical Japanese ice-sheet model, IcIES, is thus a long-term goal of IPRC's Earth system modeling capabilities. A major challenge is the development of a coupling interface between the atmospheric thermal and hydrological climate fields and the mass balance of the ice-sheet model. At present, different coupling strategies are tested offline at the IPRC using the thermomechanical ice-sheet model GLIMMER (to be replaced later by IcIES). Work has focused on the stability of the present-day Greenland ice sheet. The first time-slice experiments with climate forcing fields from the present-day ERA-40 reanalysis data and LOVECLIM's pre-industrial control simulation have been completed. When coupled to the annual mean climatological cycle of 2 m air temperature and precipitation from ERA-40, the GLIMMER simulation shows that the Greenland Ice Sheet reaches a near equilibrium state that has approximately 30% less ice volume than the initial (present-day) ice sheet (2.85 x10^6 km^3) after 10,000 model years. Central Greenland ice thickness decreases by about 1000 m, whereas the ice margins along the eastern margin grow and expand. In two additional experiments, GLIMMER was forced with climatological temperature and precipitation cycles from LOVECLIM's pre-industrial control run, one without further correction and a second with a bias correction toward the ERA-40 climatology. A precipitation bias was corrected by using a scale factor that corrects the annual-mean bias (i.e., by the ratio between LOVECLIM and ERA-40 annual-mean precipitation). Without bias correction, a dramatic reduction in ice volume occurs over Southern and Central Greenland, whereas the mean-corrected annual cycle gives similar results compared to the ERA-40 climatology, even for

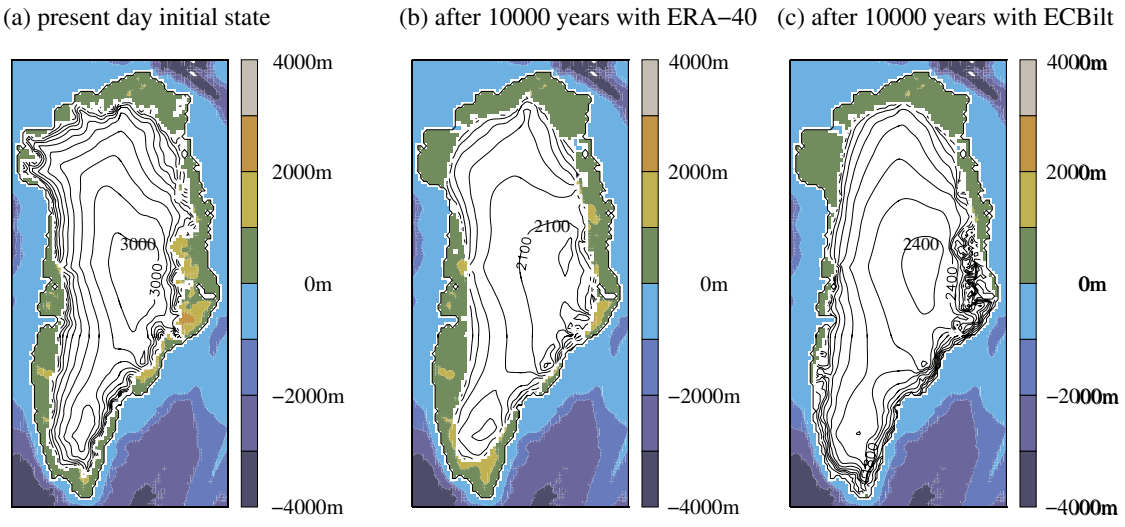

Figure 4.2. Illustration of the near-equilibrium ice-sheet simulation with GLIMMER. (a) The initial state used in the ice-sheet model based on present-day topography. The ice-sheet area is shown in white with contours (300 m interval) of its surface elevation; shades show visible Greenland and ocean topography. (b) The ice-sheet state in GLIMMER after 10000 years of forcing with climatological annual cycles in 2 m air temperature and precipitation from ERA-40 (1979–2000). (c) The ice sheet after 10000 years of forcing with bias-corrected temperatures and precipitation fields from the atmospheric model component ECBilt in the Earth system model LOVECLIM.

the coarse T21 resolution of LOVECLIM (Figure 4.2). These encouraging results are an important first step towards the two-way asynchronous coupling between LOVECLIM and GLIMMER and eventually IcIES. [O. Elison Timm (IPRC), A. Abe Ouchi (JAMSTEC), and A. Timmermann (IPRC)]

Dynamics of the descending branch of the Atlantic Meridional Overturnurning Circulation

The goal of this project was to identify the processes that cause upper-layer water to converge in the North Atlantic, thereby driving the large-scale, density-driven meridional overturning circulation (MOC). A suite of tasks was designed to isolate the dependence of the MOC on horizontal and vertical mixing and buoyancy forcing. The advantage of this approach is that analytic solutions to a variable-layer model (VLOM) are possible near the base of the hierarchy and can be compared with results from ocean general circulation model (OGCM) experiments. These analytical solutions provide valuable insights into the dynamics of the more complex, numerical solutions. The results yield a novel dynamical perspective on how large-scale mass convergence is established in response to buoyancy forcing. Key processes in a temperature-forced VLOM solution and the OGCM COCO and the MIT-OGCM are: 1) the dramatic deepening of isotherms along the eastern boundary due to Kelvin wave adjustment; 2) the westward decay of Rossby waves in the interior ocean by horizontal viscosity and subsurface temperature advection; and 3) the shallowing of isotherms along the western boundary. The zonal pressure gradient associated with the different eastern- and western-boundary density structures drives northward the upper-layer flow, which converges in the northeastern ocean at 50°N to drive the density-driven MOC. Finally, in solutions with reduced relaxation, the convergence region shifts from the northeastern ocean to the northern boundary, a consequence of temperature advection that allows stratification to extend further around the perimeter of the basin. [F. Schloesser, J. P. McCreary, R. Furue, A. Timmermann (IPRC), 2010: Dynamics of the descending branch of the Atlantic Meridional Overturnurning Circulation: Part I, to be submitted]

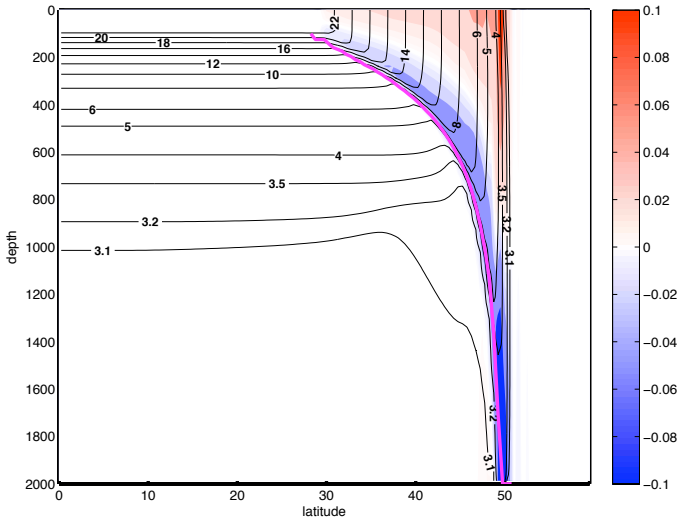

Figure 4.3. In a MIT-OGCM solution, isotherms near the eastern boundary deepen towards the north, so that the depth-integrated zonal velocities (shading, in m/s) vanish in the "upper layer", where isotherms are vertical. This layer depth agrees well with the analytical variable-layer ocean model solution (magenta line).

North Pacific Meridional Overturning Circulation during Last Glacial Termination

Around 18,000–15,000 years ago, the Atlantic Meridional Overturning Circulation (AMOC) weakened substantially in response to meltwater discharges from the disintegrating glacial ice sheets. The global

effects of this dramatic reorganization of poleward heat flow in the North Atlantic were felt as far away as Antarctica and the North Pacific. Evidence from North Pacific surface proxy data, from a compilation of marine radiocarbon-age ventilation records, and from global climate model simulations suggests that during the early stages of the Last Glacial Termination deep water was formed in the North Pacific extending to a depth of ~2500–3000 m. Resulting changes in the 3-dimensional density structure led to the establishment of a deep Pacific Meridional Overturning Cell (PMOC) and associated changes in surface climate conditions. A seesaw of Deep Water formation existed between the North Atlantic and the North Pacific, which played a key role in regulating poleward oceanic heat transport during the Last Glacial Termination. [Y. Okazaki (JAMSTEC); A. Timmermann, L. Menviel (IPRC); N. Harada, A. Abe-Ouchi, M. O. Chikamoto (JAMSTEC); A. Mouchet (U. Liege); H. Asahi (U. Tokyo), 2010: Deepwater Formation in the North Pacific During the Last Glacial Termination, *Science*, submitted]

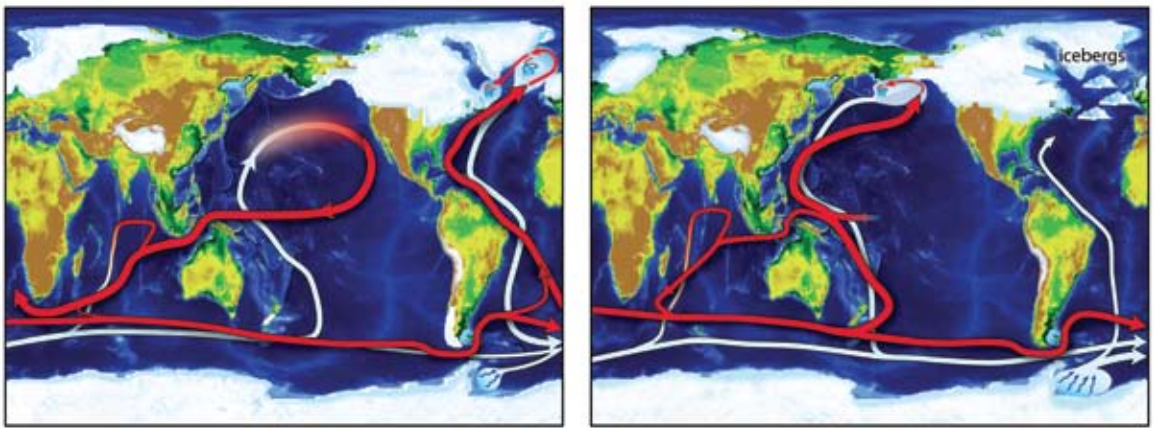

Figure 4.4. Left panel shows the glacial conveyor belt flow 21,000 years ago; right panel shows a reorganized conveyor belt flow 17,500–15,000 years ago with deep-water sinking in the North Pacific.

The Pacific Meridional Overturning Circulation and its impact on global climate and the carbon cycle

To study the effect of the establishment of a deep Pacific Meridional Overturning Circulation (PMOC) on global climate and the marine carbon cycle, an idealized experiment using an Earth system model of intermediate complexity (LOVECLIM) was performed. Imposing a negative freshwater flux in the northern North Pacific, the PMOC attains values of up to 30 Sv. The associated meridional heat transport leads to a 2.5°C warming of North Pacific waters while the Southern Ocean sea surface temperature decreases by about 0.6°C. As a result of the formation of North Pacific Deep Water (NPDW), the surface branch of the conveyor belt circulation weakens. Transport through the Indonesian Throughflow decreases by 50% as the warm and saline water from the equatorial Pacific is diverted into the North Pacific. Due to enhanced upwelling and stronger mixing at intermediate depths, the nutrient content in the euphotic zone increases by about 25%, leading to a 20% increase in export production. The greater export production is however compensated by an enhanced transport of dissolved inorganic carbon to the surface. As a result, the atmospheric CO_2 content increases by only 5 ppmv. The results further suggest that during periods of weakened Atlantic Meridional Overturning Circulation, a greater transport of salt into the North Pacific could lead to the establishment of the PMOC. [L. Menviel, A. Timmermann, O. Timm (IPRC); A. Mouchet (U. Liege); A. Abe Ouchi, M.O. Chikamoto, N. Harada, R. Ohgaito, Y. Okazaki

(JAMSTEC), 2010: The Pacific Meridional Overturning Circulation and its impact on global climate and the carbon cycle: Idealized modeling experiments, *Deep Sea Research* II, submitted.]

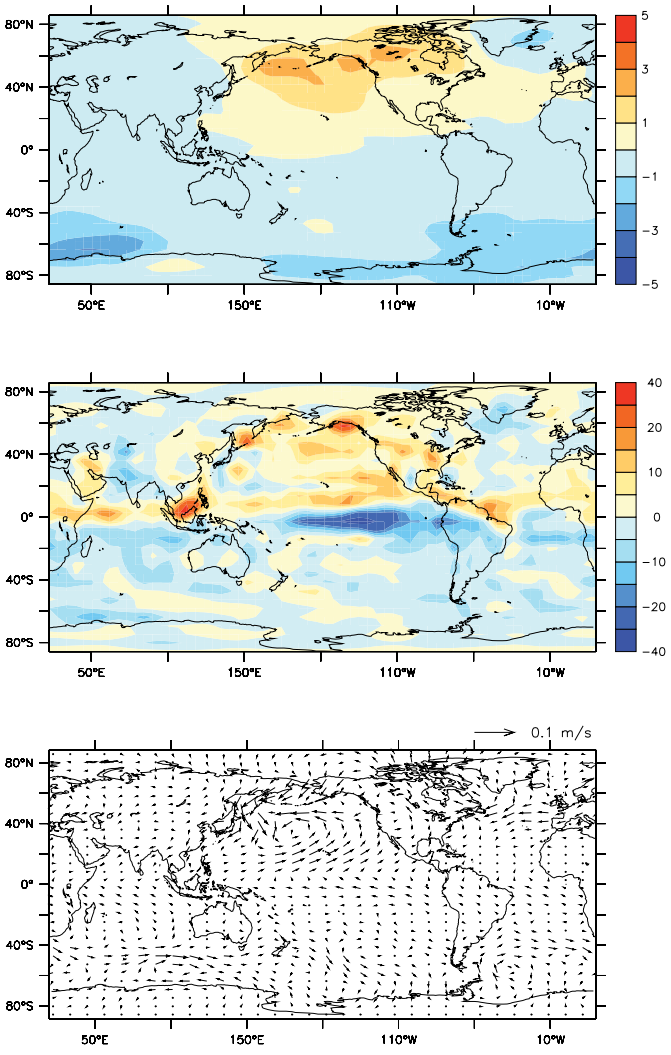

Figure 4.5. Top panel: 2-m air-temperature anomalies (°C); middle panel: precipitation anomalies (cm/yr); and bottom panel: windstress anomalies (Pa). Anomalies in the freshwater run averaged over years 900–1000 compared to the pre-industrial run.

Climate and biogeochemical responses to a rapid melting of the West Antarctic Ice Sheet during interglacial periods

In simulations with the Earth system model of intermediate complexity LOVECLIM, the effects during interglacial periods of a massive meltwater discharges from the West Antarctic Ice Sheet (WAIS) were studied on the global-climate carbon cycle. Prescribing a meltwater pulse in the Southern Ocean that mimics a rapid disintegration of the WAIS, a substantial cooling of the Southern Ocean was simulated, accompanied by an equatorward expansion of the sea-ice margin and an intensification of the Southern Hemispheric Westerlies. The strong halocline around Antarctica leads to suppression of Antarctic Bottom Water (AABW) formation and to subsurface warming in areas where under present-day conditions AABW is formed. This subsurface warming at depths between 500–1500 m could lead to a thermal weathering of the WAIS grounding line and could thus provide a positive feedback that would accelerate the meltdown of the WAIS.

The model results further demonstrate that in response to the massive expansion of sea ice, marine productivity in the Southern Ocean decreases significantly. A retreat of the WAIS however does not lead to any significant changes in atmospheric CO_2. A comparison of the climate signature of a WAIS collapse with available paleoproxies suggests that a collapse of the WAIS could have occurred during marine isotopic stage 5e. [L. Menviel, A. Timmermann (IPRC), A. Mouchet (U. Liege), O. Timm (IPRC), 2010: Climate and biogeochemical response to a rapid melting of the West Antarctic Ice Sheet, *Paleoceanography*, submitted]

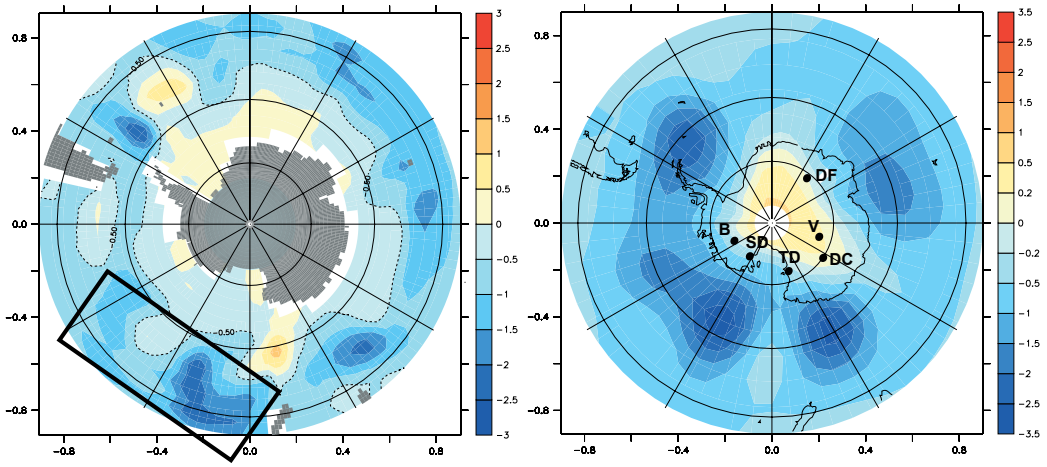

Figure 4.6. Left panel: Annual SST anomalies over the Southern Ocean 500 years into the WAIS experiment. The rectangle shows the area where a cooling due to a WAIS collapse is most likely to be recorded. Right panel: September–November 2 m air-temperature anomalies over Antarctica 500 years into the WAIS experiment. DF stands for Dome Fuji, V for Vostok station, DC for EPICA Dome C, TD for Taylor Dome, SD for Siple Dome and B for Byrd station.

The mechanism behind internally generated centennial-to-millennial-scale climate variations

The mechanism causing centennial-to-millennial-scale variability in the Atlantic Meridional Overturning Circulation (AMOC) in the Earth system model of intermediate complexity LOVECLIM was investigated. It was found that for different climate boundary conditions, such as low obliquity values (22.1) or albedo during the Last Glacial Maximum (LGM), internally generated centennial-to-millennial-scale variability occurs in the North Atlantic region. Stochastic excitations of the density-driven overturning circulation in the Nordic Seas can create regional sea-ice anomalies and a subsequent reorganization of the atmospheric circulation. The resulting remote atmospheric anomalies over Hudson Bay can release freshwater pulses into the Labrador Sea and significantly increase snowfall in this region leading to a subsequent reduction of convection. The millennial-scale AMOC oscillations disappear if LGM bathymetry (with closed Hudson Bay) is prescribed or if freshwater pulses are suppressed artificially. Furthermore, the study documents the process of the AMOC recovery as well as the response of the global marine and terrestrial carbon cycle to centennial-to-millennial-scale AMOC variability. [T. Friedrich, A. Timmermann L. Menviel, O. Timm (IPRC); A. Mouchet (U. of Liege); D. Roche (Laboratoire des Sciences du Climat et de l'Environnement), 2010: The mechanism behind internally generated centennial-to-millennial scale climate variability in an Earth system model of intermediate complexity, *Geoscientific Model Development*, submitted]

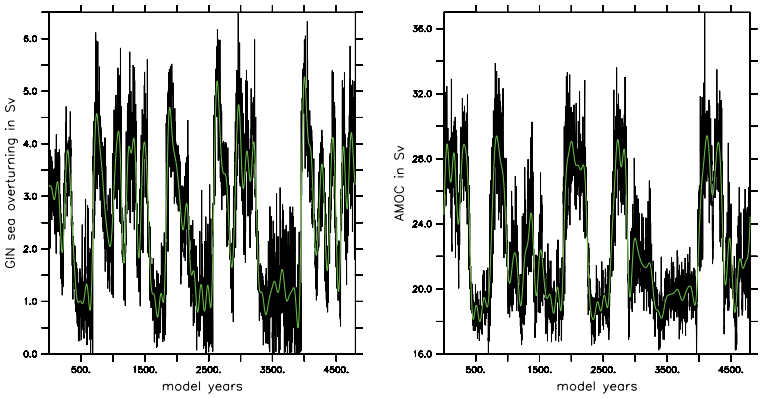

Figure 4.7. Left panel: Greenland Irminger Norwegian Sea overturning circulation; and right panel: maximum of Atlantic overturning circulation (units Sv) in a model simulation using an obliquity value of 22.1. A low-pass filter of 50 years was applied for green lines.

Precessionally paced Northern Hemispheric meltwater pulses and the build-up of the Northern Hemispheric ice sheets

Compared to the rapid glacial terminations, the build-up of glacial ice sheets in the Northern Hemisphere took tens of thousands of years. During the build-up phase, the growing ice sheets were subjected to major orbitally induced summer insolation changes, without experiencing complete disintegration. The reason for this behavior still remains elusive. Here it is proposed that between 110–60 ka B.P., increased summer insolation in high northern latitudes triggered massive instabilities of the Northern Hemispheric ice sheets about every 20 ka, leading to glacial meltwater pulses (Figure 4.8) and subsequent disruptions of the Atlantic Meridional Overturning Circulation (AMOC). Such behavior can be simulated with the Earth system model of intermediate complexity LOVECLIM using mass-balance of the Eurasian and Laurentide ice sheets. The associated severe cooling of the northern extratropics may have offset the warming trends driven by increased precessional summer insolation. This temperature response diminished the melting trend and stabilized the ice sheets. The results suggest that the competition between the direct insolation changes and the indirect climate response to AMOC disturbances may be an important factor in shaping glacial – interglacial cycles. [A. Timmermann, (IPRC), J. Knies GFZ (German Research Centre for Geosciences), O. Elison Timm (IPRC), A. Abe Ouchi (JAMSTEC), T. Friedrich (IPRC), 2010: Precessionally paced Northern Hemispheric meltwater pulses promote build-up of glacial ice sheets 60-115 ka B.P., *Paleoceanography*, doi:10.1029/2010PA001933, in press]

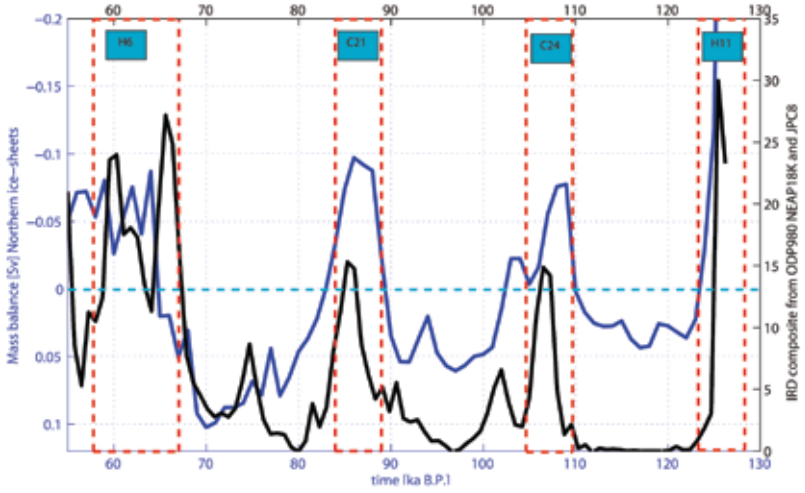

Figure 4.8. Simulated mass-balance values (Sv) for Northern Hemisphere ice sheets obtained from transient glacial–interglacial LOVECLIM climate model experiment in blue; composite of North Atlantic ice-rafted detritus (a measure for iceberg intensity) data from sediment cores NEAP18K, ODP908 and JPC8 in black.

Chapter 5: DEVELOPMENTS AT THE ASIA-PACIFIC DATA-RESEARCH CENTER (APDRC)

Data Services

The overarching goal of the APDRC data services is to provide easy access to the local and remote global climate database and products, and to provide the required data management and metadata for their easy application. This includes both the data-management (DM) tasks and the maintenance and improvements of the data-server systems (DSS). In the past, these two activities were kept as separate entities. As the APDRC continues to evolve, these two components have become more tightly integrated and are discussed together in this section.

During the past year, the APDRC maintained a wide suite of data transport and discovery servers, including OPeNDAP-based THREDDS DODS Server (TDS); GrADS DODS Server (GDS) and DAPPER; a Live Access Server (LAS); and DCHART. The LAS was upgraded to a new version and after testing, it was included as an optional service on the APDRC system (the older version provides some capabilities not available on the new version). A major effort was undertaken to produce two identical systems (additional hardware was purchased and configured) in order to provide a seamless backup in case of problems with one of the systems. Moreover, an older machine was reconfigured to be used exclusively for OFES data services.

The main increase in APDRC data archives comes from the large acquisition of OFES outputs, daily downloads of high-resolution, global ocean model output from the Navy Layered Ocean Model (NLOM) and Navy Coastal Ocean Model (NCOM), and local implementation of the Hybrid Ocean Coordinate Model (HYCOM). The downloads include daily output from a real-time simulation as well as four weekly data sets from a forecast simulation. In addition, the APDRC maintains an archive from a regional atmospheric model (run at U. Hawaii) that has a wide variety of users. In all, the APDRC has archived about 86 TB of data: 80% of this is OFES; NLOM, NCOM, IROAM, and the Hawaii atmospheric model output occupy about 10%; the remaining 10% covers all the other data sets. Upgrades to the APDRC web pages include new additions to the projects page that lists brief descriptions of the projects that the ADPRC supports, along with direct links to these projects (http://apdrc.soest.hawaii.edu/projects).

Data Products

Gridded analyses from Argo float data

The APDRC has been a leader in the development of ocean products from the Argo drifting float program. At present more than three thousand Argo floats populate the world's oceans and report every ten days temperature and salinity measurements down to one to two thousand meters. The data are available in real-time from two central global data assembly centers (GDACs), and in delayed mode from several regional DACs. The data are difficult for most users to handle, since the fields are not gridded; data are

stored by float, so profiles are functions of location. The APDRC has been trying to alleviate some of the burden on researchers and other users by creating horizontally, and optionally vertically, gridded and interpolated products. For example, using a variational interpolation technique, horizontal potential temperature, salinity, and depth on standard isopycnals are available on a 1-degree grid.

These data products are freely available at the APDRC web site and can enhance research activities beyond the IPRC. Additional effort has been placed on computed quantities, such as mixed layer depth, absolute dynamic height and other hydrographic variables at standard levels, horizontally on a 1-degree grid.

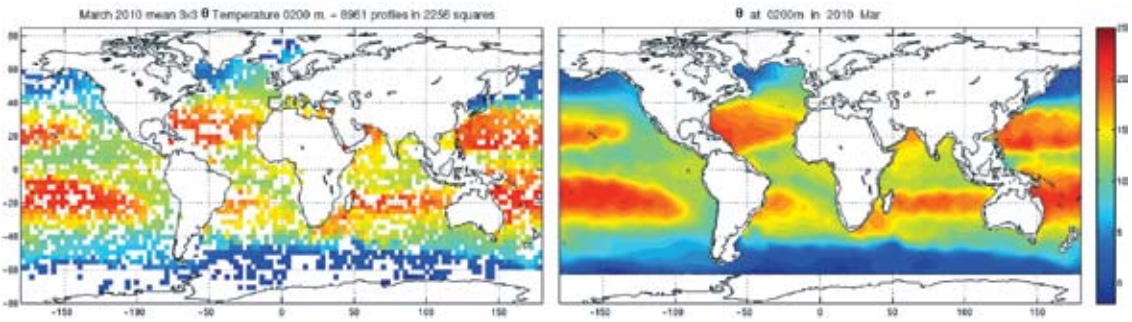

Figure 5.1. An example of the Argo plots that can be created at the APDRC project website. This sample shows potential temperature at a depth of 200 m for March 2010: (left) as observed by Argo floats averaged over 3-degree bins and (right) the interpolated IPRC product (unit is °C).

Surface CUrrents assessed from a Diagnostic model (SCUD)

A project is underway at the APDRC to produce estimates of surface current velocities. This product, called *Surface CUrrents from a Diagnostic model (SCUD)*, was produced by using satellite wind and altimetry data to estimate surface velocities consistent with trajectories of Lagrangian drifters (Figure 5.2). SCUD is for public use and freely available on the APDRC servers. The product is expected to support studies of marine debris and complements a previously developed statistical model that outlines main

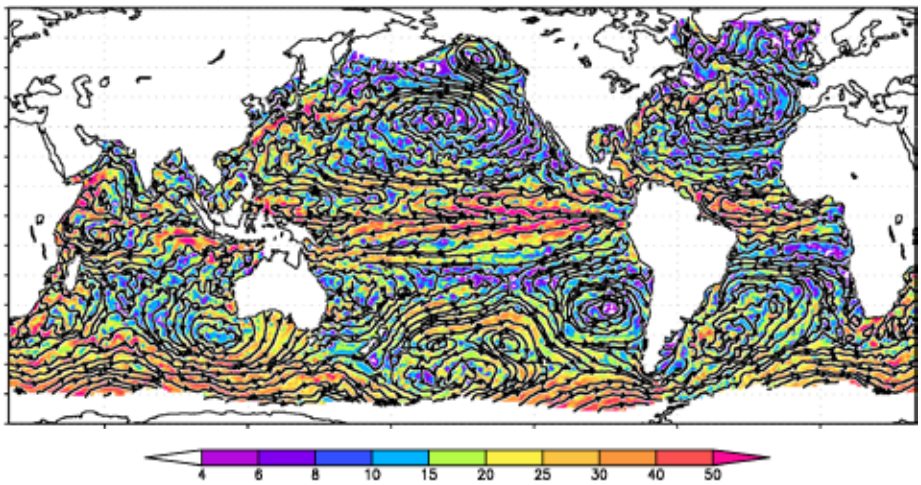

Figure 5.2. The streamlines of the Surface CUrrent Diagnostic velocity on August 20, 2008. Colors indicate speed and units are in cm/s.

areas of debris aggregation. The project is a collaboration with the NOAA Marine Debris Program, AOML, and National Fish and Wildlife Foundation. [N. Maximenko and J. Hafner (IPRC), 2010: SCUD: Surface CUrrents from diagnostic model, IPRC Tech. Note #5, 17pp.; N. Maximenko, J. Hafner (IPRC), and P. Niiler (SIO): Pathways of marine debris derived from trajectories of Lagrangian drifters, submitted]

Marine wind-product development

Surface wind speed affects air–sea interactions. Ship-based measurements of sea-surface wind speed, however, display a spurious upward trend with anemometer height measurements. To correct this bias, a new sea-surface wind dataset – the Wave and Anemometer-based Sea-surface Wind (WASWind) dataset – was constructed from ship-based observations of wind speed and wind wave height. This data set substantially reduces the spurious upward trend in wind speed, and is available from 1950 to 2008 for climate-change studies. WASWind features rich spatial structures in the trend pattern over the 58 years, making it a valuable dataset for studies of climate change on regional scales. Not only does the combination of ship-based observations of winds and wind wave-height successfully reproduce major modes of seasonal-to-decadal variability, but the trend patterns are also physically consistent with sea level pressure (SLP) measurements. WASWind is in close agreement with wind changes in satellite measurements of the Special Sensor Microwave Imager (SSM/I) for the last two decades (Figure 5.3). The agreement in trend pattern with such independent observations illustrates the utility of WASWind for climate-trend analysis. [H. Tokinaga and S.-P. Xie (IPRC): Wave and Anemometer-based Sea-surface Wind (WASWind) for climate change analysis, submitted]

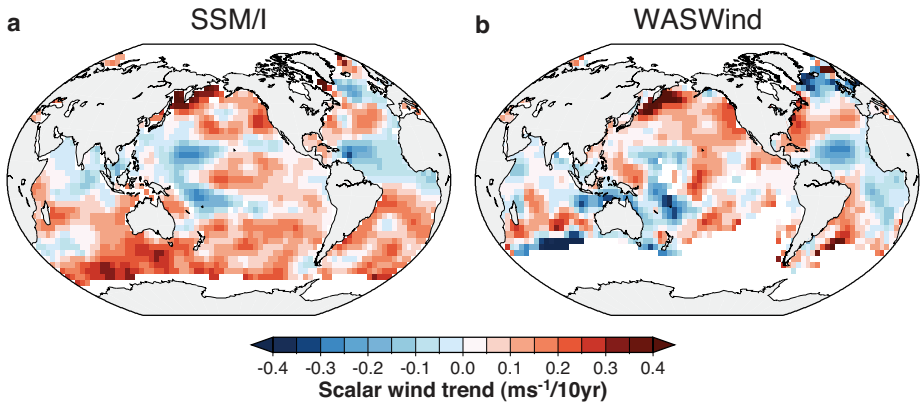

Figure 5.3. Linear trends in surface scalar-mean wind for a 20-year period from July 1987 to August 2006 derived from (a) SSM/I and (b) WASWind.

Development of a dynamical precipitation prediction system for the U.S. Affiliated Pacific Islands (USAPI) based on the CFS

The current operational seasonal precipitation prediction system for the U.S. Affiliated Pacific Islands (USAPI) is based on empirical methods. To see whether forecasts would be improved using the fully coupled NCEP Climate Forecast System (CFS), the 15-member ensemble retrospective forecasts (i.e, hindcasts) for the USAPI were analyzed for the period 1982–2005 from a deterministic [anomaly correlation coefficient (ACC)] and a probabilistic [Heidke Skill Score (HSS) and Rank Probability Skill score (RPSS)] perspective.

The CFS has ACC values higher than 0.8 (up to 7-month lead) in predicting tropical central to eastern Pacific SST anomalies, and for all seasons except boreal summer. While the mechanisms responsible for El Niño and for the regional and global impacts may differ in different years, CFS demonstrates high skill in capturing the phase and amplitude of SST anomalies associated with all the Niño indices. The model's ability to hindcast equatorial Pacific precipitation anomalies are also reflected in its high skill in capturing the teleconnection into the tropical Indian Ocean.

Figure 5.4 summarizes the overall skill (both deterministic and probabilistic) of CFS in hindcasting seasonal rainfall anomalies over the USAPI. For the west Pacific, the hindcasts for winter rainfall variations have the highest skill, followed by spring and summer; the hindcasts for boreal fall rainfall are poor. In the South Pacific, for leads of 0 to 4 months, the hindcasts for winter and spring rainfall are more skilled than for summer. For Hawaii, at shorter leads and for all seasons except fall, rainfall hindcasts are skilful and probably useful too. Results suggest that an operational dynamical system of seasonal rainfall prediction for USAPI is feasible. [K.P. Sooraj, H. Annamalai (IPRC); A. Kumar and H. Wang (Climate Prediction Center): Development of a dynamical precipitation prediction system for the U.S. Affiliated Pacific Islands, submitted]

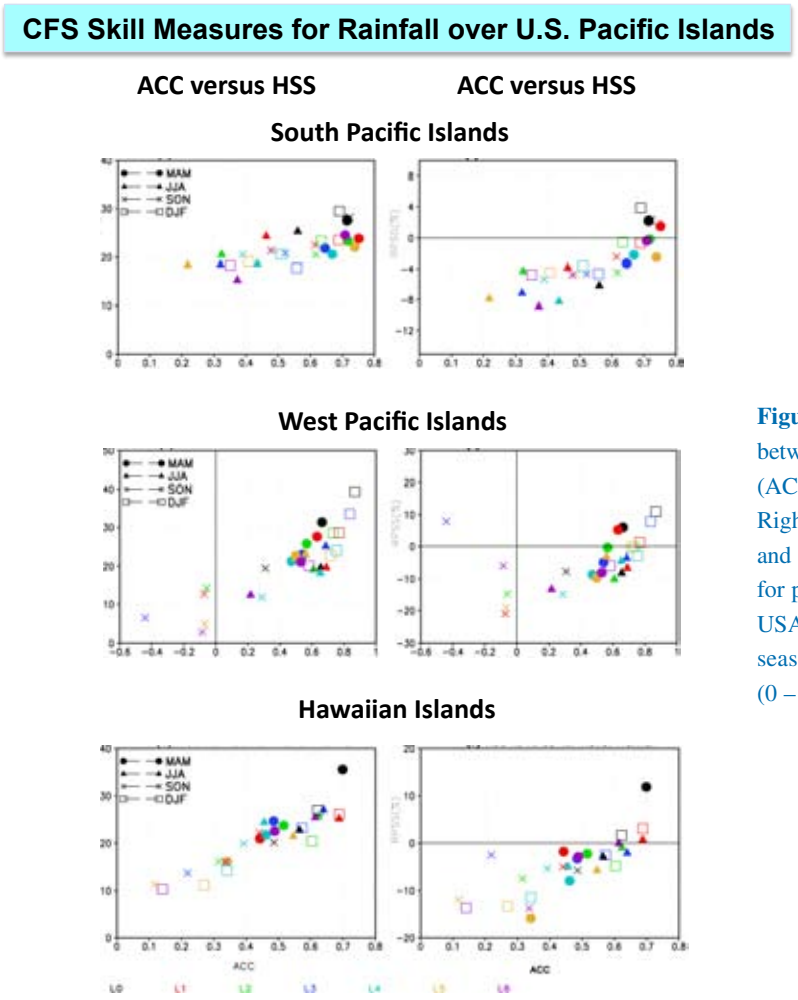

Figure 5.4. Left panels: Scatter plots between anomaly correlation coefficient (ACC) and Heidke skill scores (HSS). Right panels: scatter plots between ACC and Rank Probability skill score (RPSS) for precipitation over three regions of the USAPI. The results are for four standard seasons, and for all lead-time forecasts (0 – 6 months) shown in different colors.

PUBLICATIONS

Published Papers

2010

An, S.-I., Y.-G. Ham, J. S. Kug, A. Timmermann, J. Choi, and I.-S. Kang, 2010: The inverse effect of annual-mean state and annual-cycle changes on ENSO. *J. Climate,* **23** (5), 1095-1110, IPRC-644.

Annamalai, H., 2010: Moist dynamical linkage between the equatorial Indian Ocean and the south Asian monsoon trough. *J. Atmos. Sci*., **67**, 589-610. IPRC-635.

Calil, P. H. R., and K. J. Richards, 2010: Transient upwelling hot spots in the oligotrophic North Pacific. *J. Geophys. Res.-Oceans*, **115**, C02003, doi:10.1029/2009JC005360. IPRC-668.

Ceballos, L.I., E. Di Lorenzo, C. D. Hoyos, N. Schneider, and B. Taguchi, 2009: North Pacific Gyre Oscillation synchronizes climate fluctuations in the eastern and western boundary systems. *J. Climate*, **22** (19), 5163-5174. IPRC-590.

Ge, X., T. Li, and M. S. Peng, 2010: Cyclogenesis simulation of Typhoon Prapiroon (2000) associated with Rossby wave energy dispersion. *Mon. Weath. Rev.*, **138**, 42-54. IPRC-623.

Ge, X., T. Li, S. Zhang, and M. Peng, 2010: What causes the extremely heavy rainfall in Taiwan during Typhoon Morakot (2009)? *Atmos. Sc. Let.*, **11** (1), 46-50. IPRC-650.

McGregor, S., A. Timmermann, and O. Timm, 2010: A Unified Proxy for ENSO variability since 1650. *Climate of the Past*, **6** (1), 1-17. IPRC-637.

Sampe, T., and S.-P. Xie, 2010: Large-scale dynamics of the Meiyu-Baiu rain band: Environmental forcing by the westerly jet. *J. Climate*, **23**, 113-134. IPRC-620.

Sasaki,Y., N. Schneider, N. Maximenko, and K. Lebedev, 2010: Observational evidence for propagation of decadal spiciness anomalies in the North Pacific. *Geophys. Res. Lett.*, **37**, L07708, doi:10.1029/2010GL042716. IPRC-670.

Souma, K., and Y. Wang, 2010: A comparison between the effects of snow albedo and infiltration of melting water of Eurasian snow on East Asian summer monsoon rainfall. *J. Geophys. Res.-Atmos.*, **115**, D02115, doi:10.1029/2009JD012189. IPRC-652.

Steinhoff, T., T. Friedrich, S. E. Hartman, A. Oschlies, D. W. R. Wallace, and A. Körtzinger, 2010: Estimating mixed layer nitrate in the North Atlantic Ocean. *Biogeosciences*, **7**, 795-807. IPRC-672.

Steph, S., R. Tiedemann, M. Prange, J. Groeneveld, M. Schulz, A. Timmerman, D. Nuernberg, C. Saukel, and G.H. Haug, 2010: Early Pliocene increases in thermohaline overturning: A precondition for the development of the modern equatorial Pacific cold tongue. *Paleoceanography,* **25**, PA2202, doi:10.1029/2008PA001645. IPRC-643.

Timmermann, A., L. Menviel, Y. Okumura, A. Schilla, U. Merkel, O. Timm, A. Hu, B. Otto-Bliesner, and M. Schulz, 2010: Towards a quantitative understanding of millennial-scale Antarctic Warming events. *Quaternary Science Reviews*, **29**, 74-85. IPRC-610.

Wang, B., Z. Wu, C.-P. Chang, J. Liu, J. Li, and T. Zhou, 2010: Another look at interannual-to-interdecadal variations of the East Asian winter monsoon: The northern and southern temperature modes. *J. Climate*, **23**, 1495-1512.IPRC-653.

Wang, Y., and J. Xu, 2010: Energy production, frictional dissipation, and maximum intensity of a numerically simulated tropical cyclone. *J. Atmos. Sci.,* **67**, 97-116, IPRC-621.

Wu, S., L. Wu, Q. Liu, and S.-P. Xie, 2010: Development processes of the tropical Pacific meridional mode. *Advances in Atmospheric Sciences*, **27** (1), doi: 10.1007/s00376-009-8067-x. IPRC-609.

Xie, S.-P., C. Deser, G.A. Vecchi, J. Ma, H. Teng, and A.T. Wittenberg, 2010: Global warming pattern formation: Sea surface temperature and rainfall. *J. Climate*, **23**, 966–986. IPRC-632.

Yu, J., Y. Wang, and K. Hamilton, 2010: Response of tropical cyclone potential intensity to a global warming scenario in the IPCC AR4 CGCMs. *J. Climate*, **23**, 1354-1373. IPRC-648.

Yun, K.-S., K.-J. Ha, B. Wang, and R.-Q. Ding, 2010: Decadal cooling in the Indian summer monsoon after 1997/1998 El Niño and its impact on the East Asian summer monsoon. *Geophys. Res. Lett.*, **37**, L01805. IPRC 675.

Zeng, Z.-H., Y. Wang, and L.-S. Chen, 2010: A statistical analysis of vertical shear effect on tropical cyclone intensity change in the North Atlantic. *Geophys. Res. Lett.*, **37**, L02802. IPRC-663.

Zeng, Z.-H., Y. Wang, Y.-H. Duan, L.-S. Chen, and Z. Gao, 2010: On sea surface roughness parameterization and its effect on tropical cyclone structure and intensity. *Adv. Atmos. Sc.*, **27**, 337-355. IPRC-629.

Zheng, X.-T., S.-P. Xie, G. A. Vecchi, Q. Liu, and J. Hafner, 2010: Indian Ocean dipole response to global warming: Analysis of ocean-atmospheric feedbacks in a coupled model. *J. Climate*, **23** (5), 1240-1253. IPRC-638.

2009

Di Lorenzo, E., J. Fiechter, N. Schneider, A. Bracco, P.J.S. Franks, S. J. Bograd, A.M. Moore, A. Thomas, W. Crawford, A. Pena, and A. Herman, 2009: Nutrient and salinity decadal variations in the central and eastern North Pacific. *Geophys. Res. Lett.*, **36**, doi:10.1029/2009GL038261. IPRC-613.

Du, Y., S.-P. Xie, G. Huang, and K. Hu, 2009: Role of air-sea interaction in the long persistence of El Niño-induced North Indian Ocean warming. *J. Climate*, **22** (8), 2023-2038. IPRC-558.

Friedrich, T., and A. Oschlies, 2009: Basin-scale pCO_2 maps estimated from ARGO float data: A model study. *J. Geophys. Res.-Oceans*, **114**, C10012, doi:10.1029/2009JC005322. IPRC-624.

Friedrich, T., and A. Oschlies, 2009: Neural network-based estimates of North Atlantic surface pCO2 from satellite data: A methodological study. *J. Geophys. Res.-Oceans*, **114**, doi:10.1029/2007JC00464. IPRC-581.

Friedrich, T., A. Timmermann, L. Menviel, O. Timm, A. Mouchet, and D.M. Roche, 2009: Orbital modulation of millennial-scale climate variability in an earth system model of intermediate complexity. *Clim. Past Discuss.*, **5**, 2019-2051. IPRC-622.

Fu, X., B. Wang, Q. Bao, P. Liu, and J.-Y. Lee, 2009: Impacts of initial conditions on monsoon intraseasonal forecasting. *Geophys. Res. Lett.*, **36**, L08801; doi:10.1029/2009GL037166. IPRC-603.

Fu, X., and B. Wang, 2009: Critical roles of the stratiform rainfall in sustaining the Madden-Julian Oscillation: GCM Experiments. *J. Climate*, **22** (14) 3939–3959. IPRC-602.

Furue, R., J. P. McCreary, and Z. Yu, 2009: Dynamics of the northern Tsuchiya Jet. *J. Phys. Oceanogr.*, **39** (9), 2024-2051. IPRC-586.

Hong, C.-C., and T. Li, 2009: The extreme cold anomaly over Southeast Asia in February 2008: Roles of ISO and ENSO. *J. Climate*, **22**, 3786-3801. IPRC-580.

Kajikawa, Y., T. Yasunari, and B. Wang, 2009: Decadal change in intraseasonal variability over the South China Sea. *Geophys. Res. Lett.*, **36**, L06810; doi:10.1029/2009GL037174. IPRC-598.

Kajikawa, Y., B. Wang, and J. Yang, 2009: A multi-time scale Australian monsoon index. *Int. J. Climatol.*, doi: 10.1002/joc.1955. IPRC-608.

Kashino Y., N. Espana, F. Syamsudin, K.J. Richards, T. Jensen, P. Dutrieux and A. Ishida, 2009: Observations of the North Equatorial Current, Mindanao Current, and the Kuroshio Current system during the 2006/7 El Niño and 2007/08 La Niña. *J. Oceanogr.*, **65**, 325-333. IPRC-562.

Kida, S., and K.J. Richards, 2009: Seasonal sea surface temperature variability in the Indonesian Seas. *J. Geophys. Res.-Oceans*, **114**, C06016, doi:10.1029/2008JC005150. IPRC-607.

Kikuchi, K., and B. Wang, 2009: Global perspective of the Quasi-Biweekly Oscillation. *J. Climate,* **22** (6), 1340-1359. IPRC-550.

Kubota, H., and B. Wang, 2009: How much do tropical cyclones affect seasonal and interannual rainfall variability over the western North Pacific? *J. Climate*, **22**, 5495-5510. IPRC-676

Lauer, A., V. Eyring, J. J. Corbett, C. Wang, and J. J. Winebrake, 2009: Assessment of near-future policy instruments for oceangoing shipping: impact on atmospheric aerosol burdens and the Earth's radiation budget. *Environ. Sci. Technolol.*, **43** (15), 5592–5598. IPRC-618.

Lauer, A., Y. Wang, V. T. J. Phillips, C. S. McNaughton, R. Bennartz, and A. D. Clarke, 2009: Simulating Marine Boundary Layer Clouds over the Eastern Pacific in a Regional Climate Model with Double-Moment Cloud Microphysics. *J. Geophys. Res.-Atmos.*, **114**, D21205. IPRC-625.

Li, T., and C. Zhou, 2009: Planetary scale selection of the Madden-Julian Oscillation. *J. Atmos. Sci.*, **66**, 2429-2443. IPRC-606.

Liu, J., B. Wang, Q. Ding, X. Kuang, W. Soon, and E. Zorita, 2009: Centennial variations of the global monsoon precipitation in the sast millennium: Results from ECHO-G Model. *J. Climate*, **22** (9), 2356–2371. IPRC-627.

Liu, P., M. Satoh, B. Wang, H. Fudeyasu, T. Nasuno, T. Li, H. Miura, H. Taniguchi, H. Masunaga, X. Fu, and H. Annamalai, 2009: An MJO Simulated by the NICAM at 14-km and 7-km Resolutions. *Mon. Wea. Rev.*, **137**, 3254-3268. IPRC-614.

Liu, P., Y. Kajikawa, B. Wang, A. Kitoh, T. Yasunari, T. Li, H. Annamalai, X. Fu, K. Kikuchi, R. Mizuta, K. Rajendran, D. E. Waliser, and D. Kim, 2009: Tropical Intraseasonal Variability in the MRI-20km60L AGCM. *J. Climate*, **22** (8), 2006–2022, doi: 10.1175/2008JCLI2406.1. IPRC-556.

Loeptien, U., C. Eden, A. Timmermann, and H. Dietze, 2009: Effects of biologically induced differential heating in an eddy-permitting coupled ocean-ecosystem model. *J. Geophys. Res.-Oceans*, **114,** C06011, doi:10.1029/2008JC004936. IPRC-647.

Lu, B., L. Pandolfo, and K. Hamilton, 2009: Nonlinear representation of the quasi-biennial oscillation. *J. Atmos. Sci.,* **66**, 1886-1904. IPRC-501.

Maximenko, N., P. Niiler, M.-H. Rio, O. Melnichenko, L. Centurioni, D. Chambers, V. Zlotnicki, and B. Galperin, 2009: Mean dynamic topography of the ocean derived from satellite and drifting buoy data using three different techniques. *J. Atmos. Oceanic Tech.*, **26** (9), 1910-1919. IPRC-576.

Okumura,Y.M., C. Deser, A. Hu, A. Timmermann and S.-P. Xie, 2009: North Pacific climate response to freshwater forcing in the Subarctic North Atlantic: Oceanic and atmospheric pathways. *J. Climate*, **22** (6), doi: 10.1175/2008JCLI2511.1, IPRC-619.

Peng, J., T. Li, M.S. Peng, and X. Ge, 2009: Barotropic instability in the tropical cyclone outer region. *Quart. Jour. Royal Met. Socc*, **135**, 851-864 IPRC-588.

Phillips,V. T. J., C. Andronache, B. Christner, C. E. Morris, D. C. Sands, A. Bansemer, A. Lauer, C. McNaughton, and C. Seman, 2009: Potential impacts from biological aerosols on ensembles of continental clouds simulated numerically. *Biogeosciences*, **6**, 987-1014. IPRC-634.

Qu, T., and J. Chen, 2009: A North Pacific decadal variability in subduction rate. *Geophys. Res. Lett*, **36**, L22602, doi:10.1029/2009GL040914, IPRC-641.

Qu, T., S. Gao, I. Fukumori, R.A. Fine, and E.J. Lindstrom, 2009: Origin and pathway of equatorial 13°C water in the Pacific identified by a simulated passive tracer and its adjoint. *J. Phys. Oceanogr.*, **39** (8), 1836-1853. IPRC-

Qu, T., and Y. T. Song, 2009: Mindoro Strait and Sibutu Passage transports estimated from satellite data. *Geophys. Res. Lett.*, **36,** L09601, doi:10.1029/2009GL037314. IPRC-604.

Richards, K. J., S.-P. Xie, and T. Miyama: Vertical mixing in the ocean and its impact on the coupled ocean-atmosphere system in the Eastern Tropical Pacific. *J. Climate*, **22** (13), 3703–3719. IPRC-560.

Sato, T., H. Miura, M. Satoh, Y. N. Takayabu, and Y. Wang, 2009 : Diurnal cycle of precipitation in the tropics simulated in a global cloud-resolving model. *J. Climate,* **22**, 4809-4826. IPRC-631.

Seo, H., S.-P. Xie, R. Murtugudde, M. Jochum, and A. J. Miller, 2009: Seasonal effects of Indian Ocean freshwater forcing in a regional coupled model. *J. Climate*, **22**, 6577-6596. IPRC-626.

Small, R. J., K. J. Richards, S.-P. Xie, P. Dutrieux, and T. Miyama, 2009: Damping of Tropical Instability Waves caused by the action of surface currents on stress. *J. Geophys. Res.-Oceans*, **114**, C04009, doi:10.1029/2008JC005147 IPRC-605.

Souma, K., and Y. Wang, 2009: Improved simulation of the East Asian summer monsoon rainfall with satellite-derived snow water equivalent data. *Mon. Wea. Rev.*, **137** (6), 1790–1804. IPRC-573.

Stott, L., J. Southon, A. Timmermann, and A. Koutavas, 2009: A benthic radiocarbon age anomaly at intermediate depth in the Pacific Ocean during the last deglaciation. *Paleoceanography*, **24,** PA2223, doi:10.1029/2008PA001690. IPRC-579.

Stowasser, M., H. Annamalai, and J. Hafner, 2009: Response of the South Asian Summer Monsoon to global warming: Mean and Synoptic systems. *J. Climate,* **22** (4), 1014-1036. IPRC-545.

Taguchi, B., H. Nakamura, M. Nonaka, and S.-P. Xie, 2009: Influences of the Kuroshio/Oyashio Extensions on air-sea heat exchanges and storm-track activity as revealed in regional atmospheric model simulations for the 2003/4 cold season. *J. Climate*, **22** (24), 6536-6560. IPRC-633.

Tanimoto, Y., S.-P. Xie, K. Kai, H. Okajima, H. Tokinaga, T. Murayama, M. Nonaka, and H. Nakamura, 2009: Observations of marine atmospheric boundary layer transitions across the summer Kuroshio Extension. *J. Climate*, **22** (6), 1360-1374. IPRC-553.

Timm, O., and H. F. Diaz, 2009: Synoptic-Statistical Approach to Regional Downscaling of IPCC 21st Century Climate Projections: Seasonal Rainfall over the Hawaiian Islands. *J. Climate*, **22** (16), 4261-428. IPRC-596.

Timmermann, A., O. Timm, L. Stott, and L. Menviel, 2009: The roles of CO_2 and orbital forcing in driving Southern Hemispheric temperature variations during the last 21,000 years. *J. Climate*, **22** (7), 1626-1640. IPRC-555.

Timmermann, A., and L. Menviel, 2009: What drives climate flip-flops? *Science*, **325**, 273-274.IPRC-645.

Tokinaga, H., and S.-P. Xie, 2009: Ocean tidal cooling effect on summer sea fog over the Okhotsk Sea. *J. Geophys. Res.-Atmos.*, **114**, D14102, doi:10.1029/2008JD011477. IPRC-612.

Tokinaga, H., Y. Tanimoto, S.-P. Xie, T. Sampe, H. Tomita, and H. Ichikawa, 2009: Ocean frontal effects on the vertical development of clouds over the western North Pacific: In situ and satellite observations. *J. Climate*, **22** (16), 4241-4260. IPRC-599.

Vialard, J., S.S.C Shenoi, J. P. McCreary, D. Shankar, F. Durand, V. Fernando, and S. R. Shetye, 2009: Intraseasonal response of the Northern Indian Ocean coastal waveguide to the Madden-Julian Oscillation. *Geophys. Res. Lett.*, **36**, L14606, doi:10.1029/2009GL038450, IPRC-617.

Wang, B., J.-Y. Lee and co-authors, 2009: Advance and Prospect of Seasonal Prediction: Assessment of the APCC/CliPAS 14-model ensemble retroperspective seasonal prediction (1980-2004). *Climate Dyn.*, **33**, doi:10.1007/s00382-008-0460-0. IPRC-678.

Wang B., F. Huang, Z. Wu, J. Yang, X. Fu, and K. Kikuchi, 2009: Multi-scale climate variability of the South China Sea monsoon: A review. *Dyn. of Atmos. and Oceans*, **47** (1-3), 15-37. IPRC-554.

Wang, B., Q. Ding, and P.V. Joseph, 2009: Objective definition of the Indian summer monsoon onset. *J. Climate,* **22** (12), 3303–3316. IPRC-561.

Wang, B., J. Liu, J. Yang, T.-J. Zhou, and Z. Wu, 2009: Distinct principal modes of early and late summer rainfall anomalies in East Asia. *J. Climate*, **22** (13), 3864–3875. IPRC-589.

Wang, Y., 2009: How do outer spiral rainbands affect tropical cyclone structure and intensity? *J. Atmos. Sci.*, **66** (5), 1250-1273 PRC-572.

Wang, Y.-Q., Y. Wang, and H. Fudeyasu, 2009: Roles of Typhoon Songda (2004) in producing distantly located heavy rainfall in Japan. *Mon. Wea. Rev.*, **137**, 3699-3716. IPRC-630.

Winebrake, J. J., J. J. Corbett, E. H. Green, A. Lauer, and V. Eyring, 2009: Mitigating the health impacts of pollution from oceangoing shipping: An assessment of low-sulfur fuel mandates. *Environ. Sc. and Techn.*, **43** (13), 4776-4782. IPRC-616.

Wu, B., T. Zhou, and T. Li, 2009: Seasonally evolving dominant interannual variability modes of East Asian Climate. *J. Climate*, **22** (11), 2992–3005, IPRC-601.

Wu, B., T. Zhou, and T. Li, 2009: Contrast of rainfall-SST relationships in the western North Pacific between the ENSO developing and decaying summers. *J. Climate,* **22,** 4398-4405. IPRC-600.

Wu, Z. W., B. Wang, and J. P. Li, 2009: An empirical seasonal prediction model of the East Asian summer monsoon using ENSO and NAO. *J. Geophys. Res.*, **114**, D18120, doi:10.1029/2009JD011733. IPRC-677.

Yaremchuk, M., J. McCreary, Z. Yu, and R. Furue: The South China Sea throughflow retrieved from climatological data. *J. Phys. Oceanogr.*, **39** (3), 753-767. IPRC-543.

Yaremchuk, M., D. Nechaev, and G. Panteleev, 2009: A method of successive corrections of the control subspace in the reduced-order variational data assimilation. *Mon. Wea. Rev.,* **137**(9), 2966-2978. IPRC-583.

Zeng, L., Y. Du, S.-P. Xie, and D. Wang, 2009: Barrier Layer in the South China Sea during summer 2000. *Dyn. Atmos. and Oceans,* **47** (1-3), 38-54. IPRC-544.

Zhang, S.-P., S.-P. Xie, Q.-Y. Liu, Y.-Q., Yang, X.-G. Wang, and Z.-P. Ren, 2009: Seasonal variations of Yellow Sea fog: Observations and mechanisms. *J. Climate*, **22** (24), 6758-6772. IPRC-611.

Zhou, X., and B. Wang, 2009: From concentric eyewall to annular hurricane: A numerical study with the cloud-resolved WRF model. *Geophys. Res. Lett.*, **36**, L03802, doi:10.1029/2008GL036854, IPRC-575.

Zinke, J., M. Pfeiffer, O. Timm, W.-Ch. Dullo, and G.J.A. Brummer: Western Indian Ocean Marine and Terrestrial Records of Climate Variability: A Review and new Concepts on Land-Ocean Interactions since AD 1660. *Intern. J. Earth Sciences*, **98** (1), 115-133. IPRC-547.

In Press

Annamalai, H., S. Kida and J. Hafner: Potential impact of the tropical Indian Ocean - Indonesian Seas on El Niño characteristics. *J. Climate*, IPRC-680.

Ascani, F., E. Firing, P. Dutrieux, J. P. McCreary, A. Ishida: Deep equatorial ocean circulation induced by a forced-dissipated Yanai beam. *J. Phys. Oceanogr.*, IPRC-662.

Chen, J.-M., T. Li, and C.-F. Shih: Tropical cyclone and monsoon induced rainfall variability in Taiwan. *J. Climate*, IPRC-685.

Chowdary, J. S., S.-P. Xie, J.-J. Luo, J. Hafner, S. Behera, Y. Masumoto, and T. Yamagata: Predictability of Northwest Pacific climate during summer and the role of the tropical Indian Ocean. *Clim. Dyn.*, IPRC-640.

Gu, D., T. Li, Z. Ji, and B. Zheng: On the Western North Pacific Monsoon, Indian Monsoon and Australian Monsoon phase relations. *J. Climate*, IPRC-682.

Gu, D.-J., T. Li, Z.-P Ji, and B Zheng: Connection of the South China Sea summer monsoon to maritime continent convection and ENSO. *Journal of Tropical Meteorology*, IPRC-654.

Ham,Y.-G. J.-S. Kug, I.-S. Kang, A. Timmermann: Impact of diurnal atmosphere-ocean coupling on tropical climate in a coupled GCM. *Climate Dynamics*, IPRC-646.

Hong, C.-C., T. Li, H. Lin, and Y.-C. Chen: Asymmetry of the Indian Ocean basin-wide SST anomalies. *J. Climate*, IPRC-674.

Kikuchi, K., and B. Wang: Formation of tropical cyclones in the northern Indian Ocean associated with two types of tropical intraseasonal oscillation modes. *J. Meteor. Soc. Japan*, IPRC-657.

Kikuchi, K., and B. Wang: Spatio-temporal wavelet transform and the multiscale behavior of the Madden-Julian Oscillation. *J. Climate*, IPRC-664.

Li, C., T. Li, J. Liang, D. Gu, A. Lin and B. Zheng: Interdecadal variations of meridional winds in the South China Sea and their relationship with summer climate in China. *J. Climate*, IPRC-661.

Matsumura, S., G. Huang, S.-P. Xie, and K. Yamazaki: SST-forced and internal variability of the atmosphere in an ensemble GCM simulation. *J. Meteor. Soc. Japan*, IPRC-659.

Melnichenko, O. V., N. A. Maximenko, N. Schneider, H. Sasaki: Quasi-stationary striations in basin-scale oceanic circulation: Vorticity balance from observations and eddy-resolving model. *Ocean Dynamics*, IPRC-666.

Minobe, S., M. Miyashita, A. Kuwano-Yoshida, H. Tokinaga, S.-P. Xie: Atmospheric response to the Gulf Stream: Seasonal variations. *J. Climate*, IPRC-671.

Murakami, H., and B. Wang: Future change of North Atlantic tropical cyclone tracks: Projection by a 20-km-mesh global atmospheric model. *J. Climate*, IPRC-679.

Richter, I., and S.-P. Xie: Moisture transport from the Atlantic to the Pacific basin and its response to North Atlantic cooling and global warming. *Climate Dynamics*, IPRC-660.

Sampe, T., H. Nakamura, A. Goto, W. Ohfuchi: Significance of a midlatitude SST frontal zone in the formation of a storm track and an eddy-driven westerly jet. *J. Climate*, IPRC-656.

Sasaki, H., S.-P. Xie, B. Taguchi, M. Nonaka, and Y. Masumoto: Seasonal variations of the Hawaiian Lee Countercurrent induced by the meridional migration of the trade winds. *Ocean Dynamics*, IPRC-639.

Shankar, D., S. G. Aparna, J. P. McCreary, I. Suresh, S. Neetu, F. Durand, S. S. C. Shenoi, M., A. Al Saafani: Minima of interannual sea-level variability in the Indian Ocean. *Progress in Oceanography*, IPRC-636.

Tanimoto, Y., T. Kajitani, H. Okajima, and S.-P. Xie: A peculiar feature of the seasonal migration of the South American rain band. *J. Meteor. Soc. Japan*, IPRC-655.

Timm, O., P. Koehler, A. Timmermann, L. Menviel: Mechanisms for the onset of the African Humid Period. *J. Climate*, IPRC-642.

Wang, B., Y. Yang, Q.-H. Ding, and F. Huang: Climate Control of Global Tropical Storm Days: El Niño and Global Warming. *Geophys. Res. Lett.*, IPRC-673.

Wu, B., T. Li, and T. Zhou: Asymmetry of atmospheric circulation anomalies over the western North Pacific between El Niño and La Niña. *J. Climate*, IPRC-683.

Wu, B., T. Li, and T. Zhou: Relative contributions of the Indian Ocean and local SST anomalies to the maintenance of the western North Pacific anomalous anticyclone during El Niño decaying summer. *J. Climate*, IPRC-684.

Xie, S.-P., Y. Du, G. Huang, X.-T. Zheng, H. Tokinaga, K. Hu, and Q. Liu: Decadal shift in El Niño influences on Indo-western Pacific and East Asian climate in the 1970s. *J. Climate*, IPRC-669.

Xu, J., and Y. Wang: Sensitivity of tropical cyclone inner core size and intensity to the radial distribution of surface entropy flux. *J. Atmos. Sci.*, IPRC-667.

Yoshida, S., B. Qiu, P. Hacker: Wind generated eddy characteristics in the lee of the island of Hawaii. *J. Geophys. Res.-Oceans*, IPRC-651.

Zhu, W., T. Li, X. Fu, and J.-J. Luo: Influence of the Maritime Continent on the boreal summer intraseasonal oscillation. *J. Meteor. Soc. Japan*, IPRC-681.

Zhuang, W., S.-P. Xie, D. Wang, B. Taguchi, H. Aiki, and H. Sasaki: Intraseasonal variability in sea surface height over the South China Sea. *J. Geophys. Res.-Oceans*, IPRC-658.

THE YEAR'S WORKSHOPS AND CONFERENCES

Date	Title
March 10, 2010	Joint JAMSTEC - IPRC Data-Research Workshop
February 26, 2010	Mini-Workshop on Climate Change: Modeling and Analysis
December 9 – 10, 2009	Second OFES International Workshop and ESC-IPRC Joint Workshop on Computationally-Intensive Modeling of the Climate System
July 13 – 15, 2009	Year of Tropical Convection (YOTC) Implementation Planning Meeting
June 1 – 2, 2009	Ninth Annual IPRC Symposium

THE YEAR'S SEMINARS

April 1, 2009 – March 31, 2010

Date	Speaker	Affiliation	Title
March 1, 2010	Masaru Inatsu	Hokkaido University, Sapporo, Japan	*Connecting global and regional atmospheric models: A two-way nesting approach*
*February 10, 2010	Ding Yihui	National Climate Center, Beijing, China	*Inter-decadal weakening of the Asian summer monsoon and its projection of future change in a warmer climate*
*February 3, 2010	In-Sik Kang	Seoul National University, Seoul, Korea	*MJO predictability: Impact of initialization*
*January 27, 2010	Masahiro Watanabe and Yoshimitsu Chikamoto	Center for Climate System Research, University of Tokyo, Tokyo, Japan	*Predictability of Pacific Decadal Oscillation and tropical Atlantic variability in hindcast experiments with the coupled climate model MIROC*
**January 20, 2010	Edward R. Cook	Columbia University, New York, New York	*Asian monsoon failure and mega-drought during the last millennium*
*January 13, 2010	Hisayuki Kubota	Japan Agency for Marine-Earth Science and Technology	*The recovery of historical typhoon track data over the Western North Pacific during the early 20th century*
**January 11, 2010	Claude Frankignoul	l'Université Pierre et Marie Curie, Paris, France	*Large-scale atmospheric response to North Pacific western boundary current variability*
December 22, 2009	Ming Feng	CSIRO, Floreal, Australia	*The eastward jet in the southeast Indian Ocean and western rock lobster recruitment*
*December 16, 2009	Jerry Meehl	National Center for Atmospheric Research, Boulder, Colorado	*The influence of the 11 year solar cycle on tropical Pacific climate*
**December 3, 2009	Tobias Friedrich	IPRC	*Towards basin-scale monthly maps of CO_2 uptake in the North Atlantic Ocean*
*October 7, 2009	Kevin Hamilton	IPRC	*The Kyoto Protocol, the Montreal Protocol and a perspective for the Copenhagen Conference*
*September 16, 2009	Yuqing Wang	IPRC	*What controls the inner-core size of tropical cyclones?*

Date	Speaker	Affiliation	Title
*September 9, 2009	Qinghong Zhang	Department of Atmospheric Sciences, Peking University, Beijing, China	*Hail climatology in China 1961–2005*
*September 2, 2009	Tim Li	IPRC	*Amplitude asymmetry of El Niño and La Niña in the eastern equatorial Pacific*
August 7, 2009	Masao Kanamitsu	Scripps Institution of Oceanography, San Diego, California	*Dynamical downscaling for climate study: Basic concepts, misunderstandings, and possible solutions*
July 31, 2009	Scott Power	Bureau of Meteorology, Melbourne, Australia	*The Pacific Climate Change Science Program*
July 20, 2009	Kazuyoshi Kikuchi	IPRC	*Understanding the multi-scale interaction of tropical convection*
July 17, 2009	Hiroki Tokinaga	IPRC	*Ocean-atmosphere interaction over SST fronts: Progress and future plan*
July 16, 2009	Ping Liu	IPRC	*Simulation of the convectively coupled waves, MJO, and QBO*
July 10, 2009	Oliver Timm	IPRC	*African Humid Periods during the Last 130,000 Years*
June 25, 2009	Wilbert Weijer	Los Alamos National Laboratory, Los Alamos, New Mexico	*Modal variability of the ocean circulation*

* Joint IPRC UH Mānoa Meteorology Department Seminar
** Joint IPRC UH Mānoa Oceanography Department Seminar

LUNCHEON DISCUSSIONS

April 1, 2009 – March 31, 2010

Date	Speaker	Affiliation	Title
March 23, 2010	Gang Huang	Institute of Atmospheric Physics, Chinese Academy of Sciences, Beijing, China	*Indian Ocean warming and its effects on East Asian summer climate*
March 17, 2010	Yoshiyuki Kajikawa	Hydrospheric Atmospheric Research Center, Nagoya University, Japan	*Long-term variability of the Asian monsoon rainfall and its seasonality*
March 16, 2010	Mehera Kidston	CSIRO, Sydney, Australia	*Parameter optimisations of a marine ecosystem model in the Southern Ocean*
March 4, 2010	Prasanth Divakaran	School of Earth Sciences, University of Melbourne, Australia	*Zonal features in the Southeast Indian Ocean as seen in Bluelink Reanalysis 2.1*
January 12, 2010	Viacheslav Kremenetskiy	P.P. Shirshov Institute of Oceanology, Moscow, Russia	*Black Sea dynamics: General aspects and recent results*
April 28, 2009	Bo Wu	LASG, Institute of Atmospheric Physics, Beijing, China	*What are the mechanisms that modulate the circulation over the western North Pacific during ENSO mature winter and decaying summer?*

IPRC VISITING SCHOLARS

The IPRC has a visiting scholar program. From April 2009 through March 2010, the following scholars visited the IPRC.

Name	Affiliation	Dates
Daisuke Inazu	Tohoku University, Sendai, Japan	06/08/09–06/12/09
Tommy Jensen	Naval Research Laboratory, Stennis Space Center, Mississippi	07/09/09–07/25/09
Raleigh Hood	University of Maryland Center for Environmental Science, Cambridge, Maryland	07/07/09–07/12/09
Gottfried Kirchengast	University of Graz, Graz, Austria	07/11/09–09/05/09
Qinghong Zhang	Peking University, Beijing, China	08/30/09–09/28/09
Wataru Sasaki	Japan Agency for Marine-Earth Science and Technology	09/01/09–10/31/09
Yueqing Li	Institute of Plateau Meteorology, China Meteorological Administration, Chengdu, China	09/09/09–09/14/09
Peter Huybers	Harvard University, Cambridge, Massachusetts	09/17/09–09/22/09
Mototako Nakamura	Japan Agency for Marine-Earth Science and Technology	10/01/09–10/31/09
Sun-Seon Lee	Pusan National University, Busan, Korea	10/08/09–10/30/09
Kyung-Soon Yun	Pusan National University, Busan, Korea	10/08/09–10/30/09
Anne Mouchet	Institut d' Astrophysique, Paris, France	10/09/09–10/16/09
Ajaya Mohan R.N. Santhakumari	University of Victoria, Victoria, Canada	10/18/09–10/30/09
Shan Gao	Institute of Oceanology, Qingdao, China	11/01/09–11/15/09
Wataru Ohfuchi	Japan Agency for Marine-Earth Science and Technology	12/03/09–12/17/09
Yoshio Kawatani	Japan Agency for Marine-Earth Science and Technology	12/08/09–03/05/10
Viacheslav Kremenetskiy	Russian Academy of Sciences, Moscow, Russia	12/19/09–02/21/10
Hisayuki Kubota	Japan Agency for Marine-Earth Science and Technology	01/10/10–01/23/10
Yusuke Okazaki	Japan Agency for Marine-Earth Science and Technology	01/12/10–03/30/10
In-Sik Kang	Seoul National University, Seoul, Korea	01/17/10–02/17/10
Edward Cook	Columbia University, New York, New York	01/17/10–01/25/10
Megumi Chikamoto	Japan Agency for Marine-Earth Science and Technology	01/25/10–01/30/10
Lixin Wu	Ocean University of China, Qingdao, China	01/20/10–02/28/10
Prasanth Divakaran	University of Melbourne, Melbourne, Australia	02/27/10–03/06/10
Yusuke Udagawa	Hokkaido University, Sapporo, Japan	03/02/10–03/19/10
Yoshiyuki Kajikawa	Nagoya University, Nagoya, Japan	03/13/10–03/18/10
Jian Liu	Chinese Academy of Sciences, China	03/08/10–05/20/10

IPRC RESEARCH SUPPORT

Institutional Support

Title	PI and Co-PIs	Agency	Amount	Period
JAMSTEC YR 13 (2009 – 2010)	K. Hamilton	JAMSTEC	$2,246,000	04/01/09–03/31/10
Support of Research at the International Pacific Research Center	Not applicable	*University of Hawai'i	$690,495	04/01/09–03/31/10
Data-Intensive Research and Model Development at the International Pacific Research Center	K. Hamilton PI S.P. Xie & P. Hacker	NASA	$5,225,000	03/01/07–02/29/12
Enhancement of Data and Research Activities at the IPRC	K. Hamilton PI P. Hacker & J. Potemra	NOAA/NESDIS	$1,218,000	07/01/08–06/30/09
Enhancement of Data and Research Activities at the IPRC	K. Hamilton PI P. Hacker & J. Potemra	NOAA/NESDIS	$1,742,160	07/01/09–06/30/10

* The University of Hawai'i also provides approximately 16,500 sq. ft. of office space to the IPRC

Individual Grants

Title	PI and Co-PIs	Agency	Amount	Period
Estimating Ocean Mixing and Form Drag in the Tropical Pacific	J. McCreary, R. Furue, P. Muller, K. Richards, N. Schneider	NASA	$343,161	02/01/10 – 01/31/13
Sustaining Rice Production in a Changing Climate: Testing Climate Uncertainties and Validating Selected Adaptation Techniques on Farmers Fields	H. Annamalai	Norwegian Embassy	$153,728	01/01/10–12/31/12
Basin-Scale Circulation and Mesoscale Dynamics of the Black Sea: Implications for Climate	N. Maximenko	US CRDF	$16,000	12/01/09–11/30/11
Assessing the Quality of Aquarius Sea Surface Salinity Measurements Using an Ocean State Estimation System	T. Qu	JPL / NASA	$145,248	11/17/09–03/31/12
Aquarius Salinity Calibration Error Quantification, Signal-To-Noise Analyses, and Resolution Studies	N. Maximenko	NASA	$538,206	10/01/09–09/30/13
Improve the Representation of Convection-PBL Interactions in Two Global General Circulation Models (CAM & ECHAM)	X. Fu, B. Wang	DOE	$491,580	09/15/09–01/31/11
Collaborative Research: Eddy Dynamics and Impacts of Low-Frequency Variations in the California Current System (supplemental)	N. Schneider	NSF	$382,619	08/19/09–02/29/12
Next Generation Aerosol-Cloud Microphysics for Advanced High-Resolution Climate Predictions	K. Hamilton	Univ of Wisconsin / DOE	$292,426	08/15/09–08/14/11
Mechanisms and Effects of Tropical Indian Ocean Variability	S.P. Xie	NSF	$525,408	08/15/09–07/31/13
Evaluation and Improvements of Cloud and Precipitation Physics in the Operational Hurricane WRF Model at NOAA/EMC	Y. Wang, V. Phillips	NOAA / JHT	$203,844	08/01/09–07/31/11
Collaborative Studies on Tropical Cyclone Intensification	T. Li	NPS	$96,144	06/11/09–06/10/10
Collaborative Research: Toward Improved Projections of Abrupt Response to Anthropogenic Forcing: Combining Paleoclimate Proxy and Instrumental Observations with an Earth System Model	A. Timmermann	Penn State / NSF	$228,675	06/15/09–05/31/12

Title	PI and Co-PIs	Agency	Amount	Period
Development of a MME System for ISO Prediction and Improvement of Coupled Model Initialization	B. Wang, J.Y. Lee, Z. Wu	Pusan Nat'l Univ	$124,784	04/22/09–04/21/10
A Tropical Cyclone Genesis Forecast Model	T. Li	ONR	$176,400	02/16/09–05/31/12
Near-Real Time Debris Distribution in the North Pacific	N. Maximenko	NFWF/NOAA	$69,909	01/01/09–12/31/09
Dynamics of Anisotropic Mean and Time-Varying Structure of Ocean Circulation	N. Maximenko, E. Di Lorenzo, & N. Schneider	NASA	$719,963	10/01/08–09/30/12
Toward Reducing Climate Model Biases in the Equatorial Atlantic and Adjacent Continents	S.P. Xie & I. Richter	NOAA/CPO	$342,124	07/01/08–06/30/11
Changes of Tropical Pacific Climate Variability During the Last Millennium	A. Timmermann & O. Timm	NOAA	$191,851	07/01/08–06/30/13
Precipitation Climatology Projections for Mid and Late 21st Centuries for the Main Hawaiian Islands	K. Hamilton	USGS	$84,855	06/01/08–12/31/11
Application of Multi Satellite Radiance Products to NRL NAVDAS	T. Li & S. Zhang	DoD-PET	$74,500	06/01/08–04/30/09
Development of an Extended and Long-range Precipitation Prediction System over the Pacific Islands	H. Annamalai	NOAA	$443,586	05/01/08 - 04/30/11
Scale Interactions in the Equatorial Ocean	K. Richards & J. McCreary	NSF	$595,444	05/01/08–04/30/11
Study of Processes Leading to Tropical Cyclone Structure and Intensity Changes	Y. Wang	NSF	$398,016	04/01/08–03/31/10
Analysis and High-Resolution Modeling of Tropical Cyclogenesis during TCS-08 and TPARC Field Campaign	T. Li & M. Peng	ONR	$231,243	01/01/08–12/31/10
Climate Change and Persistent Droughts: Impacts, Vulnerability and Adaptation in Rice Growing Subdivisions of India	H. Annamalai	Norwegian Embassy	$127,053	12/07/07–11/30/10
Collaborative Research: Impacts of Ocean Physics on the Arabian Sea Oxygen Minimum Zone	J. McCreary, K. Richards, & Z. Yu	NSF	$385,570	10/01/07–09/30/10
UH/MHPCC Generation of Submesoscale	K. Richards	MHPCC-Engagement Grant	$35,174	08/25/07–06/30/09
Evaluation and Improvement of NOAA Climate GCM Air-Sea Interaction Physics: An EPIC/VOCALS Synthesis Project	Y. Wang, S.P. Xie, & S. de Szoeke	NOAA / OGP / CPPA	$275,384	08/01/07–07/31/10
Future Projections of Mean and Variability of the Asian Summer Monsoon and Indian Ocean Climate Systems	H. Annamalai	DOE	$165,836	08/01/07–07/31/11
Understanding Climate-Biogeochemical Feedbacks During the Last Glacial-Interglacial Transition: A Systematic Modeling and Paleo-Data Synthesis Approach	A. Timmermann	NSF	$314,100	07/01/07–06/30/10
PI-GCOS Server Reimbursement	J. Potemra	Bureau of Meteorology Australia	$20,000	06/01/07–05/31/09
Inter-Annual Variability and Prediction on Eddies in the Gulf of Aden and the Somali Current Region	J. McCreary	ONR	$103,050	05/01/07–09/30/09
Analysis of Climate Change in Korea and East Asia Area and Study of the Atmospheric and Ocean Effects	B. Wang	Yonsei University	$121,279	04/01/07–12/31/09
Collaborative Research: Decadal Coupled Ocean-Atmosphere Interactions in the North	N. Schneider	NSF	$72,365	03/01/07–02/28/10
Western Pacific Tropical Cyclone Reanalysis with the NRL Atmospheric Variational Data Assimilation System (NAVDAS)	T. Li & X. Zhang	ONR	$180,957	01/01/07–08/31/10
Collaborative Research: Origin, Pathway and Fate of Equatorial 13°C Water in the Pacific	T. Qu & I. Fukumori	NSF	$486,210	09/01/06–08/31/10
Dynamics of Tropical Cyclone Intensity Change	T. Li	ONR / NRL	$91,000	09/01/06–08/31/09

Title	PI and Co-PIs	Agency	Amount	Period
Orographically Induced Ocean-Atmosphere Interaction: Satellite Observations and Numerical Modeling	S.P. Xie	NASA	$248,162	06/15/06–06/24/10
Effects of the Stratospheric Quasi-biennial Oscillation on Seasonal Predictability of Tropospheric Circulation in the Northern Hemisphere Extratropics	K. Hamilton	NOAA-CLIVAR	$166,355	06/01/06–05/31/09
Collaborative Research: Eddy Dynamics and Impacts of Low Frequency Variations in the California Current System	N. Schneider	NSF	$193,340	03/01/06–02/28/10
Predictability and Diagnosis of Low Frequency Climate Processes in the Pacific	N. Schneider	DOE	$150,002	09/15/04–09/14/09
Analysis of Climate Change in Korea and East Asia Area and Study of the Atmospheric and Ocean Effects	B. Wang	Yonsei University	$149,199	06/01/04–12/31/09

IPRC STAFF*

FACULTY

HACKER, Peter
HAMILTON, Kevin
LI, Tim
McCREARY, Julian
POTEMRA, Jim
RICHARDS, Kelvin
SCHNEIDER, Niklas
TIMMERMANN, Axel
WANG, Bin
WANG, Yuqing
XIE, Shang-Ping

RESEARCHERS

ANNAMALAI, H. "Anna"
ELISON TIMM, Oliver
FU, Joshua, Xiouhua
FURUE, Ryo
KIKUCHI, Kazuyoshi
LAUER, Axel
LEE, June-Yi
MAXIMENKO, Nikolai
NATAROV, Andrei
QU, Tangdong
SEO, Hyodae
TOKINAGA, Hiroki
YU, Zuojun

TECHNICAL STAFF

BURNS, Thomas David
DeCARLO, Sharon
HAFNER, Jan
JIA, Yanli
LEBEDEV, Konstantin
LIU, Ping
MERRILL, Ronald
SHEN, Yingshuo
WANG, Kin Lik

ADMINISTRATIVE SUPPORT

HO, Jeanie
NAKAJIMA, Aimee
WAKUMOTO, Lori

OUTREACH

SPEIDEL, Gisela
TOKINAGA, Keiko

POSTDOCTORAL FELLOWS

APPUKUTTAN PILLAI, Prasanth
ASCANI, François
CHEN, Ju
CHOWDARY, Jasti Sriranga
FRIEDRICH, Tobias
FU, Bing
FUDEYASU, Hironori
GE, Xuyang
JOHNSON, Nathaniel
KADOTA, Minoru
KAJIKAWA, Yoshiyuki
KIM, Hyung Jin
KOSAKA, Yu
KWON, Min Ho
LAURIAN, Audine
LI, Jinbao
LI, Yanping
McGREGOR, Shayne
MENVIEL, Laurie
OGATA, Tomomichi
SAMPE, Takeaki
SASAKI, Yoshinori
SOMA, Kazuyoshi
SOORAJ KALLIKKAL, Puthiya Veettil
SUN, Jian
VENKATRAMAN, Prasanna
WANG, Lei
XU, Jing
YOSHIDA, Sachiko
ZHANG, Chunxi
ZHANG, Shengjun

*For all or part of the year of the report

ACRONYMS

ACC	Anomaly Correlation Coefficient
AMOC	Atlantic Meridional Overturning Circulation
AR4	Fourth Assessment Report of the Intergovernmental Panel on Climate Change
BMRC	Bureau of Meteorology Research Centre
DAC	Data Assembly Center
CAPE	Convective available potential energy
CAS	Chinese Academy of Sciences
CFS	Climate Forecast System
CMAP	Climate Prediction Center Merged Analysis of Precipitation
CTL	Control
CNTL	Control
EASM	East Asian summer monsoon
EASMI	East Asia summer monsoon intensity index
ECMWF	European Centre for Medium-Range Weather Forecasts
EEIO	Eastern equatorial Indian Ocean
E-MPI	Emanual's maximum potential intensity
ENSO	El Niño–Southern Oscillation
ERA	ECMWF re-analysis
ERSST	Extended Reconstruction Sea Surface Temperature
GCM	General circulation model
GDAC	Global data assembly center
GFDL	Geophysical Fluid Dynamics Laboratory
GHG	Greenhouse gases
GLIMMER	The Community Ice Sheet Model
HYCOM	Hybrid Coordinate Ocean Model
IcIES	Name of JAMSTEC Ice sheet model
IMAR	Inner Mongolia Autonomous Region
IOD	Indian Ocean dipole
IPCC	Intergovernmental Panel on Climate Change
iRAM	IPRC regional atmospheric model
ISCCP	International Satellite Cloud Climatology Project
ISV	Intraseasonal variability
JAMSTEC	Japan Agency for Marine-Earth Science and Technology
KE	Kuroshio Extension
KOE	Kuroshio and Oyashio Extension
LGM	Last Glacial Maximum
LOVECLIM	Acronym made from the names of the five different models that have been coupled to built the Earth system model: LOch–Vecode-Ecbilt-CLio-agIsm Model
MALR	Moist adiabatic lapse rate
MBL	Marine boundary layer
MHD	Maximum hail diameter
MIT	Massachusetts Institute of Technology
MJO	Madden–Julian Oscillation
MOC	Meridional overturning circulation
MODIS	Moderate-resolution Imaging Spectroradiometer
MPI	Maximum Potential Intensity
NAO	North Atlantic Oscillation
NAOI	NAO index
NCAR	National Center for Atmospheric Research
NCEP	National Centers for Environmental Prediction

NCOM	Navy Coastal Ocean Model
NLOM	Navy Layered Ocean Model
NPDW	North Pacific Deep Water
NRG	Northern Recirculation Gyre
OFES	Ocean General Circulation Model for the Earth Simulator
OGCM	Ocean general circulation model
OLR	Outgoing long-wave radiation
PDO	Pacific Decadal Oscillation
PMOC	Pacific Meridional Overturning Cell
POAMA	Predictive Ocean–Atmosphere Model for Australia.
PreVOCA	Preliminary VOCALS Model Assessment
QBWO	Quasi-biweekly oscillation
QuikSCAT	Quick Scatterometer
RDM	Roughness diffusivity model
RMW	Radius of maximum wind
SCS	South China Sea
SCSTF	South China Sea throughflow
SCUD	Surface CUrrents from a Diagnostic model
S-EOF	Season-reliant Empirical Orthogonal Function
SINTEX-F	Scale Interaction Experiment Global Ocean-Atmosphere Coupled GCM
SLP	Sea level pressure
STWT	Spatio-temporal wavelet transform
SRES	Special Report on Emissions Scenarios
SSH	Sea surface height
SSM/I	Special Sensor Microwave Imager
SST	Sea surface temperature
STC	Subtropical overturning cell
TC	Tropical cyclone
TCM	Tropical cyclone model
TIO	Tropical Indian Ocean
TMI	TRMM Microwave Imager
TRMM	Tropical Rainfall Measuring Mission
TS	Tropical storm
TSD	Tropical storm days
USAPI	U.S. Affiliated Pacific Islands
VOCALS	VAMOS Ocean-Cloud-Atmosphere-Land Study
WAIS	West Antarctic Ice Sheet
WASWind	Wave and Anemometer-based Sea-surface Wind
WIG	Westward propagating inertio-gravity
WNP	Western North Pacific
WNPC	Western North Pacific anomalous cyclone
WNPSM	Western North Pacific summer monsoon
VLOM	Variable-layer model
VWS	Vertical wind shear
XUAR	Xinjiang Uygur Autonomous Region

A publication of the
International Pacific Research Center
School of Ocean and Earth Science and Technology
University of Hawai'i at Mānoa
1680 East-West Road, POST Bldg., Room 401
Honolulu, Hawai'i 96822

Tel: (808) 956-5019 Fax: (808) 956-9425
Web: http://iprc.soest.hawaii.edu

The IPRC is a climate research center funded by governmental agencies in Japan and the United States and by the University of Hawai'i.